

MACHINE LEARNING BASED FAULT DETECTION AND ISOLATION IN DC MICROGRIDS



Project/Thesis ID. 2023: 3954

Session: BSc. Fall 2019

Project Supervisor: Dr. Muhammad Mehdi

Submitted By

Sameer Ahmed

Tariq Khan

Electrical Engineering

**Balochistan University of Information Technology, Engineering,
And Management Sciences**

Certification

This is to certify that **Mr. Sameer Ahmed, 50246** and **Mr. Tariq Khan, 47034** have successfully completed the final project **Machine Learning based Fault Detection and Isolation in DC Microgrids** at the **Balochistan University of Information Technology Engineering and Management Sciences** to fulfill the partial requirement of the degree **Electrical Engineering**.



External Examiner

Dr. Waleed Raza

Assistant Professor



Project Supervisor

Dr. Muhammad Mehdi

Assistant Professor



Chairman

Department of Electrical Engineering, Balochistan University of Information Technology Engineering and Management Sciences, Quetta

Project Title (Machine Learning based Fault Detection and Isolation in DC Microgrids)

Sustainable Development Goals

(Please tick the relevant SDG(s) linked with FYDP)

SDG No	Description of SDG	SDG No	Description of SDG
SDG 1	No Poverty	SDG 9	Industry, Innovation, and Infrastructure
SDG 2	Zero Hunger	SDG 10	Reduced Inequalities
SDG 3	Good Health and Well Being	SDG 11	Sustainable Cities and Communities
SDG 4	Quality Education	SDG 12	Responsible Consumption and Production
SDG 5	Gender Equality	SDG 13	Climate Change
SDG 6	Clean Water and Sanitation	SDG 14	Life Below Water
SDG 7	Affordable and Clean Energy	SDG 15	Life on Land
SDG 8	Decent Work and Economic Growth	SDG 16	Peace, Justice and Strong Institutions
		SDG 17	Partnerships for the Goals



Machine Learning based Fault Detection and Isolation in DC Microgrids

Range of Complex Problem Solving			
	Attribute	Complex Problem	
1	Range of conflicting requirements	Involve wide-ranging or conflicting technical, engineering and other issues.	
2	Depth of analysis required	Have no obvious solution and require abstract thinking, originality in analysis to formulate suitable models.	
3	Depth of knowledge required	Requires research-based knowledge much of which is at, or informed by, the forefront of the professional discipline and which allows a fundamentals-based, first principles analytical approach.	
4	Familiarity of issues	Involve infrequently encountered issues	
5	Extent of applicable codes	Are outside problems encompassed by standards and codes of practice for professional engineering.	
6	Extent of stakeholder involvement and level of conflicting requirements	Involve diverse groups of stakeholders with widely varying needs.	
7	Consequences	Have significant consequences in a range of contexts.	
8	Interdependence	Are high level problems including many component parts or sub-problems	
Range of Complex Problem Activities			
	Attribute	Complex Activities	
1	Range of resources	Involve the use of diverse resources (and for this purpose, resources include people, money, equipment, materials, information and technologies).	
2	Level of interaction	Require resolution of significant problems arising from interactions between wide ranging and conflicting technical, engineering or other issues.	
3	Innovation	Involve creative use of engineering principles and research-based knowledge in novel ways.	
4	Consequences to society and the environment	Have significant consequences in a range of contexts, characterized by difficulty of prediction and mitigation.	
5	Familiarity	Can extend beyond previous experiences by applying principles-based approaches.	

Abstract

DC microgrids have attracted considerable attention in recent years due to their higher efficiency, increased integration of renewables, and improved islanding capability over traditional AC power networks. However, ensuring effective protection for DC microgrids remains a challenge, as the failure to detect and isolate faults promptly can lead to widespread grid failure. This thesis proposes a machine learning-based fault detection and isolation algorithm to address this issue. The algorithm integrates mathematical and physical modeling of the DC microgrid using SIMULINK and incorporates a hysteresis band controller to maintain stable operation. By extracting fault-related data from the microgrid, a supervised machine learning algorithm based on neural networks is trained. The algorithm utilizes the cross-entropy loss function for effective classification and the scaled conjugate backpropagation algorithm to optimize the neural network's parameters. These choices enable the algorithm to achieve accurate fault detection and classification, making significant contributions to the field of fault detection and isolation in DC microgrids. The algorithm demonstrates remarkable fault detection capabilities, achieving detection within an impressive 0.2ms and a fault classification accuracy of 99.9%. This research contributes to enhancing the reliability and stability of DC microgrid systems. Future work can focus on expanding the algorithm's capabilities by integrating advanced machine learning techniques and validating its performance in real-world implementations.

Keywords: fault detection and isolation; machine learning; DC microgrids; neural networks

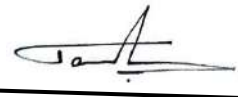
Undertaking

I certify that the project **Machine Learning based Fault Detection and Isolation in DC Microgrids** is our own work. The work has not, in whole or in part, been presented elsewhere for assessment. Where material has been used from other sources it has been properly acknowledged/ referred.



Sameer Ahmed

50246



Tariq Khan

47034

Acknowledgement

We truly acknowledge the cooperation and help made by **Dr. Muhammad Mehdi, Assistant Professor** of **BUIITEMS, Quetta**. He has been a constant source of guidance throughout the course of this project. We would also like to thank **Dr. Abdul Wahid**, from **Assistant Professor** of **BUIITEMS, Quetta** for his help and guidance throughout this project.

We are also thankful to our friends and families whose silent support led us to complete our project.

Table of Contents

Certification.....	ii
Abstract.....	v
Undertaking.....	vi
Acknowledgement	vii
Table of Contents	viii
List of Tables	x
List of Figures.....	xi
List of Acronyms	xii
Chapter 1	1
1.1 Introduction	1
1.1.1 Power Grid	1
1.1.2 DC Micro-Grid (DCMG)	3
1.2 Statement of the problem	7
1.3 Goals/Aims & Objectives.....	7
1.4 Motivation	8
1.5 FDI Methods	8
1.5.1 Model-Based FDI	8
1.5.2 Measurement-Based FDI.....	9
1.5.3 Data Driven FDI.....	10
1.6 Report Overview	12
Chapter 2.....	13
2.1 Literature Review/Related Work	13
Chapter 3.....	16
3.1 Methodology	16
3.2 Single Line Diagram of the DCMG and Elaboration.....	16
3.3 Modeling of the System	18
3.3.1 Mathematical Modeling of the System.....	19
3.3.2 Implementation of the DC Microgrid System (Physical Modeling of the DCMG).....	22
3.4 Parameters of DC Microgrid Model.....	26
3.5 Fault Modeling	27
3.5.1 Failure of Switch in Power Converter	28
3.5.2 DC transmission Cable Short-Circuit Fault.....	29
3.5.3 Busbar Short-Circuit Fault	31

3.5.4	Load Component Fault	33
3.5.5	Modeling of the Component Faults of the DCMG	35
3.6	Machine Learning Algorithm for Fault Detection and Classification.....	36
3.6.1	Supervised Learning for Fault Classification	37
3.6.2	Neural Networks for Fault Detection and Classification in Power Systems	38
3.6.3	Workflow: Fault Detection and Classification in DC Microgrid using Neural Networks..	44
3.7	Fault Classification Module	45
3.7.1	No-Fault Condition (Nof):.....	45
3.7.2	Fault Signature for the Switch Failure type Fault:.....	46
3.7.3	Fault Signature for the Short-Circuit Fault in the Transmission Cable:	46
3.7.4	Fault Signature for the Short-Circuit Fault in the Busbar:.....	47
3.7.5	Fault Signature for the Short-Circuit Fault in the Load Component:	47
Chapter 4	49
4.1	Proposed Solution/Results & Discussion.....	49
4.1.1	DCMG under Normal Operation	50
4.1.2	DCMG Under Fault Condition	52
4.1.3	Proposed FDI Training and Results.....	60
4.1.4	Results of the Proposed ML Based FDI in DCMG	64
Chapter 5	73
5.1	Summary and Future work.....	73
Chapter 6	74
6.1	Conclusion & Recommendation	74
References	75

List of Tables

Table 1: DCMG component-wise parameters.	26
Table 2: Component Fault Specifications of the DCMG.....	35
Table 3: Different Fault Scenarios and Data Sample Quantities in the DCMG	53

List of Figures

Figure 1: A generic model of the AC Power Grid	2
Figure 2: A typical DCMG construction	4
Figure 3: Circuit Diagram of Two-State Buck Converter	5
Figure 4: Circuit Diagram of Two-State Boost Converter	6
Figure 5: Workflow of the machine learning process.....	11
Figure 6: The configuration of the DC microgrid in the case study. [18].	16
Figure 7: The schematic representation of the DC microgrid in the case study [18].	18
Figure 8: DCMG under the influence of different faults [12].	18
Figure 9: Physical circuit model of the DCMG.....	22
Figure 10: Physical circuit model of the Boost Converter Circuit.	23
Figure 11: Physical circuit model of the Buck Converter Circuit.	24
Figure 12: Physical circuit model of the DC Cable	25
Figure 13: Physical circuit model of the Busbar.....	25
Figure 14: Equivalent model of a DC cable incorporating a short-circuit faults.....	30
Figure 15: Equivalent model of a DC busbar incorporating a short-circuit fault.	32
Figure 16: Architecture of Neural Networks.	38
Figure 17: Workflow depiction for Fault Detection and Classification in DC Microgrid Systems using Neural Networks.	48
Figure 18: The schematic representation of the DC microgrid in the case study	50
Figure 19: Data Generation Case-1 No-fault	51
Figure 20: Data Generation Case-2 Switch Faults.....	56
Figure 21: Data Generation Case-3 Busbar Faults	57
Figure 22: Data Generation Case-4 Cable Faults	58
Figure 23: Data Generation Case-5 Load Faults	59
Figure 24: Structure of the neural network used in this FDI	61
Figure 25: Training Performance Plots.....	62
Figure 26: Confusion Matrix Plots	63
Figure 27: FDI Case-1 Boost Converter Switch Failure Responses.....	65
Figure 28: FDI Case-1 Boost Converter Switch Failure Detection & Isolation	66
Figure 29: FDI Case-2 Transmission Cable Fault Responses	67
Figure 30: FDI Case-2 Transmission Cable Fault Detection & Isolation	68
Figure 31: FDI Case-3 Busbar Fault Response	69
Figure 32: FDI Case-3 Busbar Fault Detection & Isolation	70
Figure 33: FDI Case-4 Load Component Fault Responses	71
Figure 34: FDI Case-4 Load Component Fault Detection & Isolation.....	72

List of Acronyms

ANN	Artificial Neural Networks
CNN	Convolutional Neural Networks
DCMG	DC Micro-Grid
DER	Distributed Energy Resources
DOB	Disturbance Observer
EKF	Extended Kalman Filter
EMD	Empirical Mode Decomposition
EU	European Union
FIS	Fuzzy Inference System
HIF	High Impedance Fault
HT	Hilbert Transform
IEKF	Iterated Extended Kalman Filter
KNN	K –Nearest – Neighbors
LC	Inductor – Capacitor
LED	Light Emitting Diode
LPV	Linear Parametric Variation
MDOB	Modified Disturbance Observer
MPPT	Maximum Power Point Tracking
MRA	Multiresolution Analysis
MVDC	Medium – Voltage DC
NUIO	Nonlinear Unknown Input Observers
PG	Pole – to – Ground
PP	Pole – to – Pole
PPO	Proximal Policy Optimization
PV	Photo-Voltaic
RES	Renewable Energy Resources
RNN	Recurrent Neural Networks
STFT	Short – Time Fourier Transform
SVM	Support Vector Machines
TFA	Time – Frequency Analysis
TWP	Traveling Wave Protection
UIO	Unknown Input Observers
UKF	Unscented Kalman Filter
WMRA	Wavelet-Multi Resolution Analysis

Chapter 1

In this chapter we discuss the basic concepts of microgrids, especially the need for DC microgrids. Moreover, we will provide a brief discussion about fault-detection and isolation for the DC grids.

1.1 Introduction

The present power system is rapidly growing. This rapid growth is making the system more complicated and contributing to several issues, including an increase in reactive power loss and a decrease in the system's stability and power quality. A DC system was developed as a viable solution to many of the problems an AC power system is now experiencing. In addition to being naturally simple, DC systems are also devoid of concerns like reactive power loss and power quality problems. Therefore, DC systems are widely used for bulk power transmission. DC systems are now becoming more commonplace at distribution levels as well [1]. By 2050, carbon emissions are expected to be decreased to between 80% and 90%, achieving the exceptional carbon reduction target set by the EU. This is expected to be accomplished by using renewable energy sources and smart electricity utilization. To promote future energy sustainability and reduce dependency on the usage of fossil fuels, recent research focused on substituting conventional resources with RES and effective power management by constructing micro-grids [2].

1.1.1 Power Grid

Power grids are today regarded as one of the crucial parts of the infrastructure that supports modern society. The uninterrupted delivery of power to clients is the main goal of power system operation. However, both small- and large-scale defects and disruptions in the grid frequently result in power outages, which have an impact on the dependability of the system and consumer satisfaction [3]. There are two types of power distribution systems.

1.1.1.1 AC Power Grid

Due to its evolution since the 19th century, the AC electrical grid has subsequently become a well-developed and tested idea. Through substations, it is feasible to transmit

electric power from a power plant to homes. It also provides a straightforward and trustworthy concept of power distribution as shown in Figure 1, which has been the norm during the past century. The power transformer, which can change the amplitude of the voltage inside the grid system to make the grid system more flexible while supplying electricity to the home, is the fundamental benefit of the AC grid [4].

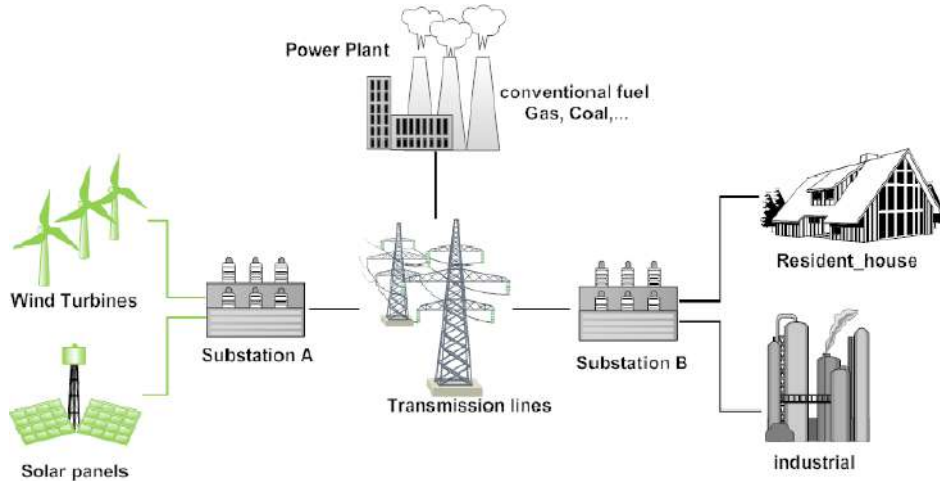


Figure 1: A generic model of the AC Power Grid

1.1.1.2 DC Power Grid

A DC power system is an electrical circuit that consists of resistors and constant current sources. The voltages and currents in the circuit are unaffected by time. The current or voltage in an electrical circuit is independent of its preceding value. Following are some of the main advantages of DC Power System [4]

- Fewer sources of failure and simpler power electronic connections.
- Using DC electricity promotes grid dependability and improves stability.
- Improved integration of dispersed renewable generation.
- Compared to AC, DC distribution has lower overall losses. Since many household appliances run on DC, generating electricity from solar energy avoids the losses associated with changing to AC.
- There are fewer conductors needed, and the skin effect is not present (compared to HVDC transmission system).
- Due to its lower cost than AC, DC is employed in high-voltage long-distance transmission in current technologies.

1.1.1.3 Concept of Micro-Grid

A micro-grid is a network of interrelated loads and distributed energy sources that, in relation to the grid, functions as a single, managed entity and is restricted within specific electrical parameters. A micro-grid may connect to and disconnect from the grid to operate in both grid-connected and island mode [5].

1.1.2 DC Micro-Grid (DCMG)

A collection of scattered generators, loads, and energy storage systems that are situated near to one another is referred to as a DC micro-grid Fig. 1-2. It presents an opportunity to utilize renewable energy sources to produce a clean, green environment. Since the DERs are located near to the load, power transmission losses are reduced to a minimum. DERs like fuel cells and solar panels create DC Power. Power electronics devices can be used to harvest wind energy and generate DC electricity. By coupling the DC terminals to electronic loads, electric cars, and batteries, a direct current micro-grid is produced. DCMG must be correctly operated and regulated to boost dependability, generate revenue, and improve performance [6]. Some of the advantages in the implementation of DC micro-grid are as follows.

- Decreased losses and improved efficiency because of using fewer converters for DC loads.
- Simpler interfaces make it easier to integrate various DC DERs such as solar PV cells, energy storage devices, and fuel cells, to the same bus.
- It provides a more effective supply to DC loads, including LED lights and electric cars.

1.1.2.1 Structure of a DC Micro-Grid

A generic grid connected DCMG configuration with solar panels, wind turbine batteries, and a load is shown in Figure 2 below.

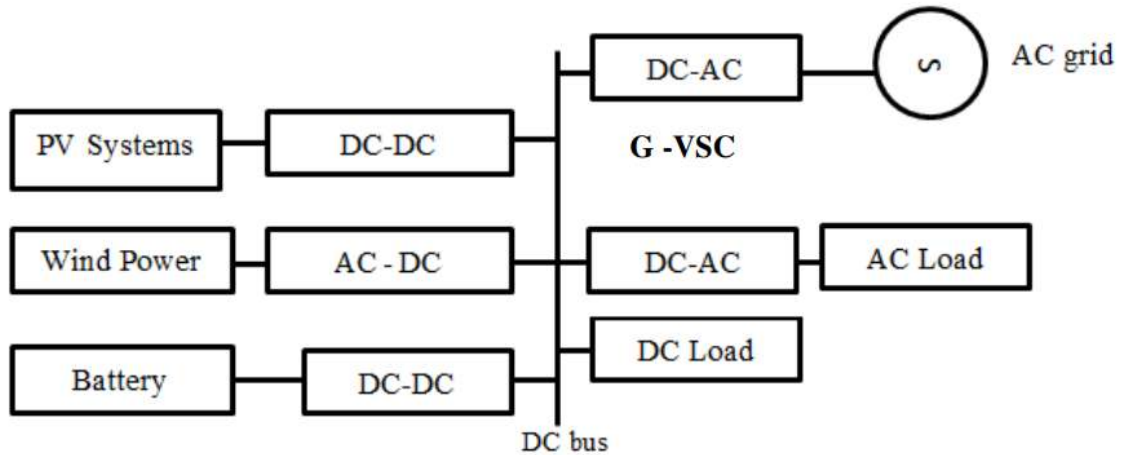


Figure 2: A typical DCMG construction

The following are the DCMG's constituent parts:

1. Generation Unit

Solar and wind energy are used as DERs in this system. While PV is joined to the DC bus using a DC-DC converter, wind power sources are connected using an AC-DC converter. Both generating sources operate in the MPPT mode, or maximum power point tracking. To capture as much wind and solar energy as possible, this is done. The network conditions may allow for the usage of the DERs in derated mode [6].

2. Battery

Using a bi-directional converter, the power storing battery is linked to the DC bus regardless of its technology (lead acid, li-ion, etc.). If the demand in the grid-connected mode is lower than the generation, the battery gets charged. In isolated mode, a battery can be used to power the load [6].

3. Load

The appropriate rated voltage load is connected to the DC bus with the help of converters, depending on whether the load is of AC or DC type. The loads with the appropriate rated voltage ratings can be connected appropriately in the case of a multilevel DC system [6].

4. Grid Linking Converter

Grid linking converters are crucial components in modern power systems that enable the seamless integration of renewable energy sources into the electrical grid [6]. These converters serve as the vital interface between different types of power systems, such as AC and DC, allowing for efficient power transmission and distribution. By

converting the electricity from one form to another, grid linking converters facilitate the stable and reliable transfer of power across diverse networks, bridging the gap between conventional power generation and renewable energy generation [7]. Their ability to control and regulate power flow ensures grid stability, enhances grid resilience, and maximizes the utilization of renewable resources. Grid linking converters play a pivotal role in shaping a sustainable and environmentally friendly energy landscape, empowering the transition towards a cleaner and greener future.

1.1.2.2 DC-DC Step-Up and Step-Down Transformer

1. DC-DC Buck Converter

A buck converter is a type of DC-DC converter (Step-Down Transformer) widely used in power electronics for voltage step-down applications. Its primary function is to efficiently reduce a higher DC voltage input to a lower DC voltage output [8]. The working principle of a buck converter involves the use of a switch (typically a transistor) that operates in a switching mode, along with an inductor, a diode, and a capacitor. Through the cyclical switching of the transistor, the buck converter regulates the output voltage by controlling the duty cycle, which determines the amount of time the switch is ON or OFF. This control mechanism enables the buck converter to efficiently step down the voltage while minimizing power losses [8]. Following is the schematic diagram of a buck converter shown in Figure 3.

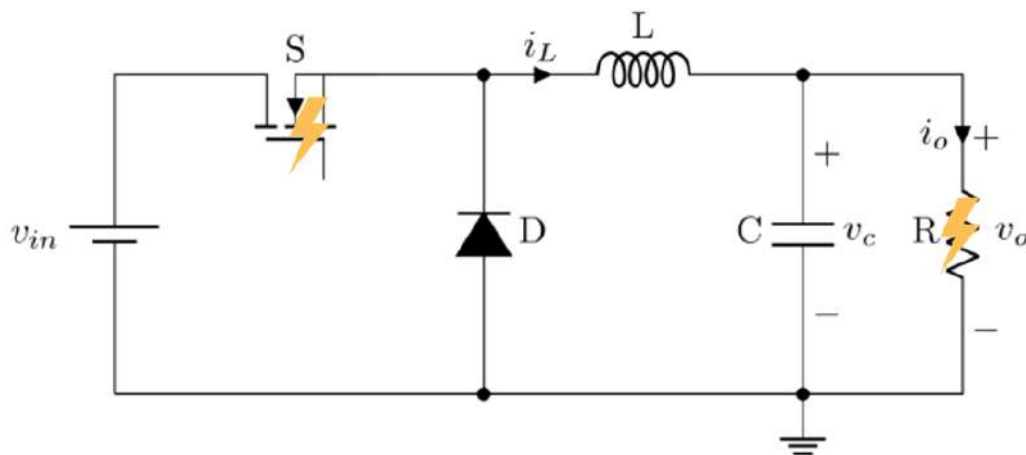


Figure 3: Circuit Diagram of Two-State Buck Converter

The circuit working dynamics can be explained by the following equations.

$$\begin{aligned}\frac{d}{dt}I_L &= -\frac{1}{L}V_C + \frac{V_{IN}}{L}D \\ \frac{d}{dt}V_C &= \frac{1}{C}I_L - \frac{1}{RC}V_C\end{aligned}\quad (1)$$

Where L is inductor and I_L the current through it. C is capacitor and V_C is the voltage across it. V_{IN} is the input voltage. R is the load resistance in *Ohms*, and D is the duty cycle of the switch.

The possible occurrences of faults are also depicted in the figure. In the first case, switch failure might occur, causing a change in duty cycle of the buck converter, similarly in second case load component fault can occur resulting in short-circuit fault.

2. DC-DC Boost Converter

A boost converter, also known as a step-up converter, is a type of DC-DC converter that is widely used in power electronics for voltage step-up applications. Its main purpose is to increase a lower DC voltage input to a higher DC voltage output [8]. The working principle of a boost converter involves a switch (usually a transistor), an inductor, a diode, and a capacitor. Through the control of the duty cycle, which determines the ratio of ON and OFF times for the switch, the boost converter regulates the output voltage [8]. Following is the schematic diagram of a boost converter shown in Figure 4.

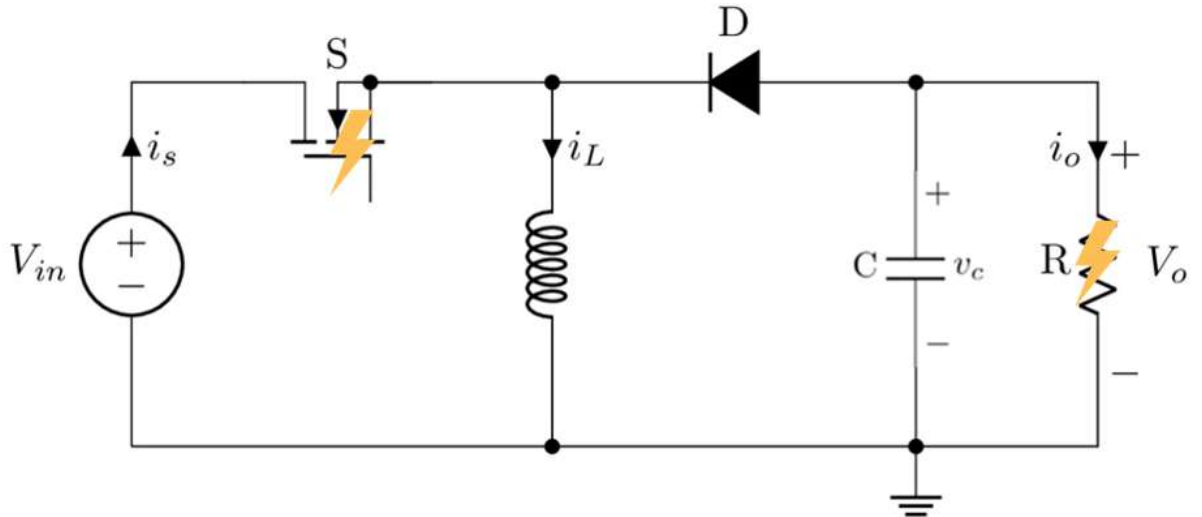


Figure 4: Circuit Diagram of Two-State Boost Converter

The circuit working dynamics can be explained by the following equations.

$$\begin{aligned}\frac{d}{dt}I_L &= -\frac{1-D}{L}V_C + \frac{1}{L}V_{IN} \\ \frac{d}{dt}V_C &= \frac{1-D}{C}I_L - \frac{1}{RC}V_C\end{aligned}\quad (2)$$

Where I_L and L is the current through inductor and inductance in H respectively. V_C and C are the voltage across the capacitor and capacitance in Farads respectively. V_{IN} is the input voltage, R is the load resistance in ohm . D is the duty cycle of the switch.

The possible occurrences of faults are also depicted in the figure. In the first case, switch failure might occur, causing a change in duty cycle of the boost converter, similarly in second case load component fault can occur resulting in short-circuit fault.

1.2 Statement of the problem

The electricity sector of the world is witnessing a major shift towards DC microgrids, driven by their enhanced efficiency, reliability, flexibility, and cost-effectiveness compared to traditional AC grids [9], [10]. This innovative shift is fueled by factors [11], [12] like decreasing power electronics costs, surging renewable energy integration, increased energy efficiency demands, and the vital need for grid resilience. As these driving forces accelerate, DC microgrids stand poised to transform the future of power distribution. However, despite their immense potential, DC microgrids are insecure because of their vulnerability to faults. High voltage, low impedance, and a lack of natural zero crossings in DCMGs make FDI challenging [13], [14], demanding advanced strategies and robust mechanisms to ensure safe, reliable operation.

1.3 Goals/Aims & Objectives

This research proposes a machine-learning-based algorithm to address the fault protection issue of the DCMG. Below are the main objectives of this study:

- Model and generate training data for the DC Microgrid.
- Train a machine-learning algorithm for fault detection.
- Test and evaluate the algorithm.
- Implement the algorithm on the DC microgrid.

1.4 Motivation

As technology advances, the need for a reliable, uninterrupted electric power supply becomes more common for everyone, from industry to homes. As a result, the global electricity sector is shifting dramatically toward DC microgrids, which outperform traditional AC grids in terms of efficiency, reliability, flexibility, and cost-effectiveness. This innovative shift is being driven by factors such as falling power electronics costs, increased renewable energy integration, rising energy efficiency demands, and the critical need for grid resilience. Despite their enormous potential, DC microgrids are insecure due to their vulnerability to faults. High voltage, low impedance, and a lack of natural zero crossings in DCMGs make fault detection and isolation difficult, necessitating advanced strategies and robust mechanisms to ensure safe, dependable operation, which is the primary motivation for undertaking this project.

1.5 FDI Methods

Equipment failure and malfunctioning are caused by faults in any system. There are many FDI techniques that have been proposed to identify the type, size, location, and time of fault. Any FDI method's primary goals are to identify the magnitude, location, and timing of the occurrence of faults and to sound an alarm if there is any change in the process. Fault isolation and fault detection are two tasks carried out by FDI. Finding a defect involves figuring out if it has already happened or not. [15]. The following are some of the basic FDI techniques.

1.5.1 Model-Based FDI

Model-based FDI approaches utilize a model of the system to determine if a failure may occur. The system model might be based on knowledge or on mathematics. There are two primary model-based FDI methods that exist [15].

1.5.1.1 Kalman Filter

The Kalman filter encompasses various algorithms and types, including the standard Kalman filter for linear systems with Gaussian noise and the EKF for nonlinear systems by linearizing models. It also includes other types such as the UKF, which

approximates system behavior using selected points, and the IEKF [15], which iteratively refines EKF estimates. This versatile filter finds applications in aerospace, robotics, finance, and more, as it enables accurate state estimation and fault detection in dynamic systems. A Kalman filter based FDI system integrates Kalman filter principles with fault detection techniques to identify abnormal behavior and faults in real-time. By analyzing sensor measurements and comparing them with expected values, the FDI system detects deviations indicating faults, while the Kalman filter's state estimation aids in fault isolation and localization, enhancing system reliability through timely maintenance [15].

1.5.1.2 Observer

A state observer or state estimator is a system that utilizes measurements of input and output from a real system to estimate its internal state [15]. It is commonly implemented using computer-based algorithms and serves as a fundamental tool in various applications. Models play a crucial role in fault detection and diagnostics within the observer approach. However, these methods face challenges such as disturbances, mismatches, noise, and uncertainties. To mitigate the impact of significant disturbances, researchers have developed techniques such as the DOB and MDOB. In the context of FDI, UIO and NUIO are frequently employed. These techniques provide operators with early warnings of any changes in the process, aiding in fault detection. [15]

1.5.2 Measurement-Based FDI

Measurement-based FDI methods play a crucial role in ensuring the health and reliability of complex systems across diverse domains, from industrial processes to large-scale power grids. These methods rely on analyzing sensor data to identify deviations from normal operation, indicating the presence and location of potential faults. The core working principle revolves around comparing actual measurements with expected values derived from models or historical data. This comparison generates residuals, which are the differences between expected and observed behavior. Exceeding predefined thresholds or analyzing abnormal patterns in these residuals triggers the fault detection alarm. Several commonly employed techniques [24] – [33] illustrate this approach:

1.5.2.1 Voltage and Current Threshold Methods

Simple but effective, setting predefined thresholds for critical parameters like voltage or current. Exceeding these thresholds indicates a potential fault, with the location narrowed down based on the affected sensor.

1.5.2.2 Current Differential Method

Compares currents at different points in a circuit. Significant disparities point to anomalies in specific sections, aiding in fault isolation.

1.5.2.3 Signal Processing Methods

Techniques like spectral analysis and time-frequency decomposition capture specific features of noisy or complex signals. Deviations from expected patterns due to faults can then be identified and localized.

1.5.2.4 LC Circuit Method

Utilizes the impedance characteristics of an LC circuit to selectively filter out background noise and amplify fault-related signals, enhancing their detection and differentiation.

1.5.3 Data Driven FDI

In this protection strategy, measurements are subjected to some mathematical or statistical computations, or a type of neural network is trained using some sort of algorithm to extract information about the fault.

1.5.3.1 Fuzzy

A mathematical model is not necessary with fuzzy approach. The modelling inaccuracy, uncertainty, and disruption are therefore not present in a fuzzy model. An issue with a complicated nonlinear system might be the lack of an adequate model. In this situation, fuzzy plays a significant role by utilizing human expertise to handle fault diagnostics more effectively. A fuzzy decision-making system is created based on fuzzy rules to determine where the error lies. Although fuzzy decision-making relies on

human expertise, it is incapable of effective learning. It is challenging to automatically tune functions of fuzzy control. Fuzzy bases decisions on data that is vague or ambiguous. The residual must first be fuzzified and evaluated using inference mechanisms like IF-THEN rules before being defuzzified to detect and isolate the fault using fuzzy [15].

1.5.3.2 Machine Learning Based FDI

Machine learning-based FDI is an emerging approach that utilizes advanced algorithms and techniques from the field of machine learning to detect and diagnose faults in complex systems. Commonly employed algorithms in this context include SVM and ANN [16]. SVM is a supervised learning algorithm that can classify normal and faulty system behavior based on labeled training data. ANN, inspired by the human brain's neural structure, is a powerful tool for pattern recognition and fault detection. These algorithms, along with others such as Decision Trees, Random Forests, and Deep Learning architectures like CNN and RNN, enable the extraction of valuable insights from large datasets and the identification of abnormal behavior associated with faults [16]. The workflow of the general machine learning algorithm is depicted in Figure 5.

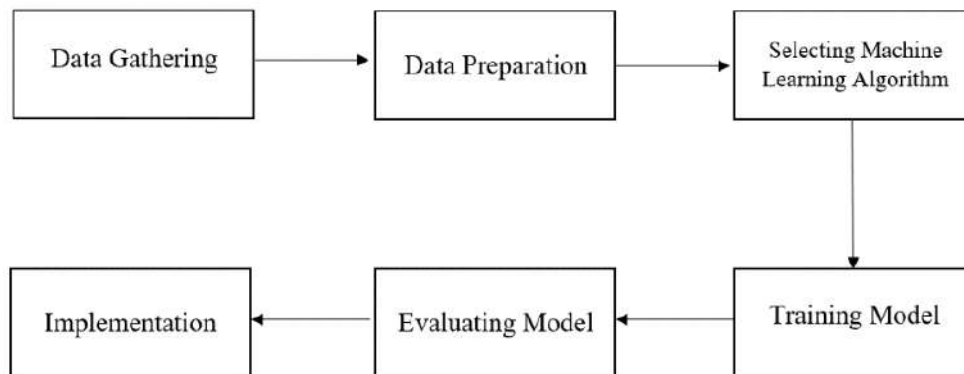


Figure 5: Workflow of the machine learning process

The following are the main classification of machine learning types.

1. Supervised Learning

Supervised learning is a type of machine learning where the algorithm is trained on labeled examples, with input-output pairs, to learn a mapping function. The training data consists of input features and corresponding output labels. The algorithm learns to predict or classify new data based on the patterns it has observed during training. Examples of supervised learning algorithms include decision trees, SVM and ANN [17].

2. Unsupervised Learning

Unsupervised learning, on the other hand, involves learning patterns and structures in unlabeled data without explicit feedback. It aims to discover hidden patterns, clusters, or relationships within the data. Unsupervised learning algorithms operate on raw data and seek to find inherent structures or groupings. Clustering algorithms, such as k-means clustering and hierarchical clustering, are commonly used in unsupervised learning [17].

3. Reinforcement Learning

Reinforcement learning is a branch of machine learning where an agent learns to make sequential decisions through interactions with an environment, aiming to maximize cumulative rewards. Algorithms such as Q-learning, Deep Q-Networks and PPO are commonly used in reinforcement learning [17].

1.6 Report Overview

We can highlight the report organization as follows: Section #2 includes a literature review of the project. Section #3 is mainly the body of the project, discussing the methodology of the machine learning algorithm. Section #4 is about the discussion of the results of the proposed protection scheme. Section #5 contains the summary of the project and future work, and Section #6 includes the conclusion and recommendations.

Chapter 2

This chapter discusses the current trends and techniques applied for the FDC of DCMG. In a detailed literature review we provide the pros and cons of the existing methods.

2.1 Literature Review/Related Work

As discussed in Section 1.5, FDI methods can be broadly categorized into three main approaches: model-based, model-free, and data-driven. This section comprehensively explores all three FDI approaches, highlighting their respective advantages and disadvantages, to provide a comprehensive understanding of the available options for ensuring the safety and reliability of DC microgrids.

Model-based FDI methods [18] – [23] utilize a mathematical model of the system to predict its normal behavior and flag any deviations as potential faults. These methods are well-suited for DC microgrids due to their well-defined physical relationships. The typical workflow involves developing a model, estimating its parameters, using an observer to detect faults, and then analyzing residuals to isolate the fault's location. In this category, observer-based FDI approaches have gained prominence due to their effectiveness and adaptability. Observer-based FDI methods employ state observers to estimate the internal states of the system, enabling the detection of faults through the comparison of estimated states to the actual system outputs. This comparison generates residuals, which serve as indicators of fault occurrence. By analyzing the patterns and characteristics of these residuals, the specific fault type (FT) can be identified. Several studies have successfully implemented observer-based FDI techniques for fault detection and isolation in DC microgrids. In [18], an FDI approach using state observers was developed for power electronic converters. Similarly, [19] presented an FDI method using reduced-order observers for DC microgrids. [20] proposed a Luenberger observer-based FDI method for bidirectional DC-DC converter interfaced microgrids. A similar, observer-based FDI has been proposed by [21] for a nonlinear DC microgrid. To overcome the nonlinearity, the researchers have proposed a LPV-based sliding mode observer. In addition to observer-based methods, other model-based FDI approaches have also been proposed. For instance, [22] introduced a Kalman filter-based method for detecting and locating series arc faults in DC microgrids. [23] presented a parameter

estimation-based method for local fault location in meshed DC microgrids. While model-based FDI is an effective approach for fault detection and isolation in DC microgrids, it is important to consider its potential drawbacks. As DC microgrids become more complex, the required analytical models become more intricate and computationally demanding. Additionally, model-based FDI methods are sensitive to model uncertainties.

Measurement-based fault detection and isolation (FDI) is a technique used to detect and locate faults in power systems by measuring electrical quantities, such as voltage, current, and power. It works by comparing the measured values to pre-defined thresholds or to expected values based on a model of the power system. If the measured values exceed the thresholds or deviate from the expected values, a fault is detected. One important approach in this category is to monitor local current and voltage thresholds and measure the resistance, called local measurement-based FDI. This method has been applied in [24] and [25] with the current and voltage thresholds, respectively. Similarly, [26] presented an FDI method using the resistance measurement method for DC microgrids. Although local measurement-based FDI methods can be a viable option for FDI, they lack in several areas, including sensitivity to system parameters such as line impedance and false positives due to noise in the measurements. Another important technique of measurement-based FDI is through TWP. TWP utilizes the high-frequency electromagnetic disturbances generated by faults to detect and locate faults in power systems. By analyzing the characteristics of traveling waves, TWP delivers fast, precise, and dependable fault detection and location capabilities. This technique has been extensively studied and refined, as evidenced by [27], [28] which propose novel TWP approaches for MVDC microgrids and MRA-based TWP schemes, respectively. TWP's benefits come with inherent trade-offs. Although powerful, it is vulnerable to noise and interference, and it may require complex signal processing algorithms to function effectively. Similarly, another crucial technique for measurement-based FDI in DC microgrids is TFA. TFA techniques provide a powerful means of analyzing and comprehending the non-stationary signals, revealing information about the signal's time and frequency content, TFA techniques can uncover hidden patterns and characteristics that may be obscured in traditional time-domain or frequency-domain analysis. Several TFA techniques have been successfully applied to FDI in DC microgrids. For instance, in [29] STFT has been

employed for fault detection, while WMRA has been used to decompose current signals and construct feature vectors for classification [30]. Additionally, a combination of EMD and HT has been proposed for local fault detection [31]. TFA techniques have certain limitations, such as its sensitivity to noise, and it loses effectiveness in some cases, for example, HIFs. Other approaches for FDI in DCMGs include fault detection based on line characteristics using an LC resonance circuit [32] and fault detection and location using differential current protection [33]. The LC resonance circuit method utilizes the resonant frequency of an LC circuit to measure the inductance and capacitance of the faulty line, enabling accurate fault detection. However, this method requires precise measurement of line parameters. Conversely, the differential current protection method compares the currents at both ends of a line to detect faults. This approach has precise fault detection and locating capabilities, but it is vulnerable to noise in differential currents.

Data driven-based FDI techniques have emerged as a promising approach in the field of DCMGs, particularly those utilizing machine learning algorithms. These techniques have demonstrated effectiveness in identifying faults based on patterns and anomalies in system data, offering significant advantages over traditional FDI methods. In the machine learning category, reinforcement learning-based methods [34] demonstrate high accuracy and efficiency in fault detection. Additionally, RNN-based methods [35] enable fault detection and location with high accuracy for both grid-connected and islanded modes. Furthermore, SVM-based methods [36] provide precise fault location even in the presence of high fault resistance. FIS-based methods, like the one in [37], facilitate rapid fault identification and isolation in low-voltage DCMGs. Data-driven FDI strategies, despite their potential, grapple with critical challenges. Notably, none of the solutions suggested in the literature have yet been designed to provide component-level protection. Furthermore, the computational complexity of these approaches may pose difficulties for real-time implementation.

Chapter 3

In this chapter we provide the two aspects of our implementation. One, the modeling of the DCMG under study. The DCMG is first modeled mathematically and then MATLAB Simulink is used for implementation for the simulation purposes. Two, machine learning based FDI.

3.1 Methodology

Figure 6 below displays a selected model of a low-voltage DC microgrid with three terminals. This model was chosen for the purpose of designing a machine learning-based FDI system. This model retains the key characteristics of multiterminal DC grids, such as the ability for power to flow in multiple directions, rapid changes during faults, and the presence of multiple sources contributing to fault currents.

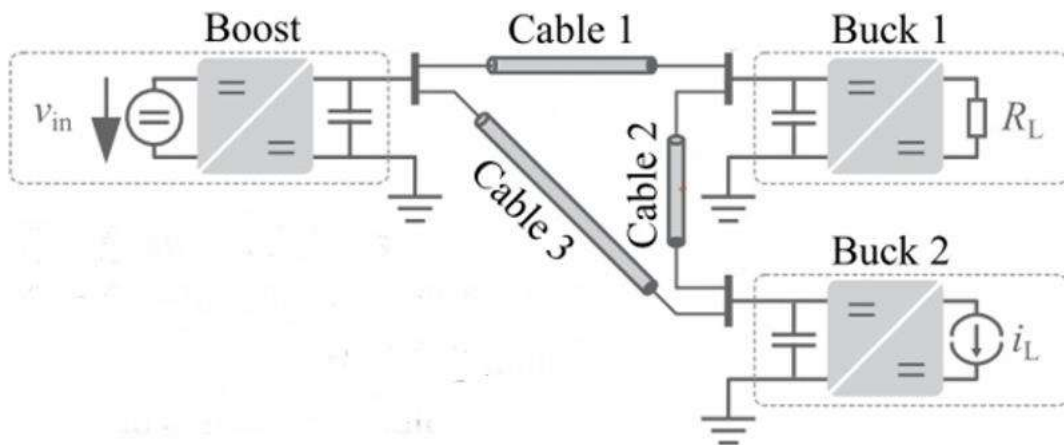


Figure 6: The configuration of the DC microgrid in the case study [18]

3.2 Single Line Diagram of the DCMG and Elaboration

The system under investigation is a three-terminal DC microgrid, which depicts the working of a whole power system. It has three power converters for transforming voltage and current up to suitable levels for transmission and distribution, three transmission cables for power flow, and three busbars, making this grid a multi-terminal system. Since this system is isolated from the utility grid supply, it has its own power generation resources, such as solar PV systems, wind turbines, micro-hydro systems, fuel cells, combined heat, and power (CHP) units, biomass generators, geothermal

systems, reciprocating engines, gas turbines, and much more. On the generation side, a boost converter (DC step-up transformer) is used to regulate the voltage and current to provide better power quality and minimize transmission losses. The DC power from the generation sources and energy storage is then distributed within the microgrid using DC power lines or busbars. These distribution networks carry DC electricity to the various loads and devices connected to the microgrid. On the load side, by using a buck converter (DC step-down transformer), power is supplied to the load with the appropriate voltage and current level. The loads in a DC microgrid can include various electrical devices and appliances, such as lights, motors, electronics, and other equipment. These loads consume the power provided by the microgrid for their operation.

A component-wise model of the DC microgrid is depicted in Figure 7 below. Inside the boost converter, there are multiple power electronics devices, namely series boost inductance L_{bo} and resistance R_{bo} , a high-frequency controllable switch, a diode, and an output link capacitor C_1 . Similarly, in the buck converters, the components are series buck inductances L_{bu1} and L_{bu2} and resistances R_{bu1} and R_{bu2} , a high-frequency power switch, a high-frequency controllable switch, a diode, and an input and output link capacitors C_{bu1} , C_{bu2} , C_2 and C_3 . In transmission cable, due to the smaller length, terminal capacitance is negligible, and only series inductances and resistances L_1, L_2, L_3, R_1, R_2 and R_3 are considered. In this microgrid, the research is focused on ten different types of faults. The failures encompassed converter switch malfunctions, short-circuit faults in DC lines and busbars, as well as a fault emerging in the load. For the illustration of busbar and line faults, this model also contains $R_{1fb}, R_{2fb}, R_{3fb}, R_{1f}, R_{2f}$ and R_{3f} fault resistances. The nominal values for the electronics components in the microgrid are provided in the table below.

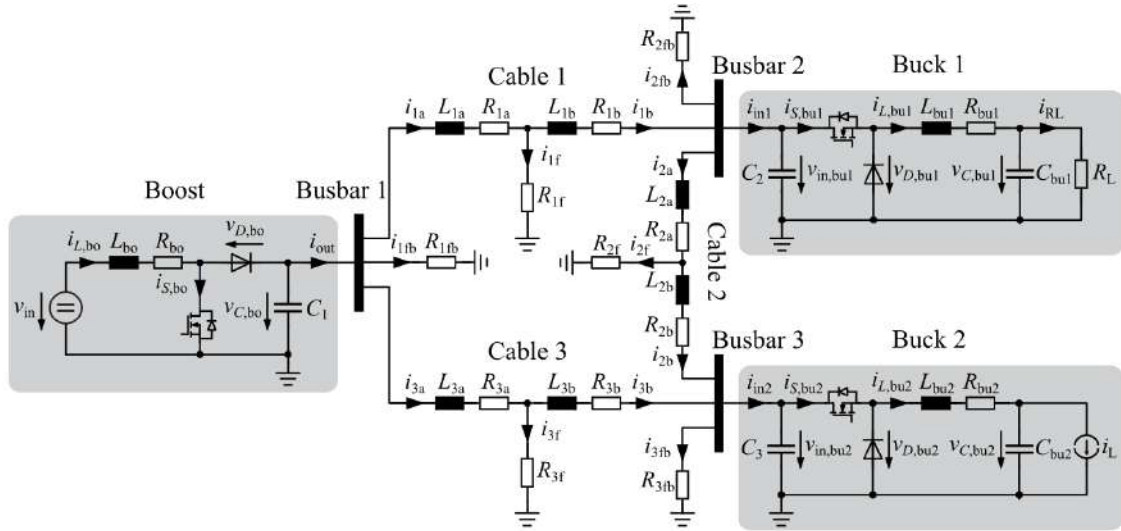


Figure 7: The schematic representation of the DC microgrid in the case study [18]

3.3 Modeling of the System

Within the study case DCMG system, a total of ten distinct faults were investigated: faults ($f_1 - f_3$) represent failures of switch in the converters, faults ($f_4 - f_6$) corresponds to short-circuit faults in DC transmission cable, faults ($f_7 - f_9$) pertain to short-circuit faults occurring in the common node busbars, and fault f_{10} signifies a fault in the load component R_L . The comprehensive diagram of the dc microgrid, including these specific faults, is presented in Figure 8 below.

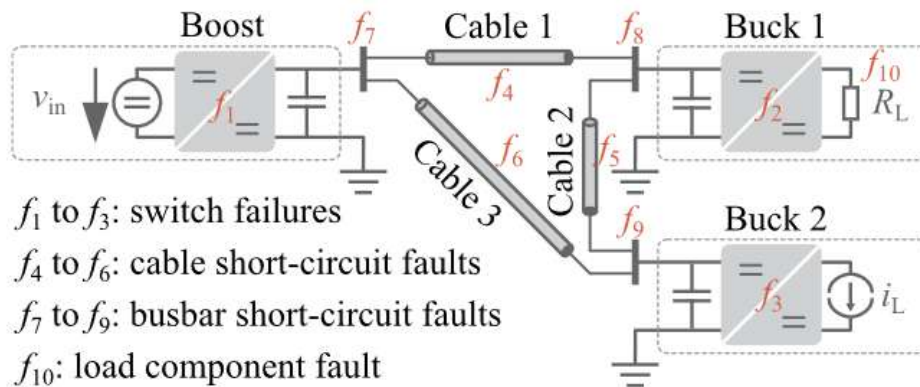


Figure 8: DCMG under the influence of different faults [18]

To comprehensively analyze the behavior and performance of the microgrid circuit, two distinct approaches were employed: mathematical modeling and physical circuit modeling on software. The mathematical modeling approach involved the development of a set of mathematical equations based on the fundamental principles

and characteristics of microgrid components. This enabled a theoretical understanding of the system's behavior and facilitated the derivation of key performance metrics. Additionally, a physical model of the circuit was utilized to simulate the microgrid circuit and validate the mathematical model. By inputting the circuit parameters and component characteristics into the software, a detailed representation of the circuit's electrical behavior was obtained. This approach offered a practical perspective, allowing for the observation of real-time responses and the analysis of system dynamics. By combining both approaches, a comprehensive understanding of the microgrid circuit was achieved, encompassing both theoretical and practical aspects.

3.3.1 Mathematical Modeling of the System

The multiterminal DC microgrid system has been mathematically modelled using a state-space approach, combining the individual models of the components, and including fault parameters. This approach allows for a comprehensive analysis of complex systems by considering the interdependencies between components and the influence of faults. State space modeling is a mathematical framework used to describe the behavior of dynamic systems. It involves two equations: the state equation and the observation equation.

- State equation:

$$x(t + 1) = Ax(t) + Bu(t) \quad (3)$$

- Observation equation:

$$y = Cx(t) + Du(t) \quad (4)$$

In these equations, $x(t)$ represents the state vector at time t , $u(t)$ represents the input vector at time t , and $y(t)$ represents the observation vector at time t . The matrices $A, B, C,$ and D capture the dynamics and relationships between the state, input, and observation variables. The component-wise derivation of the differential equation model is provided in the introduction section 1.2.2. Following is the sub-system dynamic state space system model of the DC microgrid.

The system matrix A is given as following.

$$A = [A_{11} \ A_{12} \ A_{13} \ A_{14} \ A_{15} \ A_{16}]^T \quad (5)$$

Where A_{11} is the system matrix of the Boost Converter, written as:

$$A_{11} = \begin{bmatrix} -\frac{R_{bo}}{L_{bo}} & -\frac{1-D_{bo}}{L_{bo}} & 0_{1 \times 6} & 0 & 0_{1 \times 3} & 0 & 0 \\ \frac{1-D_{bo}}{C_1} & -\frac{1}{R_{1fb}C_1} & 0_{1 \times 6} & -\frac{1}{C_1} & 0_{1 \times 3} & -\frac{1}{C_1} & 0 \end{bmatrix} \quad (6)$$

A_{12} is the system matrix of Buck Converter 1, written as:

$$A_{12} = \begin{bmatrix} 0_{1 \times 2} & -\frac{R_{bu1}}{L_{bu1}} & -\frac{1}{L_{bu1}} & \frac{D_{bu1}}{L_{bu1}} & 0_{1 \times 4} & 0 & 0 & 0_{1 \times 3} \\ 0_{1 \times 2} & \frac{1}{C_{bu1}} & -\frac{1}{R_L C_{bu1}} & 0 & 0_{1 \times 4} & 0 & 0 & 0_{1 \times 3} \\ 0_{1 \times 2} & -\frac{D_{bu1}}{C_2} & 0 & -\frac{1}{R_{2fb}C_2} & 0_{1 \times 4} & \frac{1}{C_2} & -\frac{1}{C_2} & 0_{1 \times 3} \end{bmatrix} \quad (7)$$

A_{13} is the system matrix of Buck Converter 2, written as:

$$A_{13} = \begin{bmatrix} 0_{1 \times 5} & -\frac{R_{bu2}}{L_{bu2}} & -\frac{1}{L_{bu2}} & \frac{D_{bu2}}{L_{bu2}} & 0_{1 \times 3} & 0 & 0 & 0 \\ 0_{1 \times 5} & \frac{1}{C_{bu2}} & 0 & 0 & 0_{1 \times 3} & 0 & 0 & 0 \\ 0_{1 \times 5} & -\frac{D_{bu2}}{C_3} & 0 & -\frac{1}{R_{3fb}C_3} & 0_{1 \times 3} & \frac{1}{C_3} & 0 & \frac{1}{C_3} \end{bmatrix} \quad (8)$$

A_{14} is the system matrix of Cable 1, written as:

$$A_{14} = \begin{bmatrix} 0 & \frac{p}{L_{1a}} & 0_{1 \times 2} & 0 & 0_{1 \times 3} & -\frac{R_{1a} + pR_{1f}}{L_{1a}} & \frac{pR_{1f}}{L_{1a}} & 0_{1 \times 4} \\ 0 & 0 & 0_{1 \times 2} & -\frac{p}{L_{1b}} & 0_{1 \times 3} & \frac{pR_{1f}}{L_{1b}} & -\frac{R_{1b} + pR_{1f}}{L_{1b}} & 0_{1 \times 4} \end{bmatrix} \quad (9)$$

A_{15} is the system matrix of Cable 2, written as:

$$A_{15} = \begin{bmatrix} 0_{1 \times 4} & \frac{p}{L_{2a}} & 0_{1 \times 2} & 0 & 0_{1 \times 2} & -\frac{R_{2a} + pR_{2f}}{L_{2a}} & \frac{pR_{2f}}{L_{2a}} & 0_{1 \times 2} \\ 0_{1 \times 4} & 0 & 0_{1 \times 2} & -\frac{p}{L_{2b}} & 0_{1 \times 2} & \frac{pR_{2f}}{L_{2b}} & -\frac{R_{2b} + pR_{2f}}{L_{2b}} & 0_{1 \times 2} \end{bmatrix} \quad (10)$$

A_{16} is the system matrix of Cable 3, written as:

$$A_{16} = \begin{bmatrix} 0 & \frac{p}{L_{3a}} & 0_{1 \times 5} & 0 & 0_{1 \times 4} & -\frac{R_{3a} + pR_{1f}}{L_{1a}} & \frac{pR_{3f}}{L_{1a}} \\ 0 & 0 & 0_{1 \times 5} & -\frac{p}{L_{3b}} & 0_{1 \times 4} & \frac{pR_{3f}}{L_{3b}} & -\frac{R_{3b} + pR_{3f}}{L_{3b}} \end{bmatrix} \quad (11)$$

Collectively, the whole system state-space model (A, B, C, D, x, y and u

matrices) is as follows [18]:

$$A = \begin{bmatrix} \frac{R_{bo}}{L_{bo}} & \frac{1-D_{bo}}{L_{bo}} & 0 & 0 & 0 & 0 & 0 & 0 & 0 & 0 & 0 & 0 & 0 & 0 \\ \frac{1-D_{bo}}{L_{bo}} & -\frac{1}{L_{bo}} & 0 & 0 & 0 & 0 & 0 & 0 & -\frac{1}{C_1} & 0 & 0 & 0 & 0 & -\frac{1}{C_1} \\ \frac{1}{C_1} & \frac{R_{fb}C_1}{R_{fb}C_1} & 0 & 0 & 0 & 0 & 0 & 0 & 0 & 0 & 0 & 0 & 0 & 0 \\ 0 & 0 & \frac{-R_{bu1}}{L_{bu1}} & \frac{-1}{L_{bu1}} & \frac{D_{bu1}}{L_{bu1}} & 0 & 0 & 0 & 0 & 0 & 0 & 0 & 0 & 0 \\ 0 & 0 & \frac{1}{L_{bu1}} & \frac{-1}{L_{bu1}} & \frac{1}{L_{bu1}} & 0 & 0 & 0 & 0 & 0 & 0 & 0 & 0 & 0 \\ 0 & 0 & \frac{1}{C_{bu1}} & \frac{R_{fb}C_{bu1}}{R_{fb}C_{bu1}} & 0 & 0 & 0 & 0 & 0 & 0 & 0 & 0 & 0 & 0 \\ 0 & 0 & \frac{-D_{bu1}}{C_2} & 0 & \frac{-1}{R_{fb}C_2} & 0 & 0 & 0 & 0 & \frac{1}{C_2} & -\frac{1}{C_2} & 0 & 0 & 0 \\ 0 & 0 & 0 & 0 & 0 & \frac{-R_{bu2}}{L_{bu2}} & \frac{-1}{L_{bu2}} & \frac{D_{bu2}}{L_{bu2}} & 0 & 0 & 0 & 0 & 0 & 0 \\ 0 & 0 & 0 & 0 & 0 & \frac{1}{L_{bu2}} & \frac{1}{L_{bu2}} & \frac{1}{L_{bu2}} & 0 & 0 & 0 & 0 & 0 & 0 \\ 0 & 0 & 0 & 0 & 0 & \frac{1}{C_{bu2}} & 0 & 0 & 0 & 0 & 0 & 0 & 0 & 0 \\ 0 & 0 & 0 & 0 & 0 & \frac{-D_{bu2}}{C_2} & 0 & \frac{-1}{R_{fb}C_2} & 0 & 0 & 0 & \frac{1}{C_1} & 0 & \frac{1}{C_1} \\ 0 & \frac{p}{L_{1a}} & 0 & 0 & 0 & 0 & 0 & 0 & -\frac{R_{1a} + pR_{1f}}{L_{1a}} & \frac{pR_{1f}}{L_{1a}} & 0 & 0 & 0 & 0 \\ 0 & 0 & 0 & 0 & 0 & -\frac{p}{L_{1b}} & 0 & 0 & \frac{pR_{1f}}{L_{1b}} & -\frac{R_{1b} + pR_{1f}}{L_{1b}} & 0 & 0 & 0 & 0 \\ 0 & 0 & 0 & 0 & 0 & \frac{p}{L_{2a}} & 0 & 0 & -\frac{R_{2a} + pR_{2f}}{L_{2a}} & \frac{pR_{2f}}{L_{2a}} & 0 & 0 & 0 & 0 \\ 0 & 0 & 0 & 0 & 0 & -\frac{p}{L_{2b}} & 0 & 0 & \frac{pR_{2f}}{L_{2b}} & -\frac{R_{2b} + pR_{2f}}{L_{2b}} & 0 & 0 & 0 & 0 \\ 0 & \frac{p}{L_{3a}} & 0 & 0 & 0 & 0 & 0 & 0 & 0 & 0 & 0 & -\frac{R_{3a} + pR_{3f}}{L_{3a}} & \frac{pR_{3f}}{L_{3a}} & 0 \\ 0 & 0 & 0 & 0 & 0 & 0 & 0 & 0 & 0 & 0 & 0 & \frac{pR_{3f}}{L_{3b}} & -\frac{R_{3b} + pR_{3f}}{L_{3b}} & 0 \end{bmatrix} \quad (12)$$

$$B = \begin{bmatrix} \frac{1}{L_{bo}} & 0 & 0 & 0 & 0 & 0 & 0 & 0 & 0 & 0 & 0 & 0 & 0 & 0 \\ 0 & 0 & 0 & 0 & 0 & 0 & -\frac{1}{C_{bu2}} & 0 & 0 & 0 & 0 & 0 & 0 & 0 \end{bmatrix}^T \quad (13)$$

$$C = I_{14 \times 14} \quad (14)$$

$$D = [0_{14 \times 2}] \quad (15)$$

$$x = [i_{Lbo} \quad V_{Cbo} \quad i_{1a} \quad i_{1b} \quad i_{2a} \quad i_{2b} \quad i_{3a} \quad i_{3b} \quad i_{inbu1} \quad V_{inbu1} \quad V_{outbu1} \quad i_{inbu2} \quad V_{inbu2} \quad V_{outbu2}] \quad (16)$$

$$y = C \times x \quad (17)$$

$$u = [v_{in} \quad i_L]^T \quad (18)$$

Where the states under observation are current and voltage through boost converter i_{Lbo} and V_{Cbo} , DC cables input and output current $i_{1b}, i_{1b}, i_{2a}, i_{2b}, i_{3a}$ and i_{3b} and current and voltages through the buck converters $i_{inbu1}, V_{inbu1}, V_{outbu1}, i_{inbu2}, V_{inbu2}$ and V_{outbu2} . The inputs to the model are buck source voltage and buck 2 load current V_{in} and i_L .

3.3.2 Implementation of the DC Microgrid System (Physical Modeling of the DCMG)

The circuit modeling aspect of the study involved the utilization of SIMULINK, a specialized software tool within the MATLAB environment, to simulate the behavior and performance of the microgrid circuit. This powerful software provided a comprehensive platform for modeling and analyzing complex electrical systems. The microgrid circuit was first modeled on an individual component basis, with each component represented by its respective physical circuit model. These individual component models were then integrated into a comprehensive circuit model within the SIMULINK environment. This allowed for the simulation of normal operating conditions as well as the modeling of fault disturbances such as short circuits and voltage sags. By leveraging the capabilities of SIMULINK, the interactions, coordination, and dynamics of the various components were accurately captured, facilitating a comprehensive analysis of the microgrid circuit's behavior. The use of SIMULINK in this research provided a robust and efficient platform for performance evaluation, identification of potential issues, and assessment of control strategies and protective measures within the microgrid system. Following is the whole physical circuit model of the DCMG shown in Figure 9.

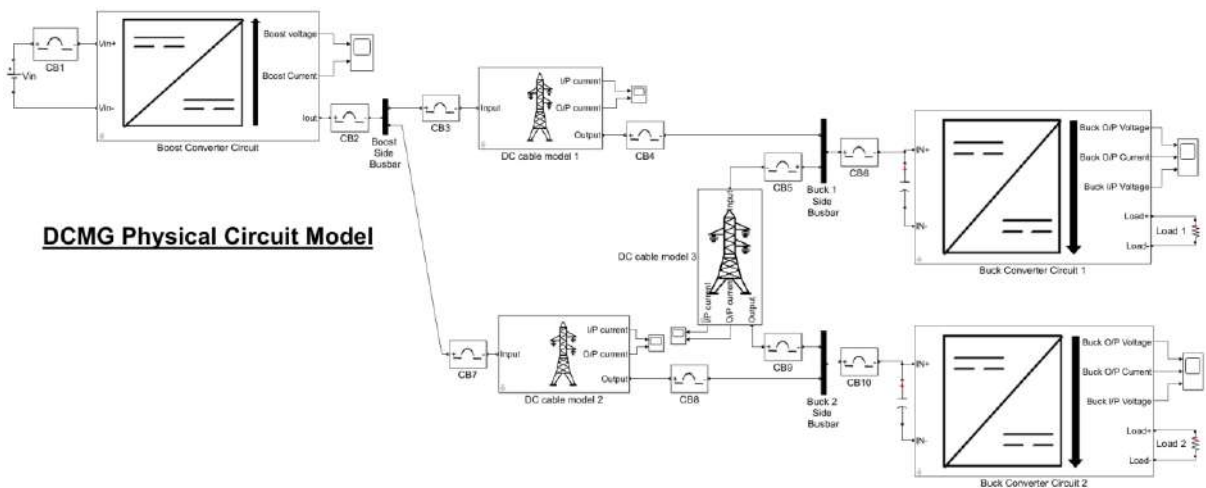


Figure 9: Physical circuit model of the DCMG

The following are the subsystem physical circuit models of the DCMG:

- 1) The boost circuit subsystem model comprises several key electronic components that facilitate its operation. These components include an inductor, a diode, a

capacitor, and a power switch. An additional switch is also connected to simulate fault behavior inside the boost circuit. A feedback hysteresis control strategy is implemented to regulate the output voltage. This control strategy dynamically adjusts the duty cycle of the switching elements based on the difference between the desired output voltage and the actual measured voltage. By employing hysteresis, a range or band around the desired output voltage is defined, within which the switching elements maintain their current state. Once the measured voltage crosses the upper or lower threshold of the hysteresis band, the control strategy triggers a change in the duty cycle to restore the voltage within the desired range. Component physical model of the Boost circuit is depicted below. Physical circuit model of the boost converter is shown in Figure 10.

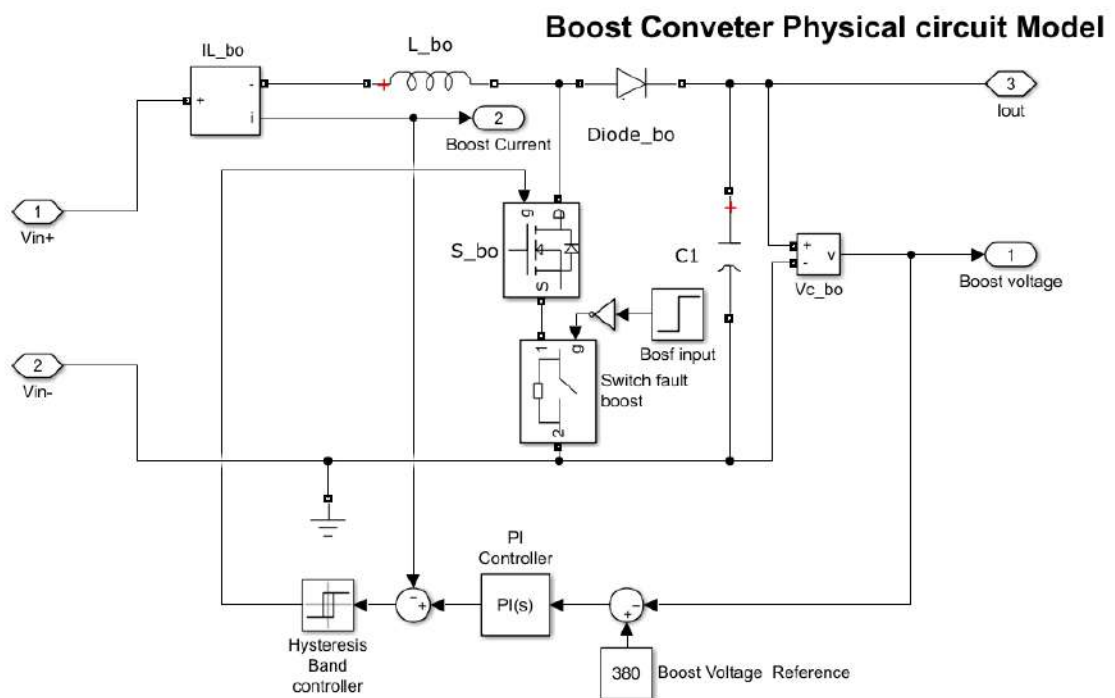


Figure 10: Physical circuit model of the Boost Converter Circuit

- 2) Similarly, the other main component of the DCMG is the buck converter. The buck circuit subsystem model consists of several essential electronic components that enable its functionality. These components include an inductor, a diode, a capacitor, and a power switch. The inductor stores energy during the on-time of the power switch and releases it during the off-time, resulting in a reduced output voltage. The diode prevents reverse current flow, ensuring proper current direction within the circuit. The capacitor aids in smoothing voltage variations, providing a more stable

output voltage. The power switch controls the flow of current through the circuit. To regulate the output voltage, a feedback hysteresis control strategy is implemented. This control strategy adjusts the duty cycle of the power switch based on the measured output voltage compared to the desired voltage. By employing hysteresis, a range or band around the desired output voltage is defined, within which the switching elements maintain their current state. This feedback hysteresis control strategy helps maintain a stable and regulated output voltage for the buck circuit subsystem. The component physical model of the Buck circuit is depicted below. The physical circuit model of the buck converter is shown in Figure 11.

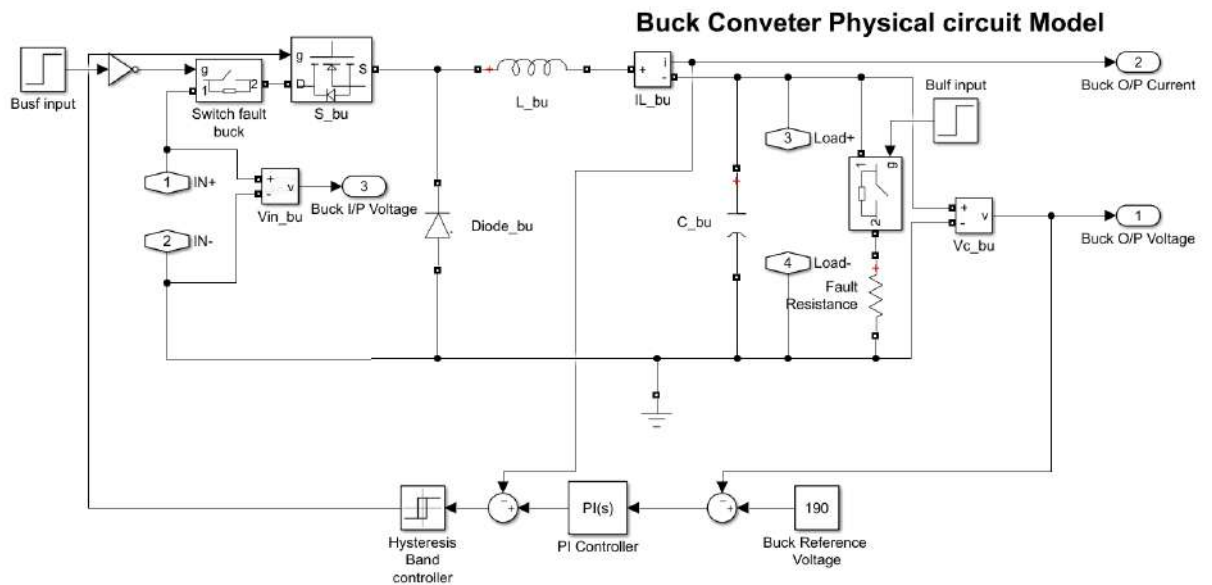


Figure 11: Physical circuit model of the Buck Converter Circuit

- 3) The DC cable component of the DCMG is simply modeled with series inductance and resistance; for the introduction of short-circuit fault in DC transmission cable, half of the total inductance and resistance is modeled on the input side and half on the output side. For this research, the line capacitance is ignored due to the shorter length of the cable. Component physical model of the DC Cable is depicted below. The physical circuit model of the DC cable is shown in Figure 12.

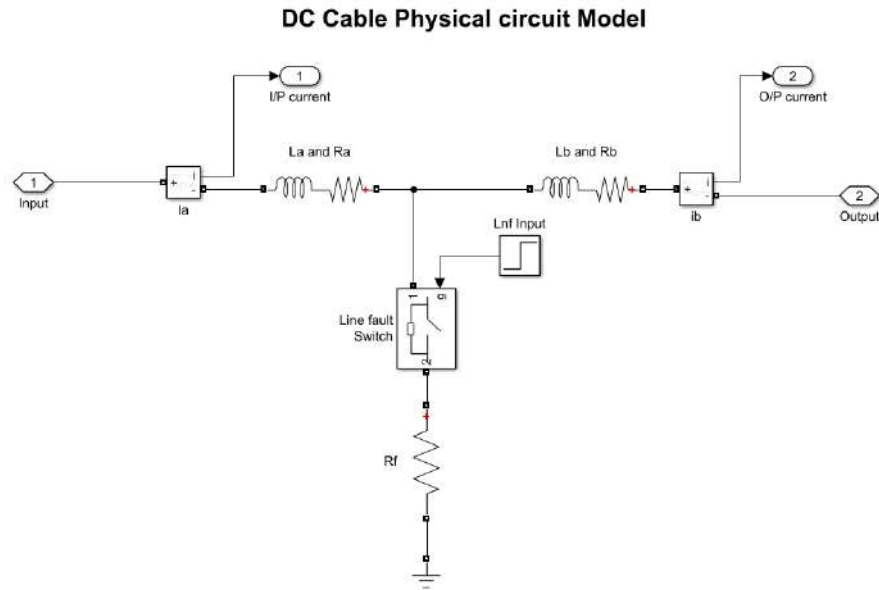


Figure 12: Physical circuit model of the DC Cable

- 4) The busbar section of the microgrid is simply modeled with a common node and incoming and outgoing lines. Fault disturbance is also included in this model. Component physical model of the Busbar is depicted below. A physical circuit model of the DC busbar is shown in Figure 13.

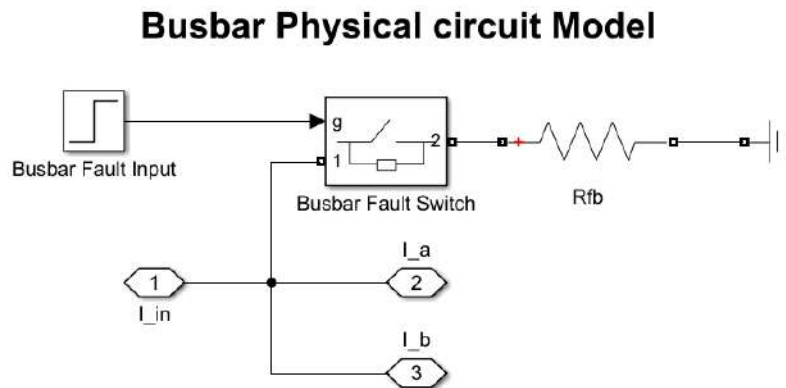


Figure 13: Physical circuit model of the Busbar

3.4 Parameters of DC Microgrid Model

Table 1 provides key parameters of the subsystem of the DC microgrid, including rated voltage, rated current, resistance, inductance, capacitance, and switching frequency. These parameters are crucial for understanding the operational characteristics, efficiency, and stability of the microgrid system.

S. No	Component	Parameter	Value
1	Boost	Rated value of v_{in}	190V
		Rated value of v_{C-bo}	380V
		Resistance R_{bo}	0.1 Ω
		Inductance L_{bo}	5mH
		DC-link Capacitance C_1	35mF
		Switching Frequency	50kHz
2	Buck 1 & 2	Rated value of v_{in-bu1} & v_{in-bu2}	380V
		Rated value of v_{C-bu1} & v_{C-bu2}	190V
		Resistances R_{bu1} & R_{bu2}	0.1 Ω
		Inductances L_{bu1} & L_{bu2}	50mH
		DC-link Capacitances C_2 & C_3	25uF
		Load Resistance R_L	10 Ω
		Switching Frequency	50kHz
3	Cable 1, 2 & 3	Line Resistance per unit length	8 Ω /km
		Line Inductance per unit length	0.45mH/km
		Line Capacitance per unit length	0.1uF/km
		Length of the Cable	0.5km

Table 1: DCMG component-wise parameters.

3.5 Fault Modeling

Fault modeling is a crucial aspect of analyzing complex systems. In state space modeling, faults are integrated as additional variables or inputs in the system's state equations. This incorporation allows for the simulation and analysis of different fault scenarios and their impact on system performance. Fault vectors define the characteristics and magnitudes of specific faults, enabling the quantification and study of fault effects. The state-space representation of a discrete-time linear time-invariant system is typically expressed in a standard form using equations 3 and 4.

$$\begin{aligned}x(t + 1) &= Ax(t) + Bu(t) \\y(i) &= Cx(t) + Du(t)\end{aligned}\tag{19}$$

In the given equation, the system state, input, and output variables are represented by $x(i)$, $u(i)$, and $y(i)$ respectively. The parameters A, B, C , and D are matrices that define the characteristics and relationships of the system. In real-world scenarios, processes are often affected by disturbances that introduce unexpected noise. To account for component faults, such as malfunctions within the sub-system, which can result in variations in the model parameters, Equation (19) can be modified to incorporate both faults and disturbances in the system representation [18].

$$\begin{aligned}x(t + 1) &= Ax(t) + Bu(t) + B_d d(t) + B_f f(t) \\y(t) &= Cx(t) + Du(t) + D_d d(t) + D_f f(t)\end{aligned}\tag{20}$$

In the extended representation, B_d and D_d are constant matrices, representing the impact of disturbances, while $d(t)$ is an unknown input vector that captures disturbances. Similarly, the fault vector $f(t)$ is time-dependent vector that represents the presence of faults within the system. The matrices, B_f and D_f are constant matrices that describe the effects of the fault on the system. The effect of disturbances is not considered in this research, so only the derivation of fault vectors and fault matrices for different types of faults is done. The following section provides a comprehensive description and derivation of various types of faults that can occur in the DC microgrid. It outlines the characteristics, causes, and implications of each fault, presenting a detailed analysis of their effects on the microgrid system.

3.5.1 Failure of Switch in Power Converter

In power converters, the occurrence of short circuits in the switch can lead to the blowing of protective fuses, causing open-circuit failures [18]. In this analysis, the specific focus is on the open-circuit failure that affects the switch. When an open-circuit failure happens, the switch remains permanently in the OFF state, resulting in a duty cycle of zero. Consequently, the impact of the switch failure can be represented by the deviation in the duty cycle, denoted as ΔD . This deviation is defined as the difference between the actual duty cycle and the expected duty cycle in the absence of the failure [18]

$$\Delta D = D' - D \quad (21)$$

In this context, D represents the duty cycle before the occurrence of the switch failure, while D' represents the equivalent duty cycle after the fault. In the case of switch failures resulting in open-circuit conditions, the equivalent duty cycle (ΔD) becomes zero.

3.5.1.1 Switch Failure in Boost Converter

The state-space model of boost converter before the occurrence of the fault is given as [12]:

$$\begin{aligned} \frac{d}{dt} I_{Lbo} &= -\frac{1 - D_{bo}}{L_{bo}} V_{Cbo} + \frac{1}{L} V_{INbo} \\ \frac{d}{dt} V_{Cbo} &= \frac{1 - D_{bo}}{C_{bo}} I_{Lbo} - \frac{1}{R_L C_{bo}} V_{Cbo} \end{aligned} \quad (22)$$

After the switch failure, the systems state-space model becomes:

$$\begin{aligned} \frac{d}{dt} I_{Lbo} &= -\frac{1 - (D_{bo} + \Delta D_{bo})}{L_{bo}} V_{Cbo} + \frac{1}{L} V_{INbo} \\ \frac{d}{dt} V_{Cbo} &= \frac{1 - (D_{bo} + \Delta D_{bo})}{C_{bo}} I_{Lbo} - \frac{1}{R_L C_{bo}} V_{Cbo} \end{aligned} \quad (23)$$

Which can be expressed as:

$$\begin{aligned} \frac{d}{dt} I_{Lbo} &= -\frac{1 - D_{bo}}{L_{bo}} V_{Cbo} + \frac{1}{L_{bo}} \Delta D_{bo} V_{Cbo} + \frac{1}{L} V_{INbo} \\ \frac{d}{dt} V_{Cbo} &= \frac{1 - D_{bo}}{C_1} I_{Lbo} - \frac{1}{C_1} \Delta D_{bo} I_{Lbo} - \frac{1}{R_L C_1} V_{Cbo} \end{aligned} \quad (24)$$

Where $\frac{1}{L_{bo}}$ and $\frac{1}{C_1}$ are part of fault matrix and $\Delta D_{bo}V_{Cbo}$ and $\Delta D_{bo}I_{Lbo}$ are the fault vectors.

3.5.1.2 Switch Failure in Buck Converter

The dynamic model of buck converter before the occurrence of the fault is given as [18]:

$$\begin{aligned}\frac{d}{dt}I_{Lbu} &= -\frac{1}{L_{bu}}V_{Cbo} + \frac{D_{bu}}{L_{bu}}V_{INbu} \\ \frac{d}{dt}V_{Cbu} &= \frac{1}{C_{bu}}I_{Lbu} - \frac{1}{R_L C_{bu}}V_{Cbu}\end{aligned}\quad (25)$$

After the switch failure, the systems state-space model becomes:

$$\begin{aligned}\frac{d}{dt}I_{Lbu} &= -\frac{1}{L_{bu}}V_{Cbo} + \frac{(D_{bu} + \Delta D_{bu})}{L_{bu}}V_{INbu} \\ \frac{d}{dt}V_{Cbu} &= \frac{1}{C_{bu}}I_{Lbu} - \frac{1}{R_L C_{bu}}V_{Cbu}\end{aligned}\quad (26)$$

Which can be expressed as:

$$\begin{aligned}\frac{d}{dt}I_{Lbu} &= -\frac{1}{L_{bu}}V_{Cbo} + \frac{D_{bu}}{L_{bu}}V_{INbu} + \frac{1}{L_{bu}}\Delta D_{bu}V_{INbu} \\ \frac{d}{dt}V_{Cbu} &= \frac{1}{C_{bu}}I_{Lbu} - \frac{1}{R_L C_{bu}}V_{Cbu}\end{aligned}\quad (27)$$

Where $\frac{1}{L_{bu}}$ is the part of fault matrix and $\Delta D_{bu}V_{INbu}$ is the fault vector.

3.5.2 DC transmission Cable Short-Circuit Fault

DC microgrids typically have a transmission range that extends from a few hundred meters to several kilometers. Given the relatively short distances involved, the capacitance of the transmission lines can be considered negligible in comparison to the capacitance of the DC-link, as outlined in Table 1. Consequently, the models for the DC cables can be simplified as RL series branches. Figure 14 illustrates the DC cable model incorporating fault resistance.

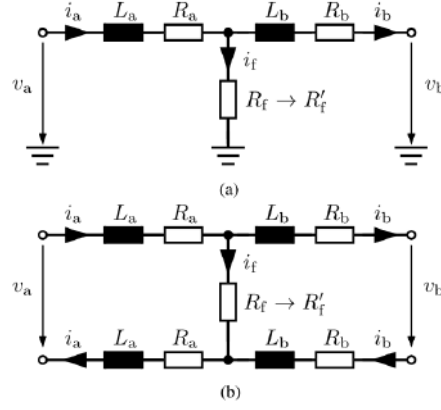


Figure 14: Equivalent model of a DC cable incorporating a short-circuit faults.

(a) PG fault. (b) PP fault.

Mathematically the system dynamic equation under short-circuit fault is as follows [18]:

$$\begin{aligned} \frac{d}{dt} I_a &= -\frac{R_a + pR_f}{L_a} I_a + \frac{pR_f}{L_a} I_b + \frac{p}{L_a} V_a \\ \frac{d}{dt} I_b &= \frac{pR_f}{L_b} I_a - \frac{R_b + pR_f}{L_b} I_b + \frac{p}{L_b} V_b \end{aligned} \quad (28)$$

For PG faults, the parameter p is assigned a value of 1. On the other hand, for PP faults, the parameter p takes a value of 0.5. The derived equivalent models of the DC line for PG and PP short-circuit faults are depicted above. These models include a grounding branch with resistance R_f , dividing the DC line into $R_a - L_a$ and $R_b - L_b$ branches. Insulation breakdown resulting from the short-circuit fault in the DC cable is represented by a sudden decrease in resistance, denoted as R'_f (where R'_f is considerably smaller than R_f). In the case of PG faults, the DC line is connected to the ground via the short-circuit branch. Similarly, for PP faults, the short-circuit branch establishes a connection between both poles of the DC line. The state-space model of DC Cable before the occurrence of the fault is given from equation 29 as:

$$\begin{aligned} \frac{d}{dt} I_a &= -\frac{R_a + pR_f}{L_a} I_a + \frac{pR_f}{L_a} I_b + \frac{p}{L_a} V_a \\ \frac{d}{dt} I_b &= \frac{pR_f}{L_b} I_a - \frac{R_b + pR_f}{L_b} I_b + \frac{p}{L_b} V_b \end{aligned} \quad (29)$$

Rewriting the equation, we get:

$$\begin{aligned}\frac{d}{dt}I_a &= -\frac{R_a}{L_a}I_a - \frac{pR_f}{L_a}I_a + \frac{pR_f}{L_a}I_b + \frac{p}{L_a}V_a \\ \frac{d}{dt}I_b &= \frac{pR_f}{L_b}I_a - \frac{R_b}{L_b}I_b - \frac{pR_f}{L_b}I_b + \frac{p}{L_b}V_b\end{aligned}\quad (30)$$

When the line short-circuit fault occurs, the systems state-space model becomes:

$$\begin{aligned}\frac{d}{dt}I_a &= -\frac{R_a}{L_a}I_a - \frac{pR'_f}{L_a}I_a + \frac{pR'_f}{L_a}I_b + \frac{p}{L_a}V_a \\ \frac{d}{dt}I_b &= \frac{pR'_f}{L_b}I_a - \frac{R_b}{L_b}I_b - \frac{pR'_f}{L_b}I_b + \frac{p}{L_b}V_b\end{aligned}\quad (31)$$

Which can be expressed as

$$\begin{aligned}\frac{d}{dt}I_a &= -\frac{R_a}{L_a}I_a - \frac{pR'_f}{L_a}(I_a - I_b) + \frac{p}{L_a}V_a \\ \frac{d}{dt}I_b &= -\frac{R_b}{L_b}I_b + \frac{pR'_f}{L_b}(I_a - I_b) + \frac{p}{L_b}V_b\end{aligned}\quad (32)$$

OR

$$\begin{aligned}\frac{d}{dt}I_a &= -\frac{R_a}{L_a}I_a - \frac{pR_f}{L_a}I_f - \frac{pR'_f}{L_a}(\Delta I_f) + \frac{p}{L_a}V_a \\ \frac{d}{dt}I_b &= -\frac{R_b}{L_b}I_b + \frac{pR_f}{L_b}I_f + \frac{pR'_f}{L_b}(\Delta I_f) + \frac{p}{L_b}V_b\end{aligned}\quad (33)$$

Where $-\frac{pR'_f}{L_a}$ and $\frac{pR'_f}{L_b}$ are part of the fault matrix and ΔI_f is the fault vector.

3.5.3 Busbar Short-Circuit Fault

Figure 3-10 represents the equivalent model of a DC busbar, comprising entering and leaving lines from common node as well as a short-circuit branch. When a short-circuit fault occurs within this busbar, the fault can be represented by an abrupt decrease in the fault resistance, transitioning from R_f to R'_f (where R'_f is substantially smaller than R_f).

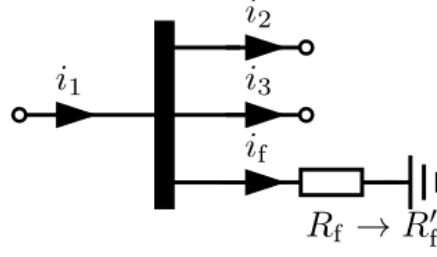


Figure 15: Equivalent model of a DC busbar incorporating a short-circuit fault

3.5.3.1 Short-Circuit Fault near Boost side Busbar

The state-space model of boost converter before the occurrence of the fault is given as [18]:

$$\begin{aligned} \frac{d}{dt} I_{Lbo} &= -\frac{1-D_{bo}}{L_{bo}} V_{Cbo} + \frac{1}{L} V_{INbo} \\ \frac{d}{dt} V_{Cbo} &= \frac{1-D_{bo}}{C_1} I_{Lbo} - \frac{1}{R_L C_1} V_{Cbo} - \frac{1}{R_{fb} C_1} V_{Cbo} \end{aligned} \quad (34)$$

After the short-circuit fault in the dc cable, the system state-space model becomes:

$$\begin{aligned} \frac{d}{dt} I_{Lbo} &= -\frac{1-D_{bo}}{L_{bo}} V_{Cbo} + \frac{1}{L} V_{INbo} \\ \frac{d}{dt} V_{Cbo} &= \frac{1-D_{bo}}{C_1} I_{Lbo} - \frac{1}{R_L C_1} V_{Cbo} - \frac{1}{(R_{fb} + \Delta R_{fb}) C_1} V_{Cbo} \end{aligned} \quad (35)$$

OR

$$\begin{aligned} \frac{d}{dt} I_{Lbo} &= -\frac{1-D_{bo}}{L_{bo}} V_{Cbo} + \frac{1}{L} V_{INbo} \\ \frac{d}{dt} V_{Cbo} &= \frac{1-D_{bo}}{C_1} I_{Lbo} - \frac{1}{R_L C_1} V_{Cbo} - \frac{1}{C_1} i_{fb} \end{aligned} \quad (36)$$

Which can be expressed as:

$$\begin{aligned} \frac{d}{dt} I_{Lbo} &= -\frac{1-D_{bo}}{L_{bo}} V_{Cbo} + \frac{1}{L} V_{INbo} \\ \frac{d}{dt} V_{Cbo} &= \frac{1-D_{bo}}{C_1} I_{Lbo} - \frac{1}{R_L C_1} V_{Cbo} - \frac{1}{R_{fb} C_1} V_{Cbo} - \frac{1}{C_1} \left(-\frac{\Delta R_{fb}}{R_{fb} + \Delta R_{fb}} \right) \frac{V_C}{R} \end{aligned} \quad (37)$$

OR

$$\begin{aligned}\frac{d}{dt}I_{Lbo} &= -\frac{1-D_{bo}}{L_{bo}}V_{Cbo} + \frac{1}{L}V_{INbo} \\ \frac{d}{dt}V_{Cbo} &= \frac{1-D_{bo}}{C_1}I_{Lbo} - \frac{1}{R_L C_1}V_{Cbo} - \frac{1}{R_{fb} C_1}V_{Cbo} - \frac{1}{C_1}\Delta i_{fb}\end{aligned}\quad (38)$$

Where $\frac{1}{C_1}$ is part of the fault matrix and Δi_{fb} is the fault vector.

3.5.4 Load Component Fault

When modeling direct current (DC) systems, the load component, which has predefined characteristics, can be depicted by its resistance. This resistance can be influenced by faults that arise within the load component. An instance of such a fault is the occurrence of short-circuits within the device, which leads to a decrease in the load resistance. Exploiting this characteristic, a fault in the load with a known equivalent resistance can be represented by the deviation of the load resistance from its initial value. The state-space model of buck converter before the occurrence of the fault is given as [18]:

$$\begin{aligned}\frac{d}{dt}I_{Lbu} &= -\frac{1}{L_{bu}}V_{Cbu} + \frac{D_{bu}}{L_{bu}}V_{INbu} \\ \frac{d}{dt}V_{Cbu} &= \frac{1}{C_{bu}}I_{Lbu} - \frac{1}{R_L C_{bu}}V_{Cbu} - \frac{1}{R_{LF} C_{bu}}V_{Cbu}\end{aligned}\quad (39)$$

After the short-circuit fault in the load component of the buck converter, the system's state-space model becomes:

$$\begin{aligned}\frac{d}{dt}I_{Lbu} &= -\frac{1}{L_{bu}}V_{Cbu} + \frac{D_{bu}}{L_{bu}}V_{INbu} \\ \frac{d}{dt}V_{Cbu} &= \frac{1}{C_{bu}}I_{Lbu} - \frac{1}{R_L C_{bu}}V_{Cbu} - \frac{1}{(R_{LF} + \Delta R_{LF})C_{bu}}V_{Cbu}\end{aligned}\quad (40)$$

OR

$$\begin{aligned}\frac{d}{dt}I_{Lbu} &= -\frac{1}{L_{bu}}V_{Cbu} + \frac{D_{bu}}{L_{bu}}V_{INbu} \\ \frac{d}{dt}V_{Cbu} &= \frac{1}{C_{bu}}I_{Lbu} - \frac{1}{R_L C_{bu}}V_{Cbu} - \frac{1}{C_{bu}}i_{RL}\end{aligned}\quad (41)$$

Which can be expressed as:

$$\begin{aligned} \frac{d}{dt} I_{Lbu} &= -\frac{1}{L_{bu}} V_{Cbo} + \frac{D_{bu}}{L_{bu}} V_{INbu} \\ \frac{d}{dt} V_{Cbu} &= \frac{1}{C_{bu}} I_{Lbu} - \frac{1}{R_L C_{bu}} V_{Cbu} - \frac{\mathbf{1}}{C_{bu}} \left(-\frac{\Delta \mathbf{R}_{LF}}{R_{LF} + \Delta \mathbf{R}_{LF}} \right) \frac{V_{Cbu}}{R_{LF}} \end{aligned} \quad (42)$$

OR

$$\begin{aligned} \frac{d}{dt} I_{Lbu} &= -\frac{1}{L_{bu}} V_{Cbo} + \frac{D_{bu}}{L_{bu}} V_{INbu} \\ \frac{d}{dt} V_{Cbu} &= \frac{1}{C_{bu}} I_{Lbu} - \frac{1}{R_L C_{bu}} V_{Cbu} - \frac{\mathbf{1}}{C_{bu}} \Delta \mathbf{i}_{RL} \end{aligned} \quad (43)$$

Where $\frac{1}{C_{bu}}$ is part of the fault matrix and $\Delta \mathbf{i}_{RL}$ is the fault vector.

3.5.5 Modeling of the Component Faults of the DCMG

Table 2 shows all the modeled component faults of the DCMG under the case study.

Fault Number	Component	Fault type	Fault Matrix B_f	Fault Vector f
f_1	Boost	Switch Failure	$\begin{bmatrix} \frac{1}{L_{bo}} & 0_{1 \times 13} \\ 0 & -\frac{1}{C_1} & 0_{1 \times 12} \end{bmatrix}^T$	$\begin{bmatrix} \Delta D_{bo} V_{Cbo} \\ \Delta D_{bo} I_{Lbo} \end{bmatrix}$
f_2	Buck 1	Switch Failure	$\begin{bmatrix} 0_{1 \times 2} & -\frac{1}{L_{bu1}} & 0_{1 \times 11} \\ 0_{1 \times 4} & -\frac{1}{C_2} & 0_{1 \times 9} \end{bmatrix}^T$	$\begin{bmatrix} \Delta D_{bu1} V_{INbu1} \\ \Delta D_{bu1} I_{Lbu1} \end{bmatrix}$
f_3	Buck 2	Switch Failure	$\begin{bmatrix} 0_{1 \times 5} & -\frac{1}{L_{bu2}} & 0_{1 \times 8} \\ 0_{1 \times 7} & -\frac{1}{C_3} & 0_{1 \times 6} \end{bmatrix}^T$	$\begin{bmatrix} \Delta D_{bu2} V_{INbu2} \\ \Delta D_{bu2} I_{Lbu2} \end{bmatrix}$
f_4	Cable 1	Short-Circuit Fault	$\begin{bmatrix} 0_{1 \times 8} & -\frac{pR'_{1f}}{L_{1a}} & \frac{pR'_{1f}}{L_{1b}} & 0_{1 \times 4} \end{bmatrix}^T$	Δi_{1f}
f_5	Cable 2	Short-Circuit Fault	$\begin{bmatrix} 0_{1 \times 10} & -\frac{pR'_{2f}}{L_{2a}} & \frac{pR'_{2f}}{L_{2b}} & 0_{1 \times 2} \end{bmatrix}^T$	Δi_{2f}
f_6	Cable 3	Short-Circuit Fault	$\begin{bmatrix} 0_{1 \times 12} & -\frac{pR'_{3f}}{L_{3a}} & \frac{pR'_{3f}}{L_{3b}} \end{bmatrix}^T$	Δi_{3f}
f_7	Busbar 1	Short-Circuit Fault	$\begin{bmatrix} 0 & -\frac{1}{C_1} & 0_{1 \times 12} \end{bmatrix}^T$	Δi_{1fb}
f_8	Busbar 2	Short-Circuit Fault	$\begin{bmatrix} 0_{1 \times 4} & -\frac{1}{C_2} & 0_{1 \times 9} \end{bmatrix}^T$	Δi_{2fb}
f_9	Busbar 3	Short-Circuit Fault	$\begin{bmatrix} 0_{1 \times 7} & -\frac{1}{C_3} & 0_{1 \times 6} \end{bmatrix}^T$	Δi_{3fb}
f_{10}	Load	Component Fault	$\begin{bmatrix} 0_{1 \times 3} & -\frac{1}{C_{bu1}} & 0_{1 \times 10} \end{bmatrix}^T$	Δi_{RL}

Table 2: Component Fault Specifications of the DCMG

3.6 Machine Learning Algorithm for Fault Detection and Classification

Detecting and classifying faults in DC microgrids is essential for maintaining their stability and ensuring uninterrupted power supply. Machine learning techniques have emerged as effective tools for automating the fault detection and classification process, offering advantages over traditional manual inspection methods [38]. Machine learning leverages the power of data analysis and pattern recognition to identify and categorize faults. By training models on historical data that includes both normal and faulty operating conditions, machine learning algorithms can learn to detect and classify faults based on patterns and features in the data. This automated approach reduces human intervention and enables faster fault detection, leading to improved system reliability [39].

One of the key advantages of applying machine learning to fault detection and classification is its ability to handle large and complex datasets. DC microgrids generate a vast amount of data, including measurements such as voltage, current, power, and environmental factors. Machine learning algorithms can effectively analyze this data to identify abnormal patterns associated with faults. Moreover, machine learning models can adapt and learn from new data, allowing for continuous improvement in fault detection accuracy over time [40]. However, applying machine learning in fault detection and classification also poses certain challenges. One such challenge is the availability of labeled training data. Building a comprehensive dataset with labeled fault data can be time-consuming and resource intensive. Additionally, the quality and representativeness of the dataset significantly impacts the performance and generalizability of the machine learning model.

Despite these challenges, machine learning techniques have shown promising results in fault detection and classification in DC microgrids. Researchers have explored various machine learning algorithms, including neural networks, decision trees, support vector machines, and ensemble methods, to improve fault detection accuracy and robustness [41].

3.6.1 Supervised Learning for Fault Classification

Supervised learning is a machine learning technique that has gained significant attention in fault classification due to its ability to learn patterns and make accurate predictions based on labeled data [42]. This type of learning involves training a model on a labeled dataset, where each data instance is associated with a known class or outcome. The model learns from this labeled data to make predictions or classify new, unseen instances. In the case of fault classification in DC microgrids, the labeled dataset contains historical records of different fault types, along with their corresponding features and characteristics [43].

There are several reasons why supervised learning a suitable approach for fault classification in DC microgrids is. Firstly, it can handle both binary (e.g., normal vs. faulty) and multiclass (e.g., short circuit, overvoltage, undervoltage) classification problems, allowing for the identification of various fault types. Supervised learning models can be trained to differentiate between different fault classes based on the patterns and features extracted from the data [44]. Secondly, supervised learning provides the ability to generalize from the training data to classify unseen instances accurately. By learning the underlying patterns and relationships in the labeled data, the model can make predictions on new data instances and classify them into the appropriate fault class. This generalization capability is crucial for fault classification in real-world scenarios where the occurrence of faults may vary.

Supervised learning algorithms commonly used for fault classification include decision trees, SVM, KNN, and ANNs. These algorithms differ in their underlying principles and approaches to classification but share the common goal of learning from labeled data to make accurate predictions [45].

The selection of supervised learning as the chosen technique for fault classification in DC microgrids was based on its ability to handle both binary and multiclass classification problems and its generalization capabilities. By utilizing a labeled dataset comprising historical fault records, we can train a supervised learning model to accurately classify different fault types based on their distinguishing features.

3.6.2 Neural Networks for Fault Detection and Classification in Power Systems

Neural networks are a class of machine learning models that have gained significant popularity due to their ability to learn complex patterns and relationships in data. Inspired by the structure and functioning of the human brain, neural networks consist of interconnected nodes, known as neurons, organized into layers. In this section, we will delve deeper into the architecture, working principles, and the utilization of pattern recognition in neural networks for fault detection in DC microgrids.

3.6.2.1 Architecture of Neural Networks

The architecture of a neural network plays a critical role in its ability to learn and make predictions. A neural network typically consists of three types of layers, as shown in Figure 16, the input layer, hidden layers, and the output layer [46].

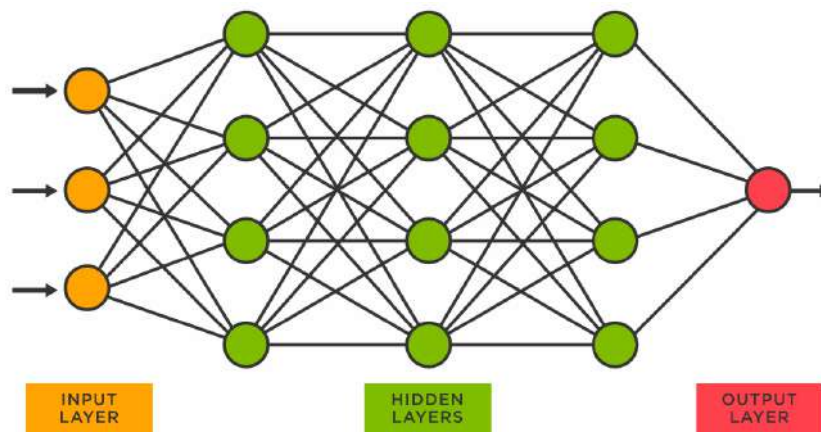


Figure 16: Architecture of Neural Networks

- The input layer is responsible for receiving the data, which could include various measurements from DC microgrid components, such as voltage, current, power, and environmental factors. Each neuron in the input layer represents a specific input feature, and its value corresponds to the value of that feature in the input data.
- The hidden layers, located between the input and output layers, perform computations on the input data and progressively learn more abstract representations of the data as information flows through the network. Hidden layers can vary in number, and each layer consists of multiple neurons. The more hidden

layers a neural network has, the more complex patterns it can learn. Each neuron in the hidden layers receives inputs from the neurons in the previous layer. It computes a weighted sum of the inputs and applies an activation function to introduce non-linearity. Mathematically, the output of a neuron in a hidden layer can be represented as follows [30]:

$$y = f\left(\sum_{i=1}^n (w_i \cdot x_i + b)\right) \quad (44)$$

In this equation, y represents the output of the neuron, x_i represents the inputs from the previous layer or the input layer, w_i represents the corresponding weights associated with each input. The weights determine the importance or influence of each input on the neuron's output, b represents the bias term, which is an additional parameter that allows the neuron to shift the decision boundary or introduce a certain level of activation.

The equation calculates a weighted sum of the inputs, represented by $\sum_{i=1}^n (w_i \cdot x_i)$, where n is the number of inputs. Each input is multiplied by its corresponding weight, and the resulting products are summed together. This weighted sum represents the total influence of the inputs on the neuron's activation.

The bias term b is then added to the weighted sum. The bias allows the neuron to have a non-zero output even when all the inputs are zero. It can be seen as a threshold that determines the neuron's activation level.

Finally, the activation function f is applied to the sum of the weighted inputs and the bias. The activation function introduces non-linearity into the computation. It determines whether the neuron should fire or be activated based on the result of the weighted sum and bias. Different activation functions have different characteristics, such as being sigmoidal, piecewise linear, or rectified. They enable the neural network to model complex relationships between inputs and outputs.

The output of the activation function y , represents the neuron's output. It serves as input to the neurons in the subsequent layers of the neural network.

By adjusting the weights and biases in the neural network during the training process, the network learns to find the optimal values that minimize the difference between the predicted outputs and the true outputs. This optimization process, often using techniques like backpropagation and gradient descent, allows the neural

network to learn the patterns and relationships in the data, enabling it to make accurate predictions or classifications.

- The output layer is the final layer of the neural network. It produces the network's predictions or classifications based on the computations performed in the hidden layers. The number of neurons in the output layer depends on the nature of the problem. For fault detection in a DC microgrid, the output layer could consist of neurons representing different fault types, with each neuron providing the probability or confidence score of a particular fault class.

3.6.2.2 Working Principles of Neural Networks

The power of neural networks lies in their ability to learn from labeled data and generalize to unseen instances. During the training phase, the network adjusts the weights and biases associated with the connections between neurons to minimize the difference between the predicted output and the actual output. This adjustment process, known as backpropagation, utilizes optimization algorithms to iteratively update the parameters of the network.

1. Training Parameters

One commonly used optimization algorithm is **Scaled Conjugate Backpropagation**. It combines the conjugate gradient method with scaling techniques to efficiently train neural networks [47]. This technique adjusts the weights and biases in the network by calculating the gradients of the loss function with respect to these parameters and updating them in a way that minimizes the loss.

The key equations involved in scaled conjugate backpropagation are as follows [48].

a) Weight Update

For each weight w in the network, the update is performed using the following equation:

$$w_{new} = w - \alpha \cdot p \cdot \text{sign}(g) \cdot \frac{\Delta w}{\Delta g} \quad (45)$$

where w_{new} is the updated weight, α is a scaling factor, p is the step size adjustment factor, g is the gradient of the weight, and $\frac{\Delta w}{\Delta g}$ is the ratio of the weight change to the gradient change.

b) Bias Update

Like weight updates, the bias b in the network is updated using the following equation:

$$b_{new} = b - \alpha \cdot p \cdot \text{sign}(g) \cdot \frac{\Delta b}{\Delta g} \quad (46)$$

Where b_{new} is the updated bias, $\frac{\Delta b}{\Delta g}$ is the ratio of the bias change to the gradient change.

c) Error Update

The error E in the network is updated using the following equation:

$$E_{new} = E - \alpha \cdot p \cdot \text{sign}(g) \cdot \frac{\Delta E}{\Delta g} \quad (47)$$

Where E_{new} is the updated error, $\frac{\Delta E}{\Delta g}$ is the ratio of the error change to the gradient change.

The scaling factor α and the step size adjustment factor p are dynamically adjusted during the training process to ensure efficient convergence.

Scaled conjugate backpropagation algorithm offers several advantages, such as faster convergence, improved stability, and better handling of ill-conditioned problems. It enables neural networks to effectively learn the underlying patterns and relationships in the data, leading to improved fault detection and classification performance. By leveraging the principles of scaled conjugate backpropagation, neural networks can efficiently adjust their parameters and optimize their performance during the training process.

2. Hyperparameters

In addition to the trainable parameters, neural networks also have hyperparameters, which are set manually before training and control the behavior and

performance of the network [49]. Following are some of the important hyperparameters commonly used in neural networks:

a) Learning Rate

The learning rate determines the step size at which the network's parameters are updated during backpropagation. A high learning rate may cause the network to converge quickly but risk overshooting the optimal solution, while a low learning rate may lead to slow convergence. It is important to find an optimal learning rate that balances convergence speed and accuracy.

b) Number of Hidden Layers and Neurons

The choice of the number of hidden layers and the number of neurons in each layer is crucial. Adding more layers or neurons can increase the network's capacity to learn complex patterns but may also lead to overfitting. On the other hand, using too few layers or neurons may result in underfitting, where the network fails to capture important patterns in the data. Finding an optimal architecture requires experimentation and validation.

c) Activation Functions

Activation functions introduce non-linearity to the network, enabling it to learn complex relationships between inputs and outputs. Common activation functions include the sigmoid, tanh, and ReLU (Rectified Linear Unit) functions. The choice of activation functions can impact the network's ability to model non-linear relationships and affect training stability.

d) Regularization Techniques

Regularization techniques help prevent overfitting by adding penalty terms to the loss function. L1 and L2 regularization are commonly used methods that control the complexity of the network by discouraging large weights and encouraging sparsity in the learned parameters. The regularization strength or coefficients are hyperparameters that need to be set based on the specific problem and dataset.

e) Batch Size

During training, the data is divided into batches, and the network's parameters are updated based on the average gradient computed over each batch. The batch size determines how many instances are processed before updating the weights. Choosing an appropriate batch size can affect the training time, memory usage, and the generalization ability of the network.

f) Dropout Rate

Dropout is a regularization technique that randomly drops out a fraction of neurons during training to prevent overfitting. The dropout rate determines the probability of a neuron being dropped out at each training iteration. It helps the network to learn more robust and generalized representations by reducing interdependencies between neurons.

g) Initialization Scheme

The initial values of the weights and biases in the network can influence the training process and convergence. There are different initialization schemes, such as random initialization, Xavier initialization, or He initialization, that can be used to set the initial parameter values [50].

3.6.2.3 Pattern Recognition in Neural Networks for Fault Detection

Neural networks excel in pattern recognition, making them well-suited for fault detection in DC microgrids [51]. Through the training process, neural networks learn to recognize patterns associated with different fault types, allowing them to accurately classify faults based on the input data.

Pattern recognition in neural networks involves two main aspects: feature extraction and decision-making.

Feature extraction refers to the process of identifying relevant patterns or features in the input data that are indicative of different fault types. Neural networks can automatically extract relevant features from raw data, eliminating the need for manual feature engineering [52]. This ability is particularly valuable in fault detection, as fault patterns may not always have explicit definitions or be easily discernible. By

learning the underlying representations of the data through the hidden layers, neural networks can capture intricate patterns and relationships that might not be apparent in the original measurements.

Once relevant features are extracted, the neural network utilizes its learned parameters to make decisions about the presence or absence of faults [53]. The network assigns input instances to different fault classes based on the patterns and features it has learned during training. By comparing the extracted features of the input data with the learned patterns, the neural network can accurately identify and classify different types of faults.

The ability of neural networks to recognize complex patterns and extract meaningful features from raw data contributes to their effectiveness in fault detection. Through extensive training on labeled fault data, neural networks can learn to generalize and accurately detect faults in DC microgrids.

3.6.3 Workflow: Fault Detection and Classification in DC Microgrid using Neural Networks

The flowchart, shown in Figure 17, illustrates the comprehensive workflow for fault detection and classification in DC microgrid systems using neural networks. The workflow begins with data collection, where relevant parameters such as voltage and current are gathered from the DC microgrid. The collected data is then preprocessed to remove noise and outliers, followed by feature extraction to identify informative patterns. Subsequently, the data is divided into training, validation, and testing datasets to prepare for model development. A suitable neural network architecture is selected, and the model is trained using the training dataset, employing techniques such as scaled conjugate backpropagation for optimization. The hyperparameters of the neural network, including the learning rate, batch size, and number of hidden layers, are carefully tuned using the validation dataset to improve the model's performance and generalization capabilities. The training process involves iterative forward and backward passes, where the model learns to minimize the loss function and adjust the weights and biases. Once the training is complete, the model's performance is evaluated using the testing dataset, measuring metrics such as accuracy, precision, recall, and F1 score. In the next step, the trained model is applied to real-time data from the DC microgrid, enabling the detection and classification of faults. The output of the model

provides valuable insights into the presence and types of faults in the microgrid, aiding in timely decision-making and maintenance. Throughout the workflow, performance analysis and improvement techniques are employed to refine the model, considering both the training and validation results. This iterative process ensures that the neural network model is optimized and reliable for accurate fault detection and classification in DC microgrid systems. Finally, the results and conclusions of the entire workflow are summarized, providing a comprehensive understanding of the effectiveness and practical implications of utilizing neural networks for fault detection and classification in DC microgrid systems.

3.7 Fault Classification Module

For fault identification, classification type supervised learning technique is employed, utilizing this type of algorithm to categorize input data into their respective classes based on distinct features. In our research work, we studied 11 different types of faults, each associated with a specific output class within the machine learning algorithm. Once trained using the fault samples dataset, the algorithm can effectively classify faults into their appropriate classes using feature detection techniques, as demonstrated by the equation below. This approach enhances the efficiency and accuracy of fault classification, enabling timely identification and appropriate response to ensure the reliable operation of the DCMG system.

$$y_j = \begin{cases} 1 & \text{if any type of fault } j \text{ is detected} \\ 0 & \text{otherwise} \end{cases} \quad (48)$$

Below is a detailed description of the fault classes associated with the different types of faults studied in this research. Each fault class represents a specific fault scenario and plays a crucial role in accurately identifying and classifying faults within the DCMG system. The comprehensive understanding of these fault classes enables effective fault detection and response strategies, contributing to the overall reliability and performance of the microgrid system.

3.7.1 No-Fault Condition (Nof):

The first fault signature corresponds to the No-fault condition (Nof), indicating that the DCMG is operating in its normal condition without any faults. This fault class is assigned the output class vector y , which is defined as:

$$y_1 = [1 \ 0_{1 \times 11}] \quad (49)$$

This output class vector serves as a representation of the fault-free state of the system and plays a crucial role in accurately identifying and classifying this specific condition during fault detection and classification processes.

3.7.2 Fault Signature for the Switch Failure type Fault:

The next fault signature corresponds to the switch failure type fault in the DCMG, which can occur in both the Boost converter and the Buck converters. This fault class represents the malfunction or failure of the switches in these converters. The output class vector y for this fault signature is defined as:

$$y_j = \begin{cases} [0 \ 1 \ 0_{1 \times 10}] & \text{when } j = 2 \\ [0_{1 \times 2} \ 1 \ 0_{1 \times 9}] & \text{when } j = 3 \\ [0_{1 \times 3} \ 1 \ 0_{1 \times 8}] & \text{when } j = 4 \end{cases} \dots (50) \quad (50)$$

Here, the output class vector is denoted as y_j , where $j = 2$ represents the Boost converter switch fault, $j = 3$ represents the Buck converter 1 switch fault, and $j = 4$ represents the Buck converter 2 switch fault. By assigning this specific output class vector, the fault classification module can accurately identify and classify instances of switch failure in the Boost converter and the Buck converters. With the help of feature detection and the defined output class vector, the machine learning algorithm can effectively detect and classify switch failure faults within the DCMG system.

3.7.3 Fault Signature for the Short-Circuit Fault in the Transmission Cable:

In the fault classification module, the fault signature for the transmission cable short circuit fault is given special consideration. This fault class specifically refers to the occurrence of a short circuit fault in one of the transmission cables within the DCMG system. The output class vector y , associated with this fault signature, is defined as:

$$y_j = \begin{cases} [0_{1 \times 4} \ 1 \ 0_{1 \times 7}] & \text{when } j = 5 \\ [0_{1 \times 5} \ 1 \ 0_{1 \times 6}] & \text{when } j = 6 \\ [0_{1 \times 6} \ 1 \ 0_{1 \times 5}] & \text{when } j = 7 \end{cases} \dots (51) \quad (51)$$

Since the DCMG system consists of three cables, each corresponding to a specific fault scenario, the fault classification algorithm assigns a unique output class vector for accurate identification and classification. Specifically, the output class vector

is denoted as y_j , where $j = 5$ corresponds to cable 1 short circuit fault, $j = 6$ corresponds to cable 2 short circuit fault, and $j = 7$ corresponds to cable 3 short circuit fault. By utilizing feature detection techniques and the defined output class vector, the machine learning algorithm demonstrates its capability to effectively detect and classify short circuit faults occurring in the transmission cables of the DCMG system.

3.7.4 Fault Signature for the Short-Circuit Fault in the Busbar:

In a similar manner, the fault signature related to the short circuit fault in the busbars of the DCMG is considered within the fault classification module. This fault class refers to the occurrence of a short circuit fault in one of the busbars of the DCMG system. The corresponding output class vector y for this fault signature is defined as:

$$y_j = \begin{cases} [0_{1 \times 7} & 1 & 0_{1 \times 4}] & \text{when } j = 8 \\ [0_{1 \times 8} & 1 & 0_{1 \times 3}] & \text{when } j = 9 \\ [0_{1 \times 9} & 1 & 0_{1 \times 2}] & \text{when } j = 10 \end{cases} \quad (52)$$

The output class vector is denoted as y_j , where $j = 8$ corresponds to busbar 1 short circuit fault, $j = 9$ corresponds to busbar 2 short circuit fault, and $j = 10$ corresponds to busbar 3 short circuit fault. By utilizing feature detection techniques and considering the defined output class vector, the fault classification algorithm becomes capable of effectively detecting and classifying short circuit faults in the busbars of the DCMG system.

3.7.5 Fault Signature for the Short-Circuit Fault in the Load Component:

Similarly, the fault signature related to the short circuit fault in the load components of the DCMG is considered within the fault classification module. This fault class represents the occurrence of a short circuit fault in one of the load components connected to the DCMG system. The corresponding output class vector y for this fault signature is defined as:

$$y_j = \begin{cases} [0_{1 \times 10} & 1 & 0] & \text{when } j = 11 \\ [0_{1 \times 11} & 1] & & \text{when } j = 12 \end{cases} \quad (53)$$

Where the output class vector is represented as y_j , where $j = 11$ corresponds to the buck converter 1 side load component fault, and $j = 12$ corresponds to the buck converter 2 side load component fault. By incorporating feature detection techniques and considering the defined output class vector, the fault classification algorithm

effectively detects and classifies short circuit faults in the load components of the DCMG system.

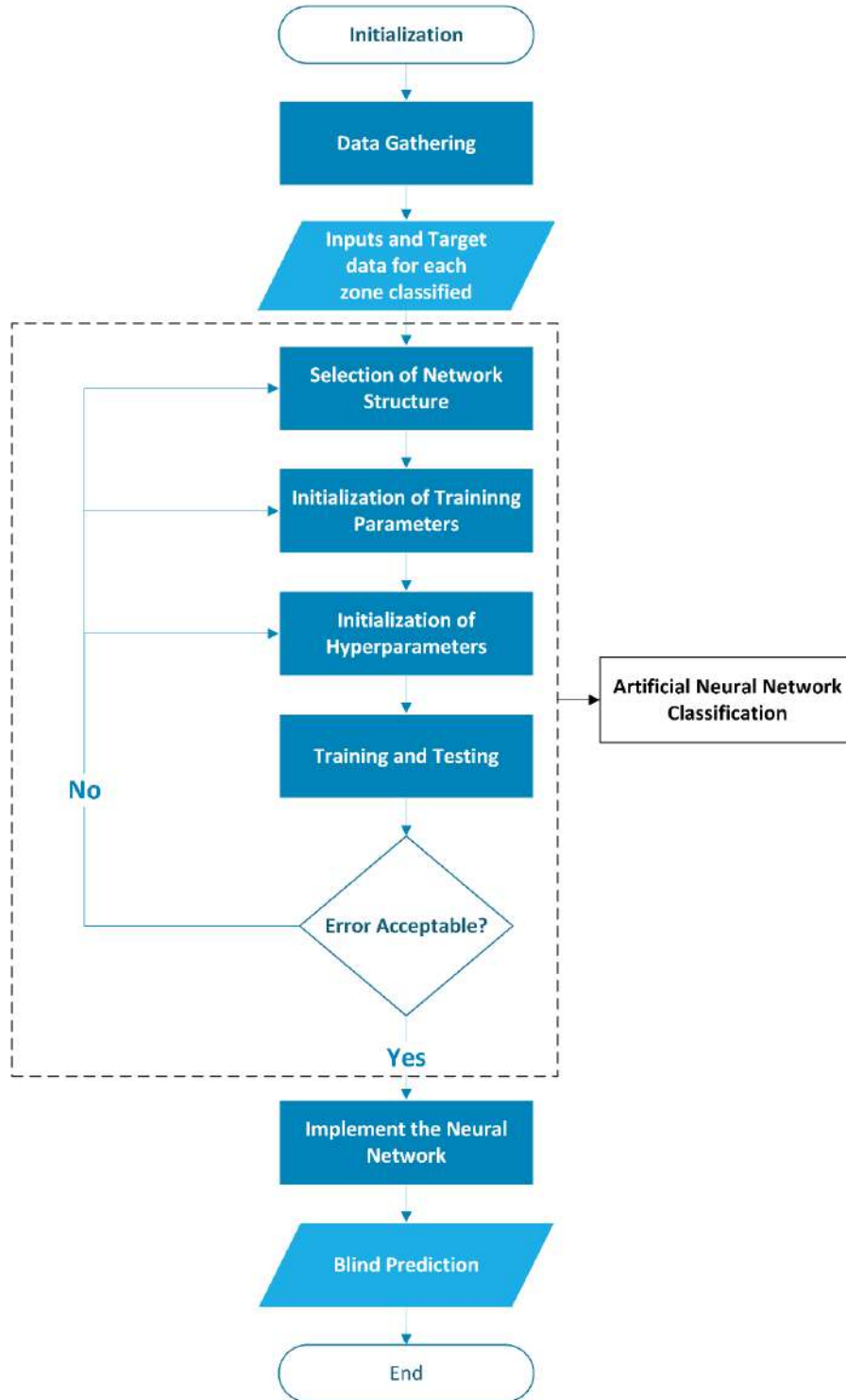


Figure 17: Workflow depiction for Fault Detection and Classification in DC Microgrid Systems using Neural Networks

Chapter 4

In this section, the results and discussion of the developed machine learning based FDI for the DCMG under study is presented.

4.1 Proposed Solution/Results & Discussion

To address the component-level protection and model uncertainty limitations inherent in existing FDI algorithms for DCMGs, this research presents an ANN-based algorithm as a solution. The algorithm employs component-wise state-space modeling and physical modeling to obtain a comprehensive training dataset, trains the ANN using fault-related data extracted from the microgrid, and utilizes the cross-entropy loss function for classification and the scaled conjugate backpropagation algorithm for optimization.

To begin with, we first provide simulation results for the DCMG under no-fault condition. We discuss this scenario by observing different plots of voltages and currents in the converters and transmission cables of the system, the simulation results of the DC microgrid under a no-fault condition are provided, including voltage and current plots of converters and transmission cables. This analysis establishes a baseline for comparison with subsequent fault scenarios. In addition to the first baseline comparison data, we also provide the generated fault data. This data is obtained by introducing various faults such as line, converter switch, and load to the DCMG. Moving on, the fault detection results are provided, accompanied by a detailed explanation of how the machine learning algorithm effectively identifies and classifies faults within the microgrid system. Moreover, the efficiency of the algorithm in isolating faults is discussed, elucidating the steps taken to pinpoint the precise location of the fault within the network.

The DC microgrid under study and its characteristics are comprehensively discussed in Section 3.2 of this thesis. The SLD of the DCMG under study mentioning the faults is provided here as Figure 18. The system encompasses boost converters, buck converters, DC busbars, DC circuit breakers, and DC transmission cables.

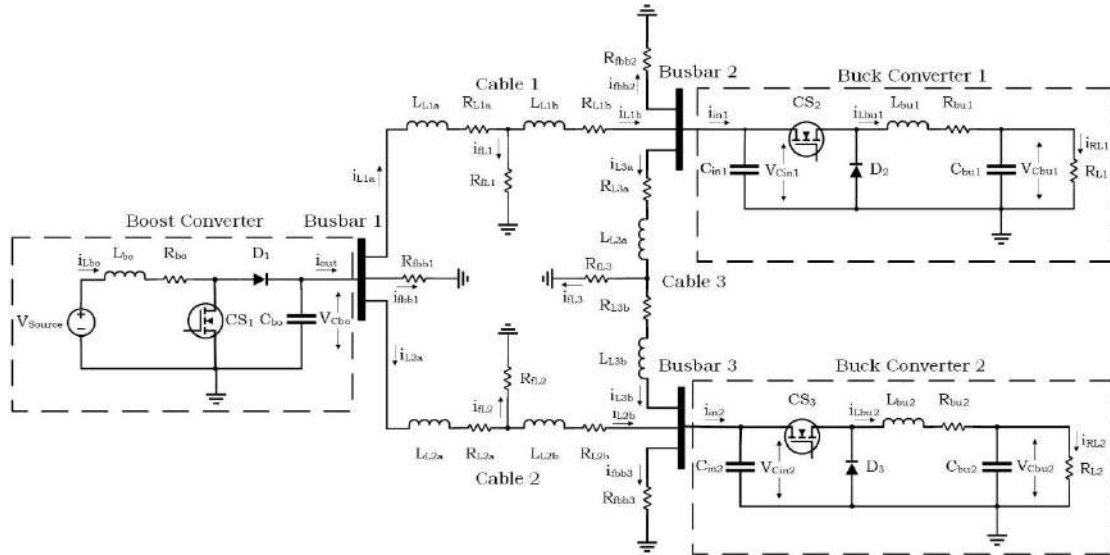


Figure 18: The schematic representation of the DC microgrid in the case study

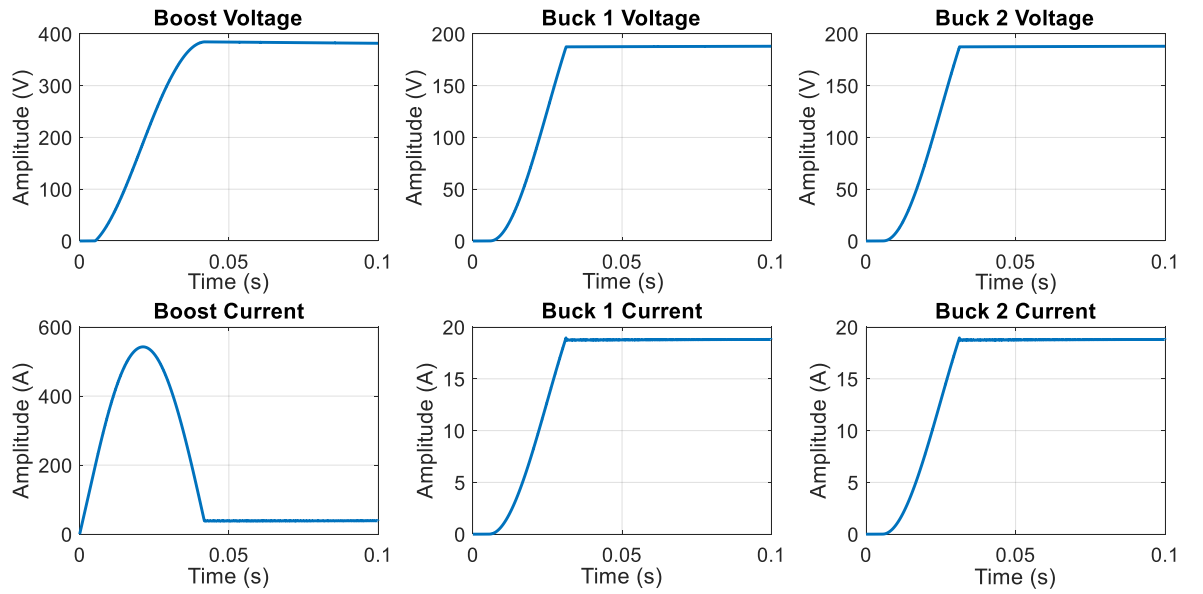
4.1.1 DCMG under Normal Operation

This subsection focuses on analyzing the response of the three-terminal DC microgrid during normal operation, i.e., devoid of any faults. Through simulation, we can observe the behavior and interaction of these components within the microgrid. This analysis establishes a baseline for evaluating the system's performance and provides valuable insights for subsequent comparison with fault scenarios. The behavior of the DCMG under normal condition is shown in Figure 19(a) and 19(b). For convenience we call this scenario Case 1.

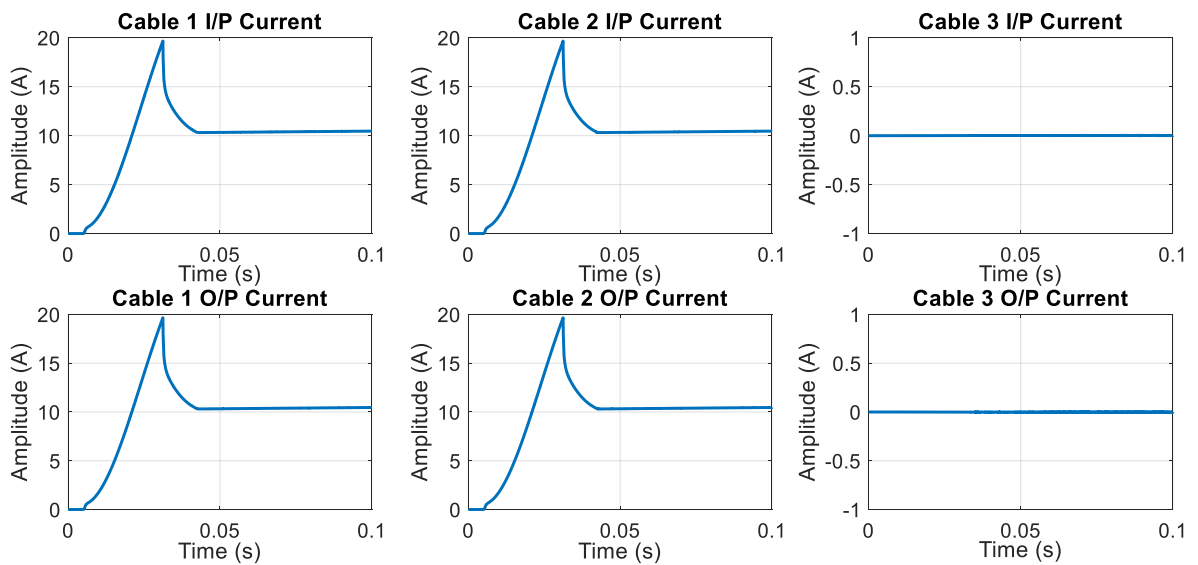
4.1.1.1 Data Generation Case 1: No-Fault Condition

Figure 19(a) illustrates the voltage and current plots of the DC-DC converters within the DC microgrid (DCMG). In this scenario all initial conditions of the DCMG are kept zero. Therefore, we can see in Figure 19(a) that the Buck and Boost terminals go through a transient phase prior achieving their rated steady-state values. The system's steady-state is achieved via a local closed-loop controller at each converter. It is observed in Figure 19(a) that the local controllers achieve steady-state voltage and current within 0.04 sec.

Machine Learning based Fault Detection and Isolation in DC Microgrids



(a)



(b)

Figure 19: Data Generation Case-1 No-fault

(a) Converters Voltage & Current, (b) Transmission Cables Current.

The transient and steady-state response of the DCMG transmission cables is shown in Figure 19(b). In this figure, both input and output current of the transmission lines are provided. Like the converter states we find that the local controllers have achieved steady-state cable current within 0.04sec; moreover, by examining this plot we can observe that there is distinct behavior among the different cable branches. Cable

1 and Cable 2 exhibit a gradual increase in current until they reach their steady-state values. This increase is intuitive as it shows the supply of power to the load connected with the buck converter. Conversely, Cable 3 demonstrates no current flow during the normal operation of the DCMG. Its primary function is to serve as an alternative power source in the event of line two or line one failure. Thus, under normal conditions, Cable 3 remains inactive, ensuring the system's reliability by providing a backup or contingency.

These plots provide critical observations regarding the dynamic behavior and performance of the DC-DC converters and the DC transmission cables within the DCMG. By analyzing these visual representations, which are derived from the circuit model of the system, we obtain a comprehensive understanding of the system's operation. The simulation results shed light on the system's capability to maintain stable voltage and current levels, guaranteeing uninterrupted power supply to the connected load. This analysis validates the efficacy and reliability of the system's design, demonstrating its robust performance under normal operating conditions.

4.1.2 DCMG Under Fault Condition

In this section, a comprehensive description of the fault parameters, number of training data samples, and fault scenarios is presented. The primary objective of this phase is to generate a dataset which will be utilized for training the machine learning algorithm. Detailed information regarding the types of faults, their characteristics, and the corresponding fault scenarios are provided. Additionally, the simulation results of these faults are presented, which serve as the basis for extracting the fault data required for training the machine learning algorithm. Thus, a diverse dataset is generated, enabling the algorithm to learn and identify different fault conditions accurately.

Fault Parameters and Dataset Description:

As indicated in Section 3 of the thesis, an essential aspect of the research involves the modeling and simulation of various fault scenarios within the DCMG. By utilizing a circuit model implemented in MATLAB/SIMULINK, therefore, 11 different fault types are carefully created and simulated. Employing a supervised learning approach, the fault data samples are associated with their respective fault classes, enabling accurate fault classification as discussed in Section 3.6. A detailed description of the

different fault scenarios, along with the number of data samples, is provided in Table 3 below.

S.No	Fault Description	Scenarios	Data Samples
1	No-Fault Condition (Nof)	1	30,001
2	Boost Converter Side Busbar Short-Circuit Fault	5	200,004
3	Buck Converter 1 Side Busbar Short-Circuit Fault	2	40,002
4	Buck Converter 2 Side Busbar Short-Circuit Fault	2	40,002
5	Transmission Cable 1 Short-Circuit Fault	2	40,002
6	Transmission Cable 2 Short-Circuit Fault	2	40,002
7	Transmission Cable 3 Short-Circuit Fault	2	40,002
8	Boost Converter Switch Fault	2	40,002
9	Buck Converter 1 Switch Fault	2	40,002
10	Buck Converter 2 Switch Fault	2	40,002
11	Buck Converter 1 Load Fault	2	40,002
12	Buck Converter 2 Load Fault	2	40,002
Total fault Cases		26	630,025

Table 3: Different Fault Scenarios and Data Sample Quantities in the DCMG

As depicted in the table, a comprehensive dataset comprising a total of 630,025 samples is generated to capture the various fault scenarios in the DCMG. This dataset is particularly significant considering the presence of 27 different simulation scenarios, ensuring a diverse range of fault scenarios. Moreover, the dataset is versatile due to the inclusion of 12 distinct features. These features encompass essential parameters such as boost converter output voltage and internal current, V_{bo} and I_{bo} , as well as the input and output currents of cables 1, 2, and 3, I_{ia} and I_{ib} where $i = 1, 2$ and 3. Additionally, the dataset includes the output voltage and current of buck converters 1 and 2, V_{bui} and I_{bui} where $i = 1$ and 2. The inclusion of these 12 distinct features provides a rich and comprehensive representation of DCMG's behavior under different fault conditions. A detailed description of different fault scenarios along with the number of data samples in each category is provided below.

To further enhance the efficiency of the machine learning fault detection system, an additional supervised machine learning algorithm is integrated in series with the

previously trained algorithm. This subsequent algorithm is trained using the output of the first algorithm, employing the same number of data samples, and utilizing the same target dataset. By cascading these algorithms, the fault detection system benefits from the combined capabilities and insights offered by both algorithms. This sequential approach strengthens the fault detection mechanism and improves its overall performance in accurately identifying and isolating faults within the DCMG. The integration of the second algorithm, trained on the output of the first, contributes to the system's robustness and enhances its fault detection capabilities.

The division of the entire dataset into distinct subsets for each algorithm is illustrated below. This approach serves a crucial role in minimizing the risk of overfitting and facilitates effective training, testing, and validation of the machine learning models, ensuring their optimal performance. The division of the data samples in these subsets is completely random.

Pre-Cascade Algorithm	Post-Cascade Algorithm
<ul style="list-style-type: none"> ○ Training Dataset: 70% of the dataset is dedicated to training the machine learning algorithm, enabling it to learn and optimize the weights and biases that govern its decision-making process. ○ Testing Dataset: 15% of the dataset is allocated for validation purposes during the learning process. This subset is used to assess the algorithm's performance, fine-tune hyperparameters, and ensure generalization beyond the training data. ○ Validation Dataset: The remaining 15% of the dataset is reserved for testing the fully trained algorithm's performance. This independent evaluation allows for an objective assessment of the algorithm's accuracy, robustness, and effectiveness in real-world scenarios. 	<ul style="list-style-type: none"> ○ Most of the dataset, approximately 70%, is utilized for training the machine learning algorithm. This dedicated portion allows the algorithm to learn and optimize its weights and biases, which are essential for accurate decision-making. ○ Around 15% of the dataset is set aside for validation purposes during the learning process. This subset serves as an evaluative tool to gauge the algorithm's performance, fine-tune hyperparameters, and ensure that it can generalize well beyond the training data. ○ The remaining 15% of the dataset is exclusively reserved for testing the fully trained algorithm's performance. This independent evaluation provides an objective assessment of the algorithm's accuracy, robustness, and real-world effectiveness, as it operates on unseen data.

Fault Data Generation Cases:

To obtain the necessary training data samples for the machine learning algorithm, the DCMG circuit model is simulated under various fault scenarios. This simulation-based approach is highly effective in observing and analyzing the voltage and current characteristics of the system under different fault conditions. By introducing faults in the simulation, the behavior of the DCMG can be closely examined, and the changes in voltage and current patterns can be observed. This comprehensive analysis provides valuable insights into the distinct fault signatures that can later be used for fault detection and classification. The simulation results of these fault scenarios serve as a crucial foundation for extracting the training data required to train the machine learning algorithm. The following section presents the plots depicting the response of the DCMG under different fault scenarios, showcasing the dynamic behavior of the system and the characteristic voltage and current patterns associated with each fault.

- Data Generation Case 2: Converters Switch failures
- Data Generation Case 3: Busbar faults
- Data Generation Case 4: Transmission Cable faults
- Data Generation Case 5: Load Component faults

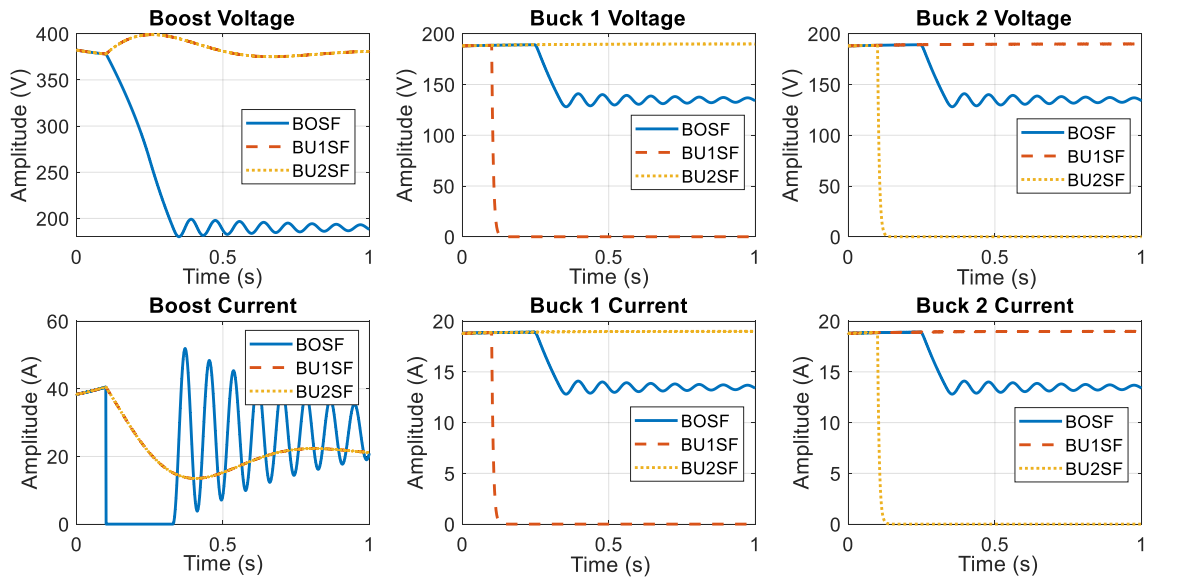
Note that Case 1, the no-fault scenario has been discussed in previous section 4.1.1.1

4.1.2.1 Data Generation Case 2: Converter Switch Failures

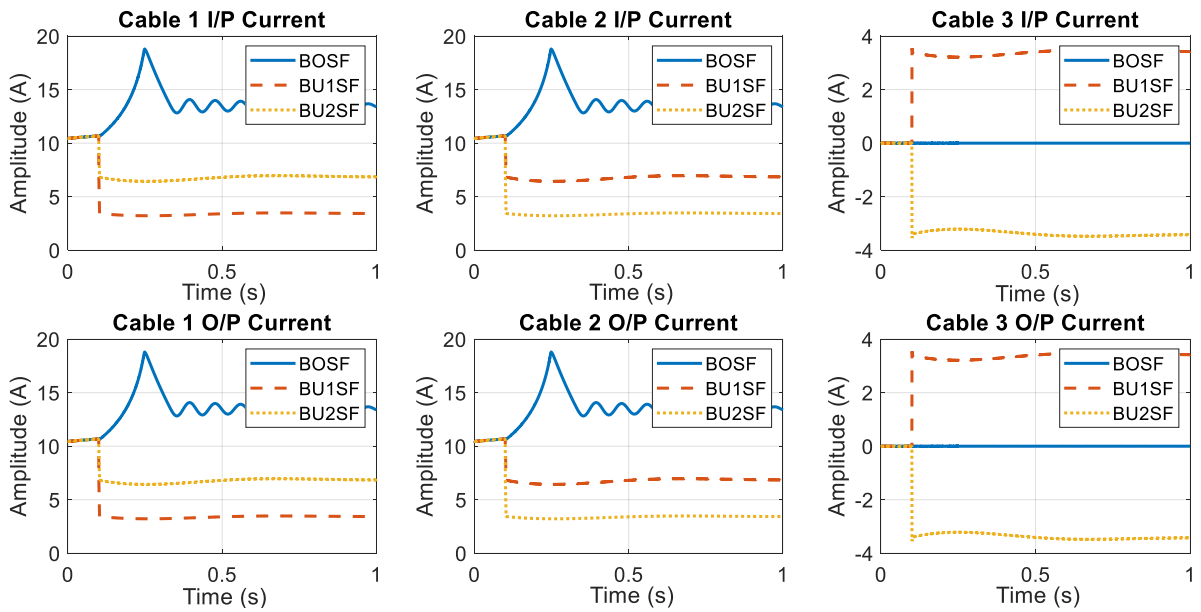
Figure 20(a) shows the Switch failures in the DCMG. These faults have been introduced at 0.1 seconds. As we can see, before the commencement of the fault, DCMG is operating in steady state which changes at the inception of the fault. Therefore, the curves in the plot illustrate the changes in voltage and current characteristics, highlighting the impact of the fault on the system's behavior.

Similarly, the Transmission cable current response of the DCMG under switch fault scenario can be observed in Figure 20(b). As observed, the current of Cable 1 & 2 increases due to *BOSF* whereas Cable 3 current remains unchanged. In contrast to the *BOSF*, the Cable 1 & 2 current decreases when *BU1SF and BU2SF* occurs. Moreover, Cable 3 also observes the effect of the Buck converters faults.

Machine Learning based Fault Detection and Isolation in DC Microgrids



(a)



(b)

Figure 20: Data Generation Case-2 Switch Faults

(a) Converters Voltage & Current, (b) Transmission Cables Current

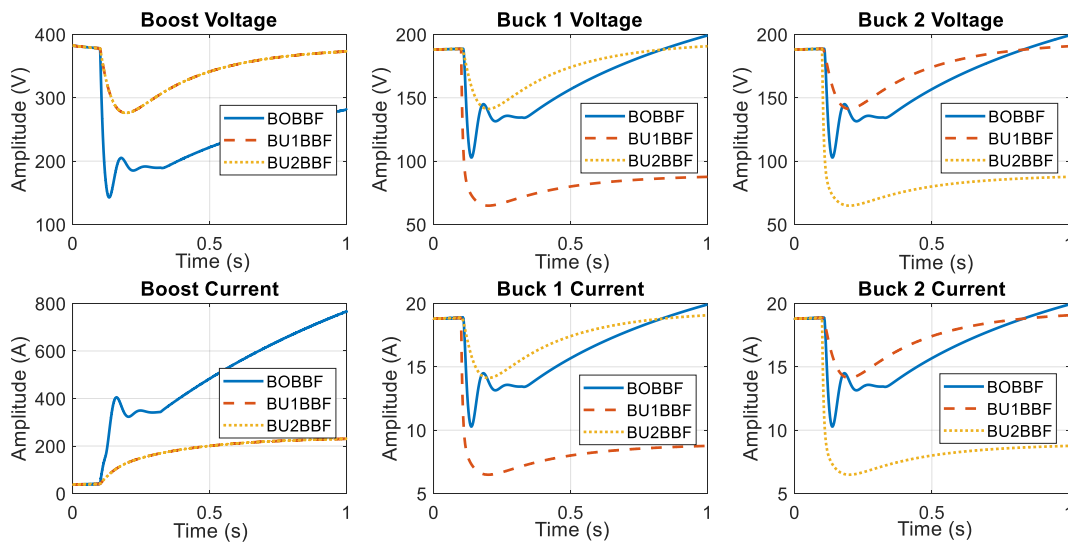
4.1.2.2 Data Generation Case 3 Busbar Faults

This case discusses the Busbar short-circuit fault scenario (Figure 21) of DCMG. These fault scenarios have been simulated at 0.1 seconds. Prior to the fault occurrence, the DCMG operates in a steady state. However, the plot reveals the changes

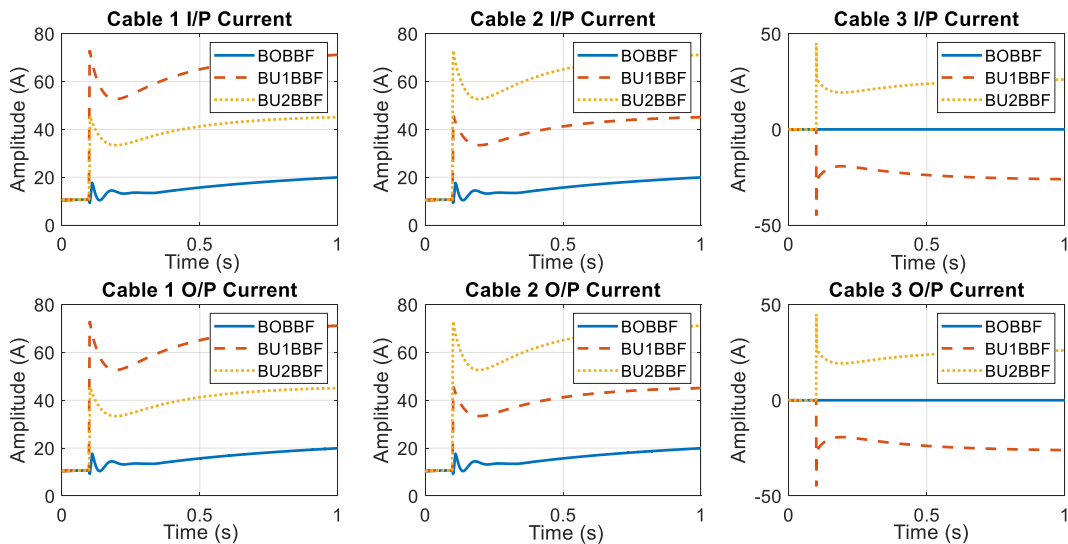
in voltage and current characteristics that occur after the fault, showcasing the impact on the system's behavior.

Figure 21(a) shows the three converters voltage and current due to the Busbar faults. As we can see that the most sever fault in this the DCMG is the BOBBF fault. Nonetheless, all faults are of equal importance for the protection of the grid.

The behavior of the Transmission Cables upon the occurrence of Busbar faults are given ad Figure 21(b). Where we can observe that the cables output and input currents behave nearly the same in this scenario.



(a)



(b)

Figure 21: Data Generation Case-3 Busbar Faults

(a) Converters Voltage & Current, (b) Transmission Cables Current.

4.1.2.3 Data Generation Case 4: Transmission Cable Faults

Case 4 provides the results of the Short-Circuit Fault in Transmission cables (Figure 22) of the DCMG. These faults were simulated at 0.1 seconds. Prior to the fault occurrence, the DCMG operated in a stable state. However, the displayed curves in the plot demonstrate significant changes in voltage and current characteristics, clearly indicating the impact of the fault on the system's behavior.

Voltage and current behavior of the converters under the influence of the transmission cable faults are provided in Figure 22(a). Similarly, the input and output current variation of the transmission cable is in Figure 22(b). We see that each converter and cable influenced differently under the introduction of the Transmission line faults.

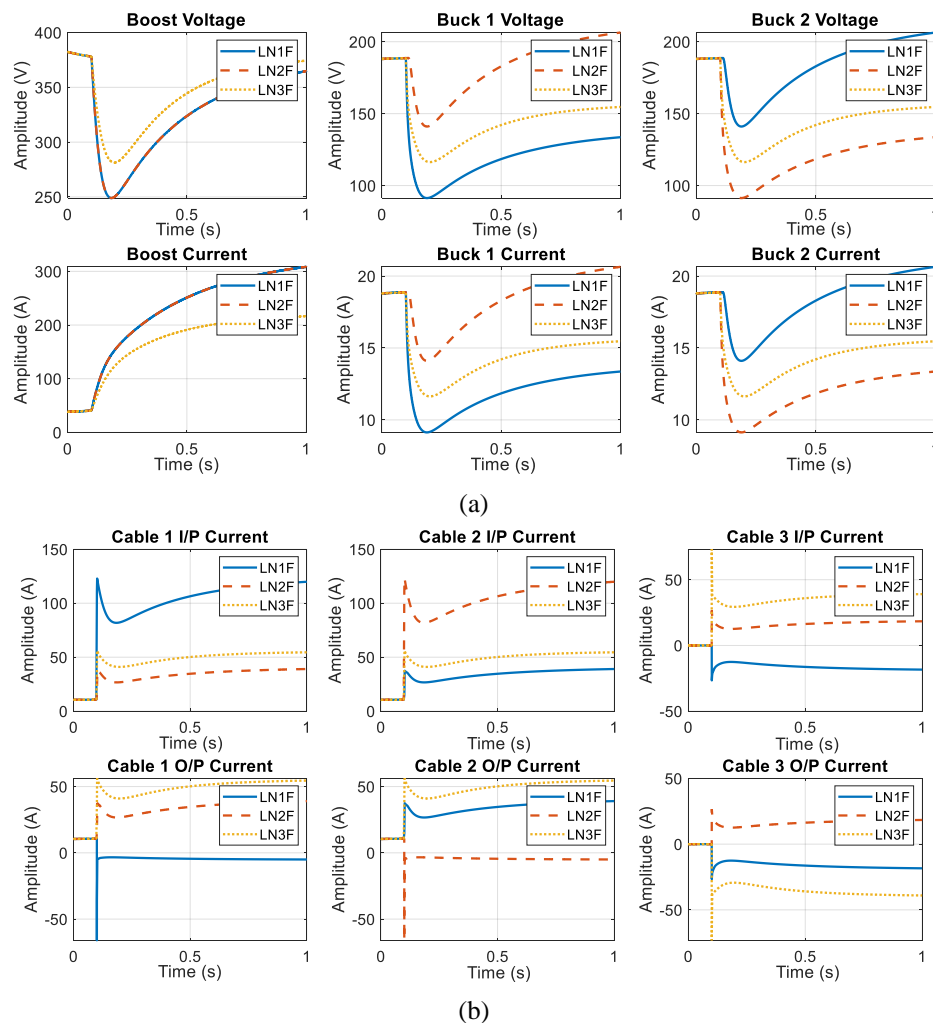


Figure 22: Data Generation Case-4 Cable Faults

(a) Converters Voltage & Current, (b) Transmission Cables Current.

4.1.2.4 Data Generation Case 5: Load Component Faults

Shown below is the depiction of a Short-Circuit Faults in the Load Component (Figure 23) of the DCMG. These faults were simulated at 0.1 seconds. Prior to the fault, the DCMG was operating in a steady-state condition. However, after the fault occurrence, the plot demonstrates notable changes in voltage and current characteristics, revealing the effect of the fault on the system's behavior.

Figure 23(a) shows the converters voltages and current for the load fault. We see that the load faults on the two Buck converters induce nearly similar responses in the Boost converter's voltage and current. Similarly, the influence of the load faults of the two Buck converters are shown in Figure 23(b). The two load faults are propagated differently into the Transmission Cables.

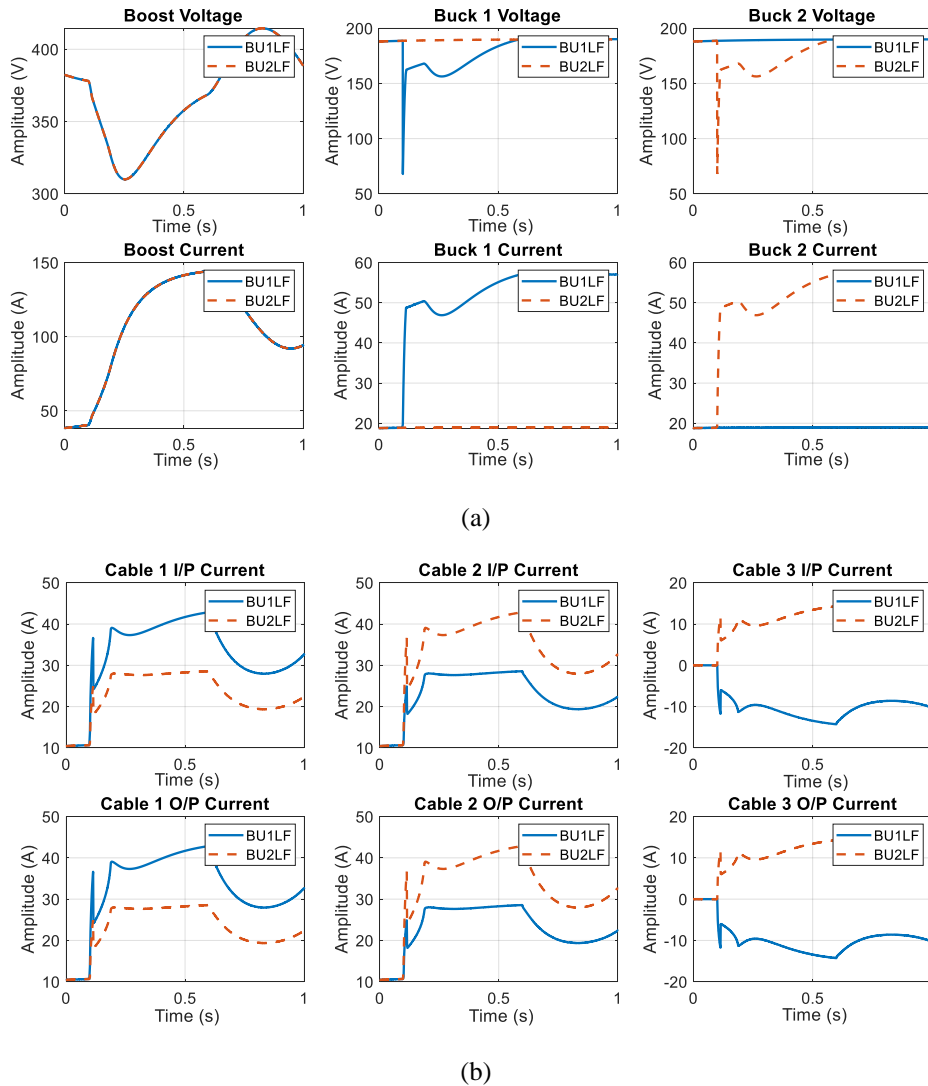


Figure 23: Data Generation Case-5 Load Faults

(a) Converters Voltage & Current, (b) Transmission Cable Current.

4.1.3 Proposed FDI Training and Results

This section presents the results obtained from the fault-type detection process using the trained machine learning algorithm. It encompasses the training outcomes of the algorithm, along with the simulation results that demonstrate the accurate detection and isolation of faults within the DCMG system. The effectiveness of the developed fault detection methodology is assessed by analyzing the performance metrics and evaluating the algorithm's ability to classify various fault types accurately. The following subsections provide an in-depth analysis of the training results and the simulation outcomes, highlighting the successful fault detection and isolation achieved through the implemented methodology.

4.1.3.1 NN Training and Performance

The training results of the neural network algorithm in this study demonstrate its effectiveness in fault detection and classification. The scaled conjugate backpropagation optimization technique, discussed in Section 3.6.2.2, ensures efficient training. The confusion matrix evaluation provides valuable insights into the algorithm's performance, allowing for accurate classification of fault types. The performance plot, based on cross-entropy as the performance measure, depicts the algorithm's convergence and provides a visual representation of its learning progress over training epochs. The depicted neural network structures for the pre-cascaded and post-cascaded algorithms illustrate their connectivity and organization within the fault classification module. The iterative process of determining the appropriate number of hidden layers contributes to achieving desired fault classification outcomes. The optimal number of hidden layers of the Pre-Cascaded and Post-Cascaded structures are 130 and 40, respectively, which is shown as Figure 24 below.

Moreover, the performance of the Neural Networks training shown in Figure 24 is presented here in Figure 25 as cross-entropy error which exhibits a consistent decrease with an increasing number of iterations, highlighting the efficient learning process of the machine learning algorithm.

Figure 25(a) shows the Pre-Cascaded Neural Network training performance plots. We find that the best validation of the training occurs on 159 epochs with a cross-entropy value of 133.24×10^{-6} . Similarly, Figure 25(b) shows that the best Post-

Cascaded Neural Network training performance results on 38th epoch with a performance value of 54.915×10^{-6} . Notably, the pre-cascaded system requires a larger number of iterations, approximately 160, compared to the post-cascaded system, which converges around 40 iterations. This significant improvement in fault classification underscores the algorithm's effectiveness in accurately identifying and categorizing faults within the DCMG system.

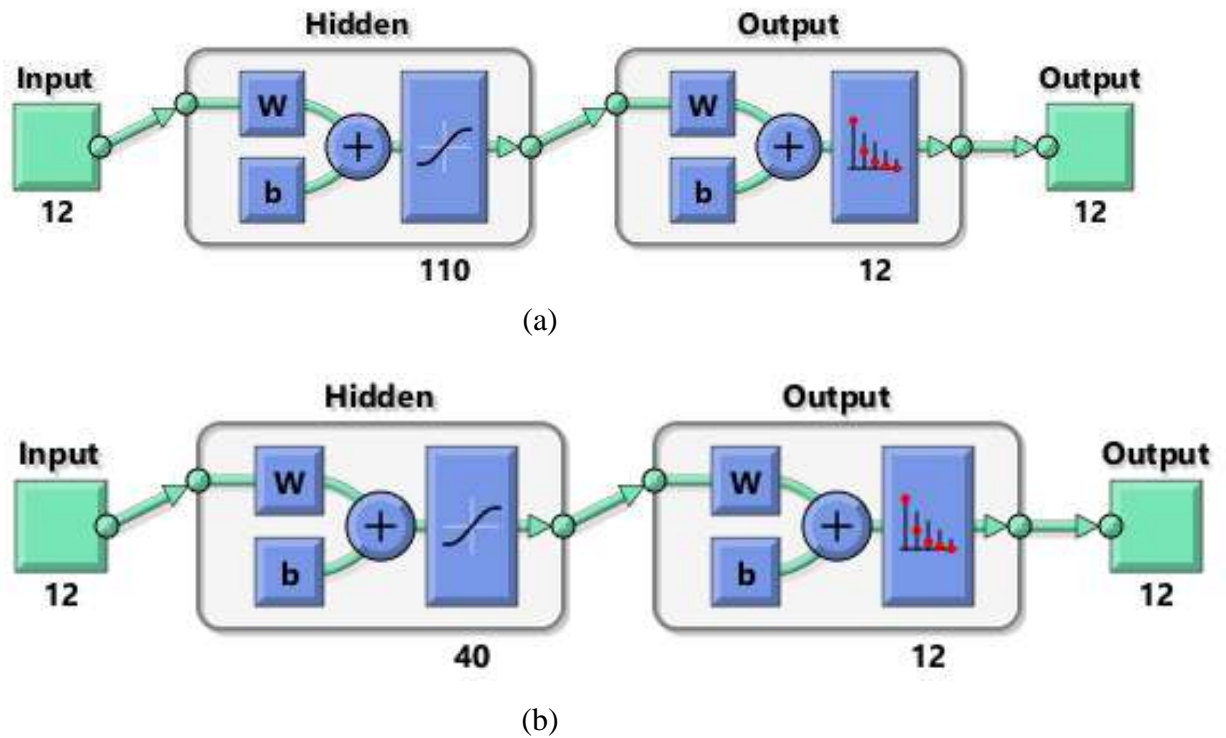
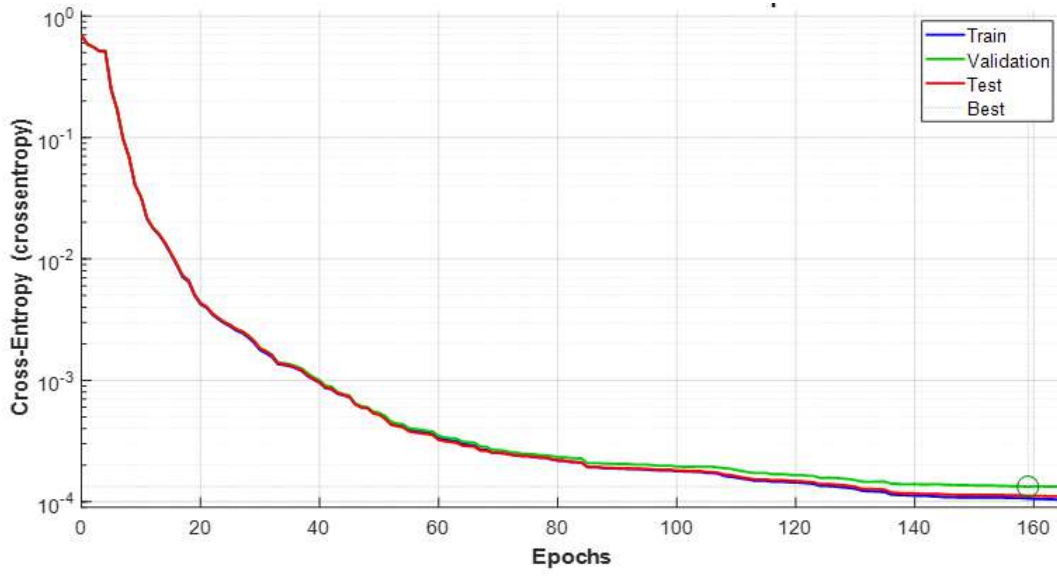


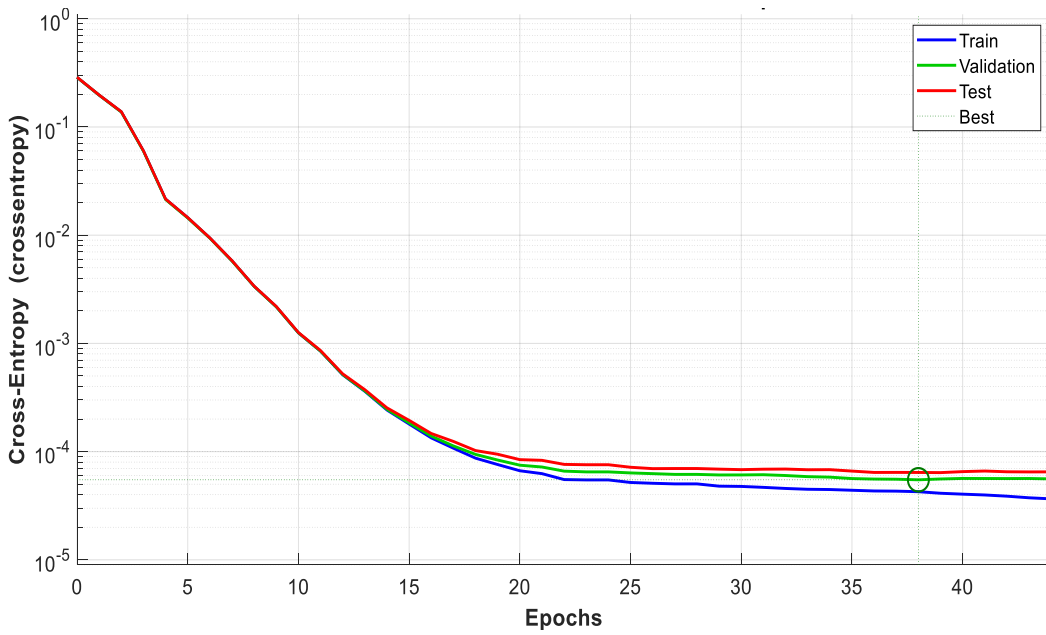
Figure 24: Structure of the neural network used in this FDI

(a) Pre-Cascaded System (b) Post-Cascaded System

The next performance criterion for the neural networks is the confusion matrix. And the results are shown as Figure 26, where we see that for both the pre-cascaded and post-cascaded systems demonstrate high classification accuracy. In the pre-cascaded system, the classification accuracy ranges from 99.8% to 100%, indicating its efficiency in fault identification. The post-cascaded system exhibits even higher accuracy, amplifying the classification rate to between 99.9% and 100%. These impressive results highlight the effectiveness of both systems in accurately identifying and classifying faults within the DCMG.



(a)



(b)

Figure 25: Training Performance Plots

(a) Pre-Cascaded System: Best validation at epoch 159 with value 133.24×10^{-6} (b)
 Post-Cascaded System: Best validation at epoch 38 with value 54.915×10^{-6} .

Machine Learning based Fault Detection and Isolation in DC Microgrids

Predicted Fault Type	Actual Fault Type												
	NoF	BOSF	BU1SF	BU2SF	LN1F	LN2F	LN3F	BOBBF	BU1BBF	BU2BBF	BU1LF	BU2BBF	
NoF	35101 5.6%	11 0.0%	0 0.0%	0 0.0%	1 0.0%	1 0.0%	0 0.0%	28 0.0%	0 0.0%	0 0.0%	2 0.0%	1 0.0%	99.9% 0.1%
BOSF	0 0.0%	35509 5.6%	0 0.0%	0 0.0%	0 0.0%	0 0.0%	0 0.0%	0 0.0%	0 0.0%	0 0.0%	0 0.0%	0 0.0%	100% 0.0%
BU1SF	0 0.0%	0 0.0%	39841 6.3%	0 0.0%	0 0.0%	0 0.0%	0 0.0%	0 0.0%	0 0.0%	0 0.0%	0 0.0%	0 0.0%	100% 0.0%
BU2SF	0 0.0%	0 0.0%	0 0.0%	39841 6.3%	0 0.0%	0 0.0%	0 0.0%	0 0.0%	0 0.0%	0 0.0%	0 0.0%	0 0.0%	100% 0.0%
LN1F	0 0.0%	0 0.0%	0 0.0%	0 0.0%	39999 6.3%	0 0.0%	0 0.0%	0 0.0%	0 0.0%	0 0.0%	0 0.0%	0 0.0%	100% 0.0%
LN2F	0 0.0%	0 0.0%	0 0.0%	0 0.0%	0 0.0%	39999 6.3%	0 0.0%	0 0.0%	0 0.0%	0 0.0%	0 0.0%	0 0.0%	100% 0.0%
LN3F	0 0.0%	0 0.0%	0 0.0%	0 0.0%	0 0.0%	0 0.0%	40000 6.3%	0 0.0%	0 0.0%	0 0.0%	0 0.0%	0 0.0%	100% 0.0%
BOBBF	16 0.0%	0 0.0%	0 0.0%	0 0.0%	0 0.0%	0 0.0%	0 0.0%	199747 31.7%	0 0.0%	0 0.0%	0 0.0%	0 0.0%	100.0% 0.0%
BU1BBF	2 0.0%	0 0.0%	0 0.0%	0 0.0%	0 0.0%	0 0.0%	0 0.0%	0 0.0%	39967 6.3%	0 0.0%	0 0.0%	0 0.0%	100.0% 0.0%
BU2BBF	1 0.0%	0 0.0%	0 0.0%	0 0.0%	0 0.0%	0 0.0%	0 0.0%	0 0.0%	0 0.0%	39967 6.3%	0 0.0%	0 0.0%	100.0% 0.0%
BU1LF	0 0.0%	0 0.0%	0 0.0%	0 0.0%	0 0.0%	0 0.0%	0 0.0%	0 0.0%	0 0.0%	0 0.0%	39995 6.3%	0 0.0%	100% 0.0%
BU2BBF	0 0.0%	0 0.0%	0 0.0%	0 0.0%	0 0.0%	0 0.0%	0 0.0%	0 0.0%	0 0.0%	0 0.0%	0 0.0%	39996 6.3%	100% 0.0%
	99.9% 0.1%	0.0% 0.0%	100% 0.0%	100% 0.0%	0.0% 0.0%	0.0% 0.0%	100% 0.0%	0.0% 0.0%	100% 0.0%	100% 0.0%	0.0% 0.0%	0.0% 0.0%	0.0% 0.0%

(a)

Predicted Fault Type	Actual Fault Type												
	NoF	BOSF	BU1SF	BU2SF	LN1F	LN2F	LN3F	BOBBF	BU1BBF	BU2BBF	BU1LF	BU2LF	
NoF	35078 5.6%	0 0.0%	0 0.0%	2 0.0%	1 0.0%	1 0.0%	0 0.0%	48 0.0%	0 0.0%	0 0.0%	2 0.0%	1 0.0%	99.8% 0.2%
BOSF	20 0.0%	35520 5.6%	0 0.0%	0 0.0%	0 0.0%	0 0.0%	0 0.0%	0 0.0%	0 0.0%	0 0.0%	0 0.0%	0 0.0%	99.9% 0.1%
BU1SF	2 0.0%	0 0.0%	39841 6.3%	0 0.0%	0 0.0%	0 0.0%	0 0.0%	0 0.0%	0 0.0%	0 0.0%	0 0.0%	0 0.0%	100.0% 0.0%
BU2SF	0 0.0%	0 0.0%	0 0.0%	39839 6.3%	0 0.0%	0 0.0%	0 0.0%	0 0.0%	0 0.0%	0 0.0%	0 0.0%	0 0.0%	100% 0.0%
LN1F	0 0.0%	0 0.0%	0 0.0%	0 0.0%	39999 6.3%	0 0.0%	0 0.0%	0 0.0%	0 0.0%	0 0.0%	0 0.0%	0 0.0%	100% 0.0%
LN2F	0 0.0%	0 0.0%	0 0.0%	0 0.0%	0 0.0%	39999 6.3%	0 0.0%	0 0.0%	0 0.0%	0 0.0%	0 0.0%	0 0.0%	100% 0.0%
LN3F	0 0.0%	0 0.0%	0 0.0%	0 0.0%	0 0.0%	0 0.0%	40000 6.3%	0 0.0%	0 0.0%	0 0.0%	0 0.0%	0 0.0%	100% 0.0%
BOBBF	15 0.0%	0 0.0%	0 0.0%	0 0.0%	0 0.0%	0 0.0%	0 0.0%	199727 31.7%	0 0.0%	0 0.0%	0 0.0%	0 0.0%	100.0% 0.0%
BU1BBF	3 0.0%	0 0.0%	0 0.0%	0 0.0%	0 0.0%	0 0.0%	0 0.0%	0 0.0%	39967 6.3%	0 0.0%	0 0.0%	0 0.0%	100.0% 0.0%
BU2BBF	2 0.0%	0 0.0%	0 0.0%	0 0.0%	0 0.0%	0 0.0%	0 0.0%	0 0.0%	0 0.0%	39967 6.3%	0 0.0%	0 0.0%	100.0% 0.0%
BU1LF	0 0.0%	0 0.0%	0 0.0%	0 0.0%	0 0.0%	0 0.0%	0 0.0%	0 0.0%	0 0.0%	0 0.0%	39995 6.3%	0 0.0%	100% 0.0%
BU2LF	0 0.0%	0 0.0%	0 0.0%	0 0.0%	0 0.0%	0 0.0%	0 0.0%	0 0.0%	0 0.0%	0 0.0%	0 0.0%	39996 6.3%	100% 0.0%
	99.9% 0.1%	100% 0.0%	100% 0.0%	0.0% 0.0%	0.0% 0.0%	0.0% 0.0%	100% 0.0%	0.0% 0.0%	100% 0.0%	100% 0.0%	0.0% 0.0%	0.0% 0.0%	0.0% 0.0%

(b)

Figure 26: Confusion Matrix Plots

(a) Pre-Cascaded System (b) Post-Cascaded System.

4.1.4 Results of the Proposed ML Based FDI in DCMG

After training both the pre-cascaded and post-cascaded systems, a fault detection module is established to detect and isolate faults in the DCMG system. This module considers the voltage and current parameters of the DCMG and generates fault signals of different types as outputs. These fault signals are represented as binary values, with "1" indicating the presence of a fault and "0" indicating a no-fault condition. The generated fault signals serve as triggers for the operation of circuit breakers within the microgrid. A value of "0" implies that the circuit breaker is closed, while a value of "1" indicates that the circuit breaker is opened in response to the fault signal. To enhance the reliability and selectivity of the fault detection process, the DCMG system is divided into zones, with separate circuit breakers assigned to each zone. This zoning approach, as discussed in Section 3.2 of the thesis, helps localize the effects of faults and facilitates prompt and targeted response to fault conditions, ensuring effective fault detection and isolation in the DCMG system.

Below is a demonstration of the effective fault detection and isolation achieved through the Neural Network-based Fault Detector. To validate the system's effectiveness, the algorithm is tested with unknown fault samples as inputs. These fault samples include faults with varying resistances and different occurrence times. By subjecting the system to such diverse fault scenarios, its ability to accurately detect and isolate faults under different conditions is thoroughly assessed. This robust testing process serves as a testament to the fault detector's reliability and adaptability, highlighting its capability to handle a wide range of fault scenarios and ensure the overall stability and safety of the DCMG system.

- FDI Case 1: Converter Switch failure in Boost Converter
- FDI Case 2: Transmission Cable Short-Circuit fault in Cable 2
- FDI Case 3: Busbar Short-Circuit fault at Bus 2
- FDI Case 4: Load Component Fault at Load 1

4.1.4.1 FDI Case 1: Switch Failure

As discussed previously, the DCMG under study has three power converters and the switches of these converters can face fault. The proposed NN has been trained to detect all these switch faults. However, in this study we perform FDI for the Switch failure scenario in the Boost Converter *BOSF*. The converters voltage and current responses upon the Boost Converter's switch fault is shown in Figure 27(a). The Transmission Cable current responses are shown in Figure 27(b). Comparing the response with the Non-FDI Data Generation Case 2, we find that the proposed FDI has successfully detected and isolated the BOSF.

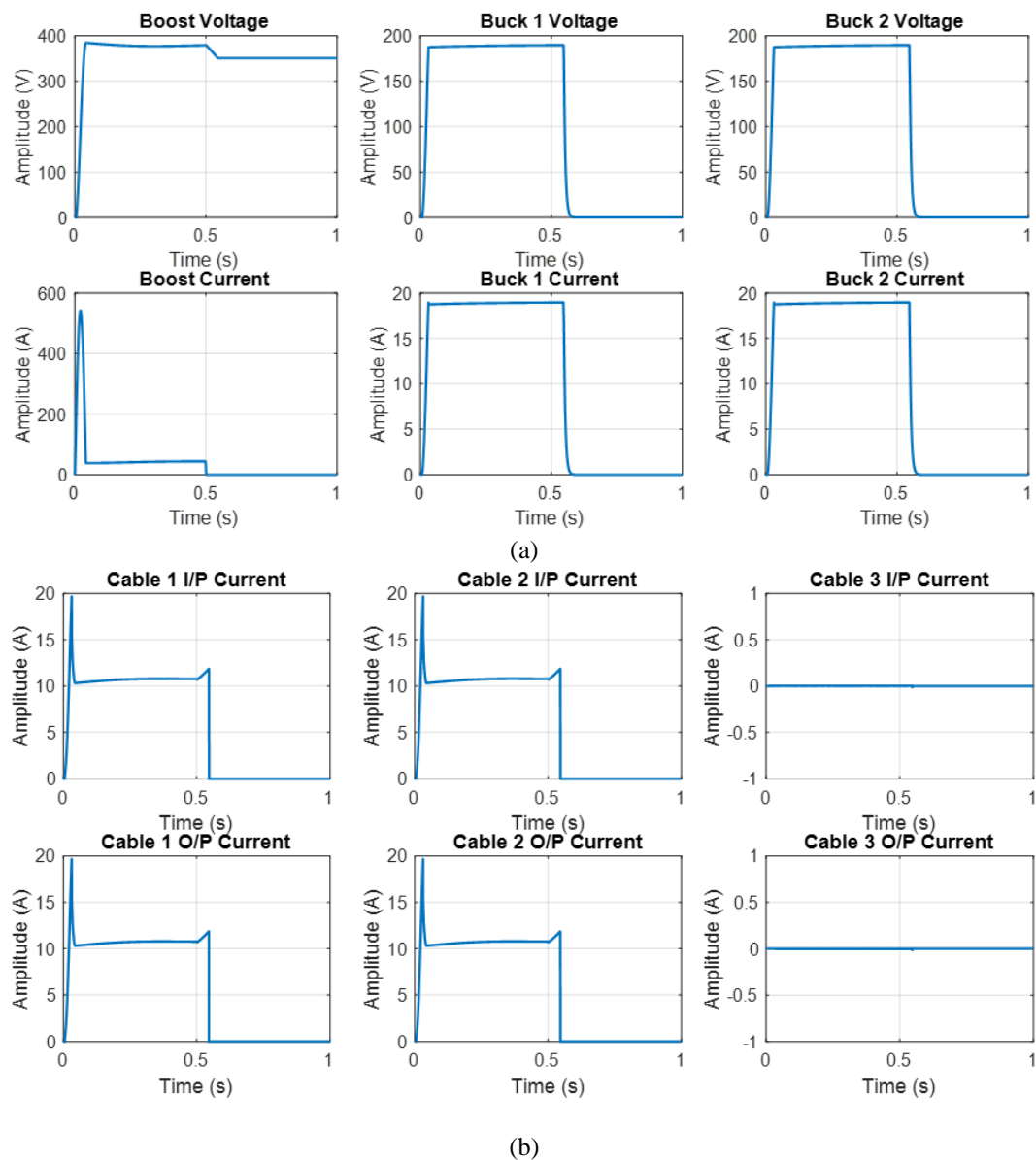
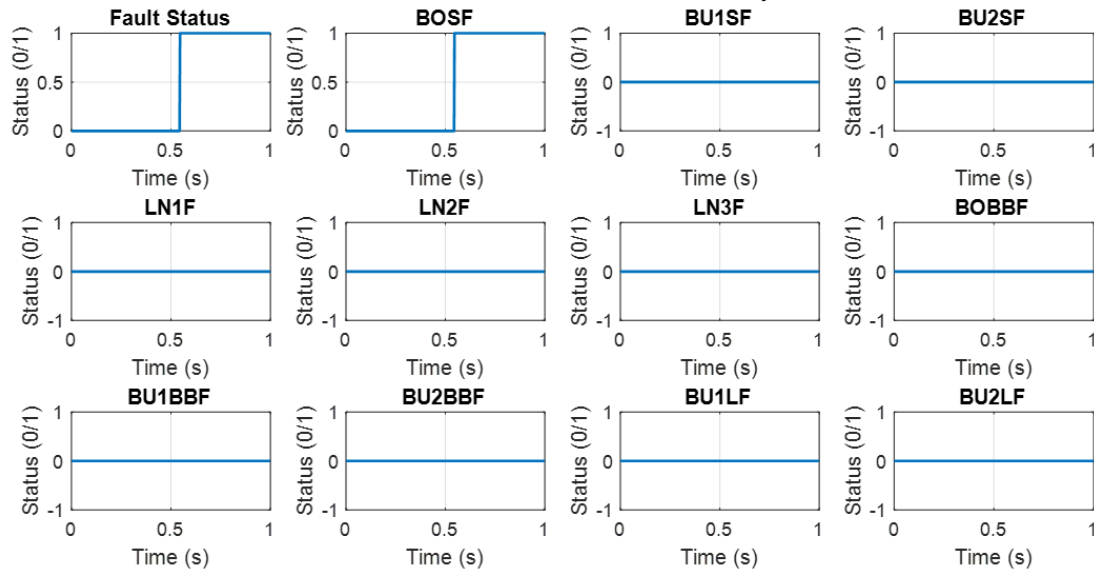
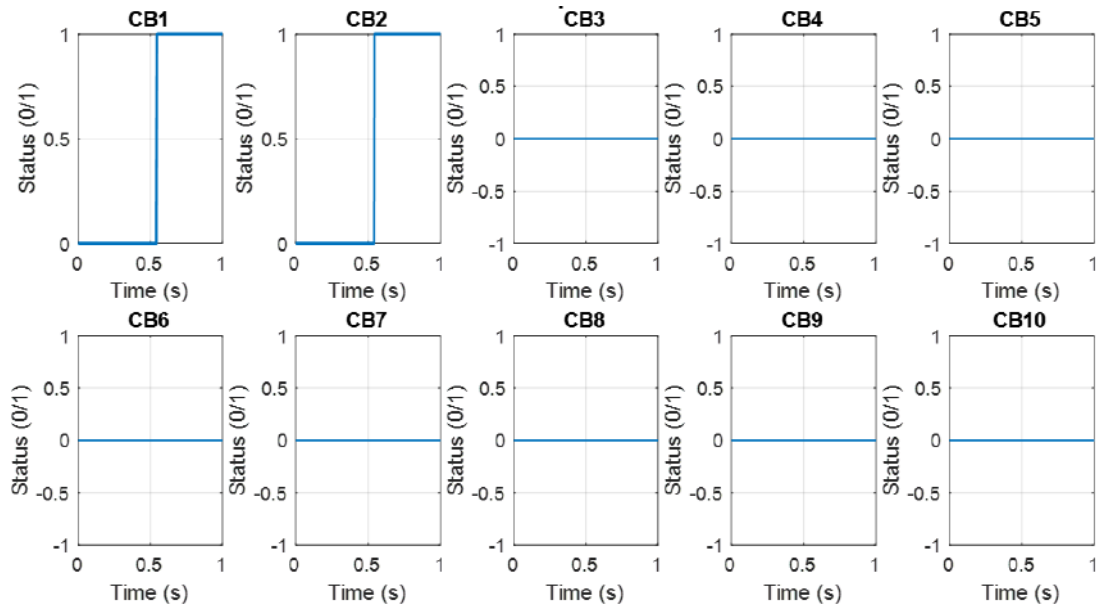


Figure 27: FDI Case-1 Boost Converter Switch Failure Responses
(a) Converters Voltage & Current, (b) Transmission Cables Current.

Figure 28(a) shows the fault detection for the *BOSF*. We see that the status of *BOSF* is “1” whereas all other fault statuses have not responded to this scenario i.e., their values are “0”. In response to the fault detection CB1 has been operated for the fault isolation purpose.



(a)



(b)

Figure 28: FDI Case-1 Boost Converter Switch Failure Detection & Isolation

(a) Detection- Fault Status, (b) Isolation- Circuit Breakers Response.

4.1.4.2 FDI Case 2: Transmission Cable Fault

To check the performance of the proposed FDI for the Transmission Cable faults; a short circuit fault has been introduced on Cable 2 called *LN2F* at 0.2 seconds. The responses of DCMG states for this fault are shown in Figure 29. The plots demonstrate the algorithm's swift and precise fault detection. The FDI responded within 0.2ms, it triggered the opening of CB1 and CB2 (Figure 30(b)), isolating the faulty boost converter and ensuring microgrid system protection.

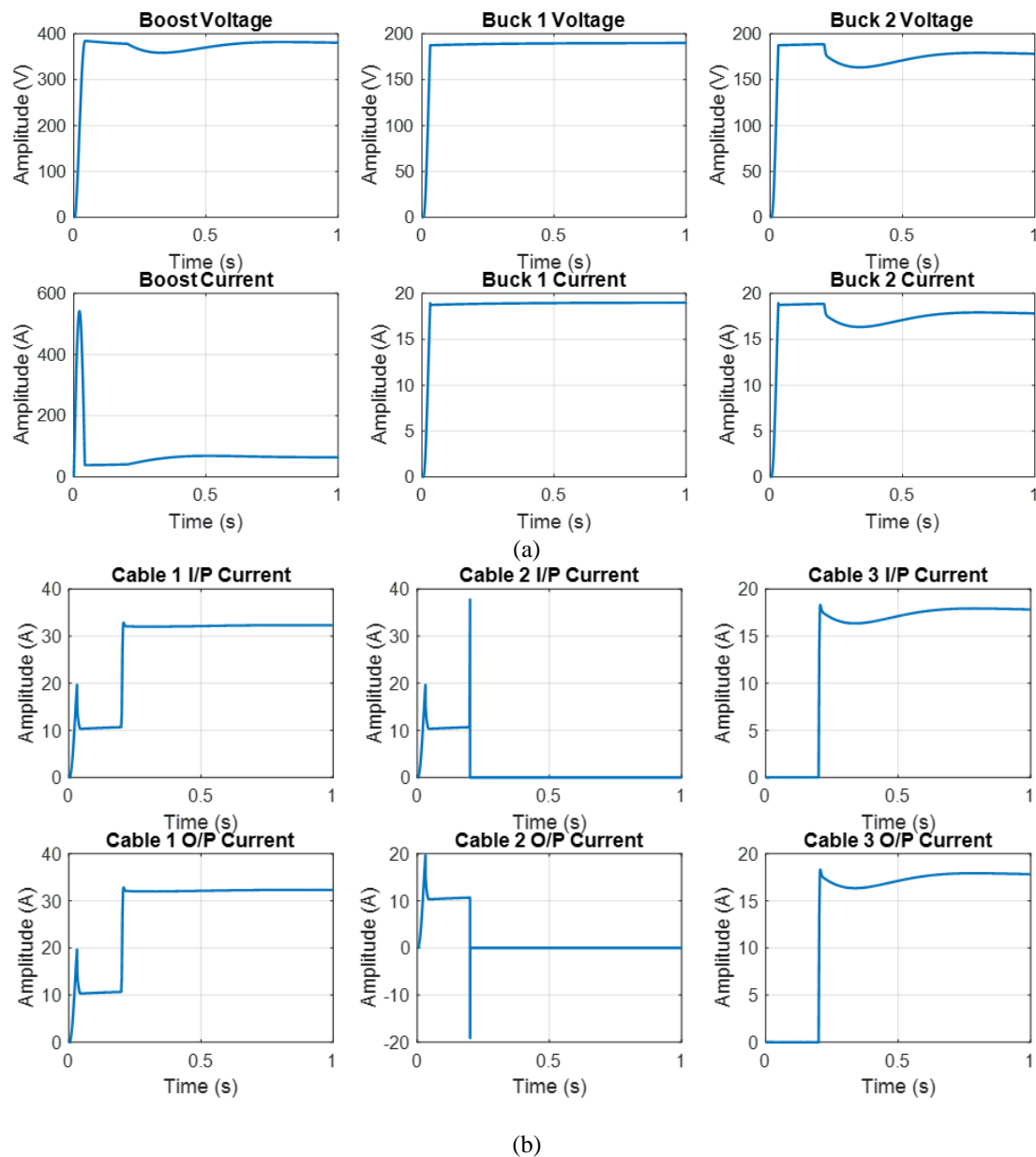
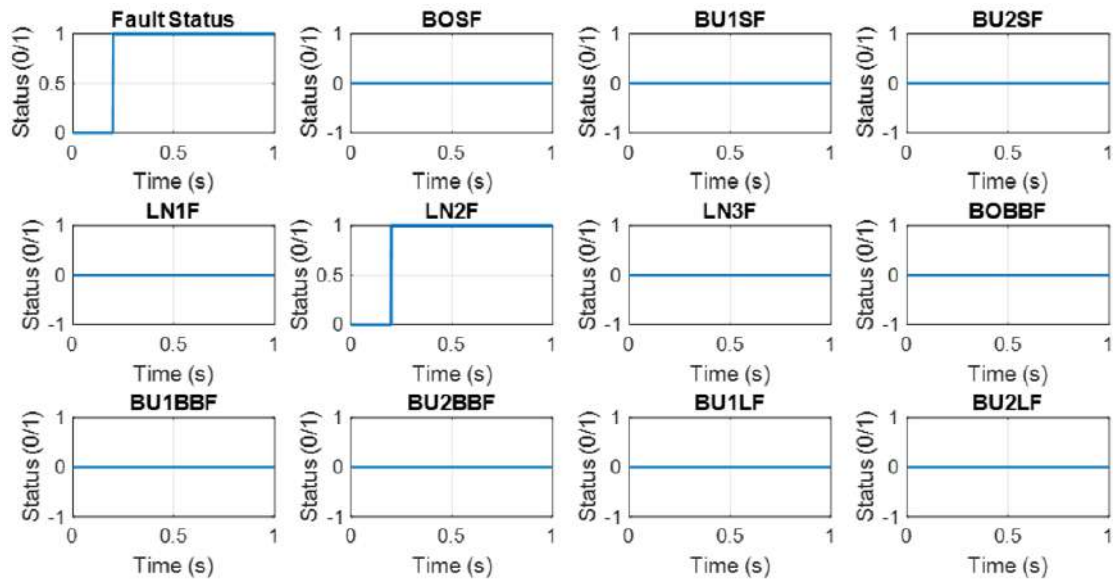
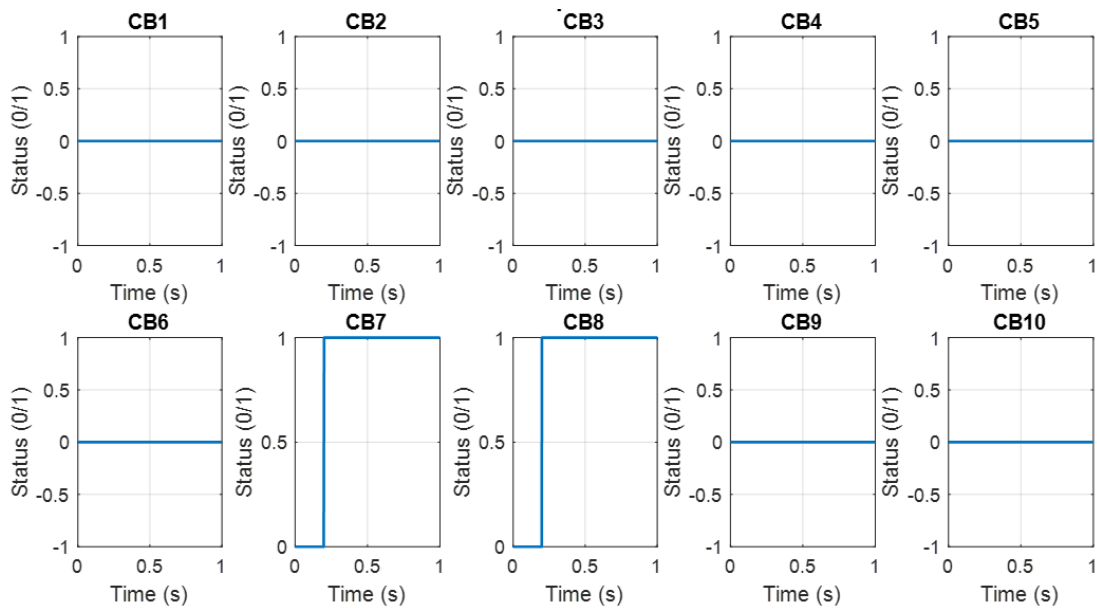


Figure 29: FDI Case-2 Transmission Cable Fault Responses

(a) Converters Voltage & Current, (b) Transmission Cables Current.



(a)

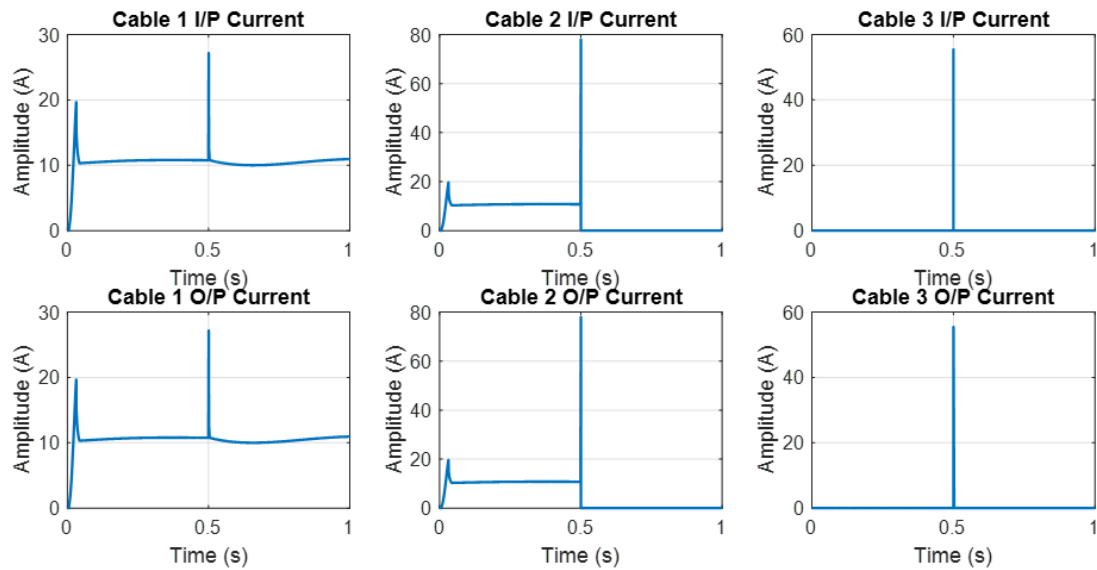


(b)

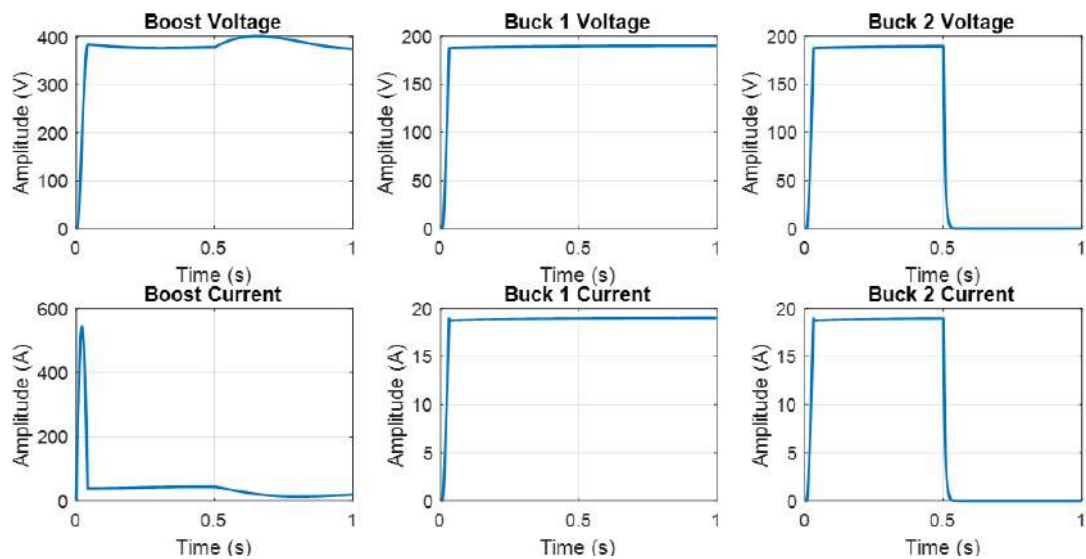
Figure 30: FDI Case-2 Transmission Cable Fault Detection & Isolation
 (a) Detection- Fault Status, (b) Isolation- Circuit Breakers Response.

4.1.4.3 FDI Case 3: Busbar Fault

For this scenario *BU2BBF* i.e., Busbar 2 fault has been tested. The plots in Figure 31 showcase the algorithm's rapid and accurate fault detection capabilities. As can be observed in Figure 32 that the proposed FDI responded in just 0.2ms, the algorithm activates CB7 and CB8, successfully isolating the faulty transmission cable 2 from the system and ensuring its stability.



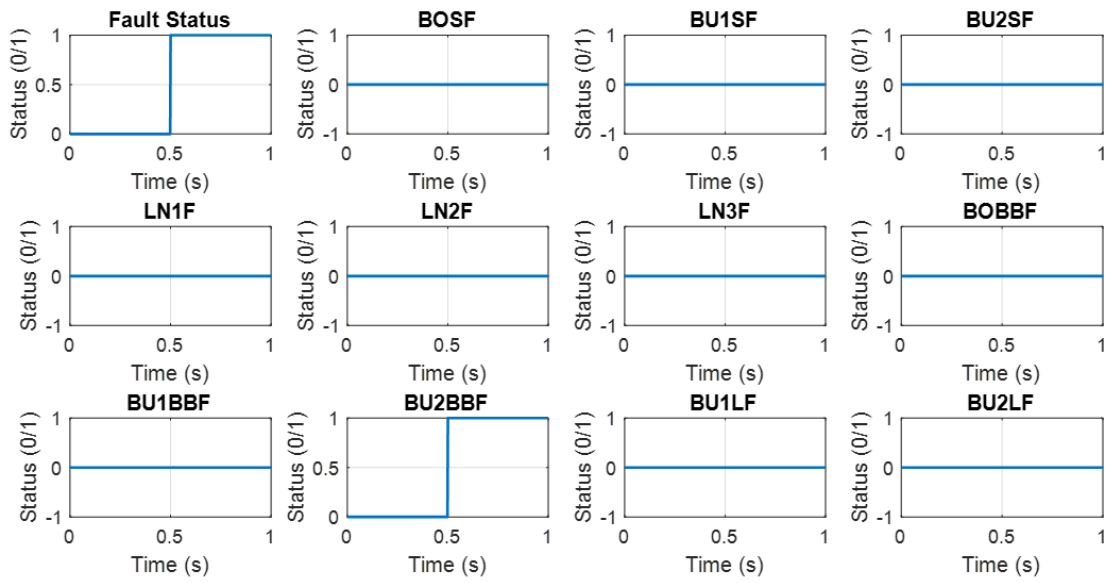
(a)



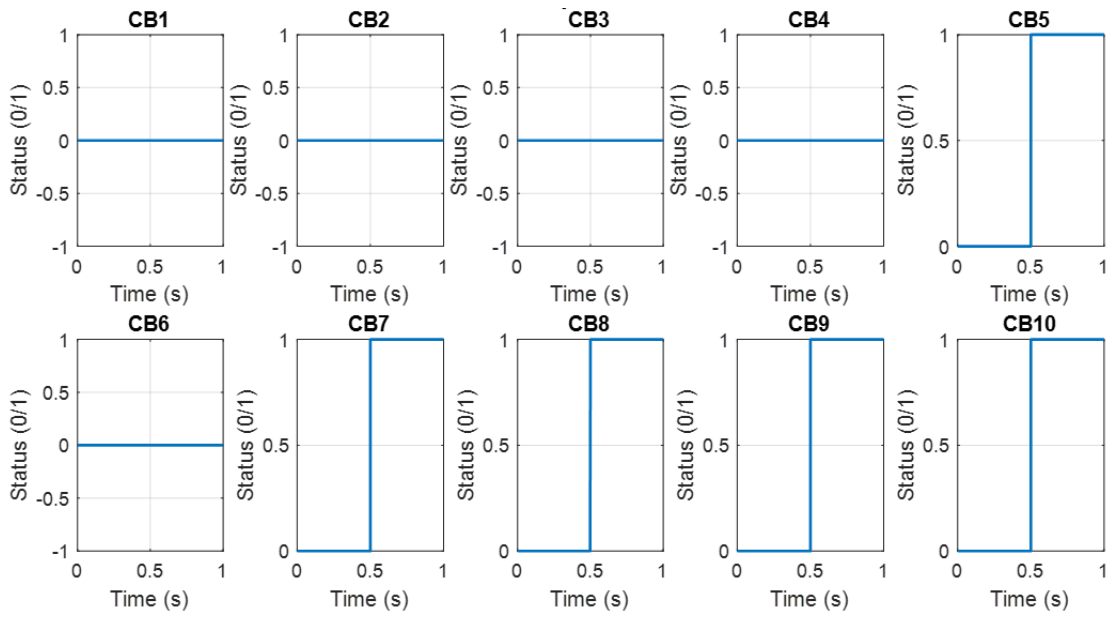
(b)

Figure 31: FDI Case-3 Busbar Fault Response

(a) Converters Voltage & Current, (b) Transmission Cables Current.



(a)



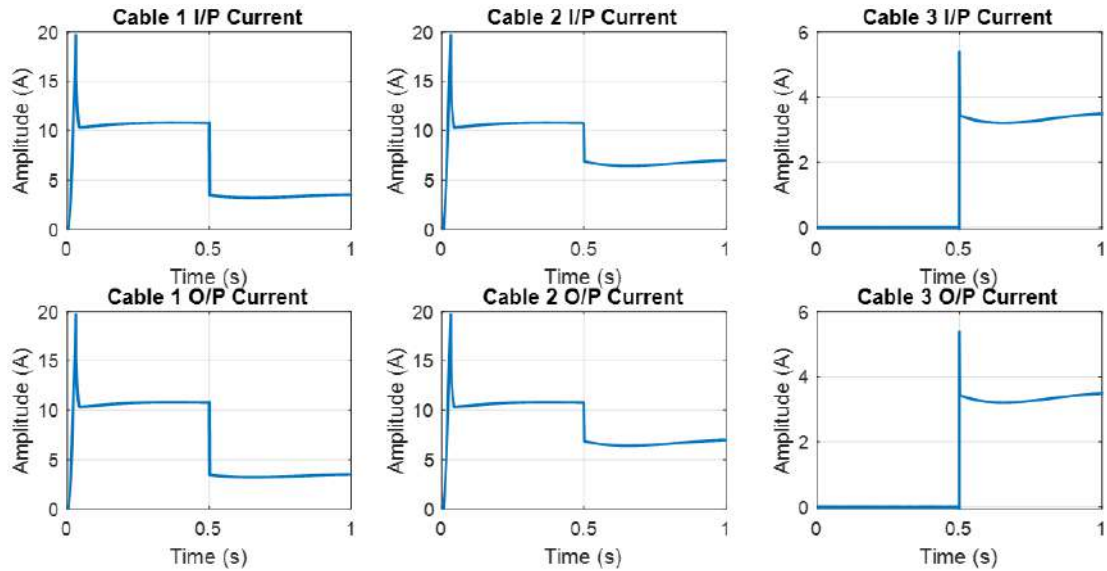
(b)

Figure 32: FDI Case-3 Busbar Fault Detection & Isolation

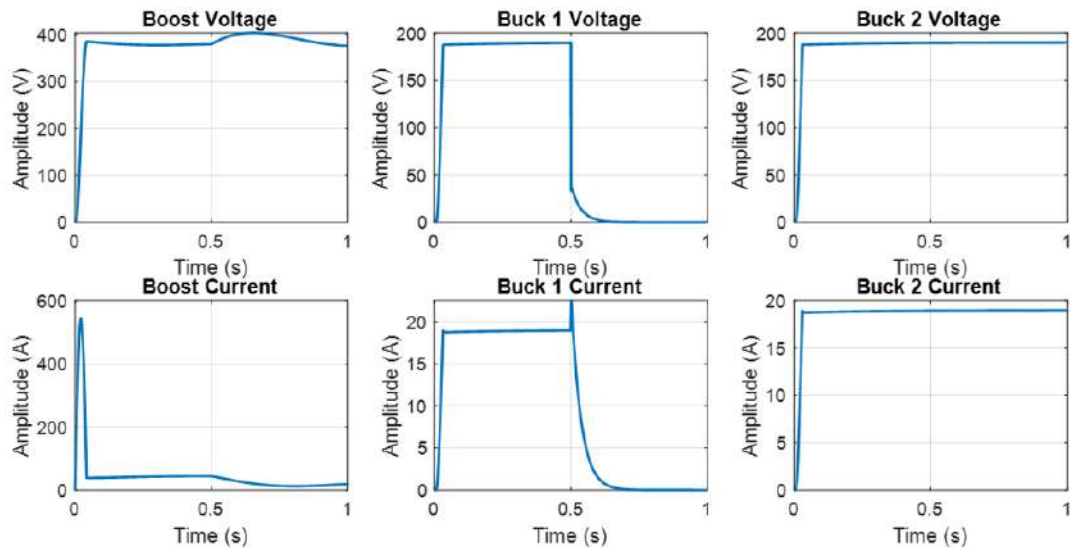
(a) Detection- Fault Status, (b) Isolation- Circuit Breakers Response.

4.1.4.4 FDI Case 4: Load Component Fault

The response of the DCMG upon the introduction of the BU1LF fault is shown in Figure 4-15. The trained NN FDI swiftly detects faults (Figure 33) and activates CB7, CB8, CB9, and CB10 (Figure 34(b)), effectively isolating the faulty components within 0.2ms. This ensures the stability of the microgrid system.



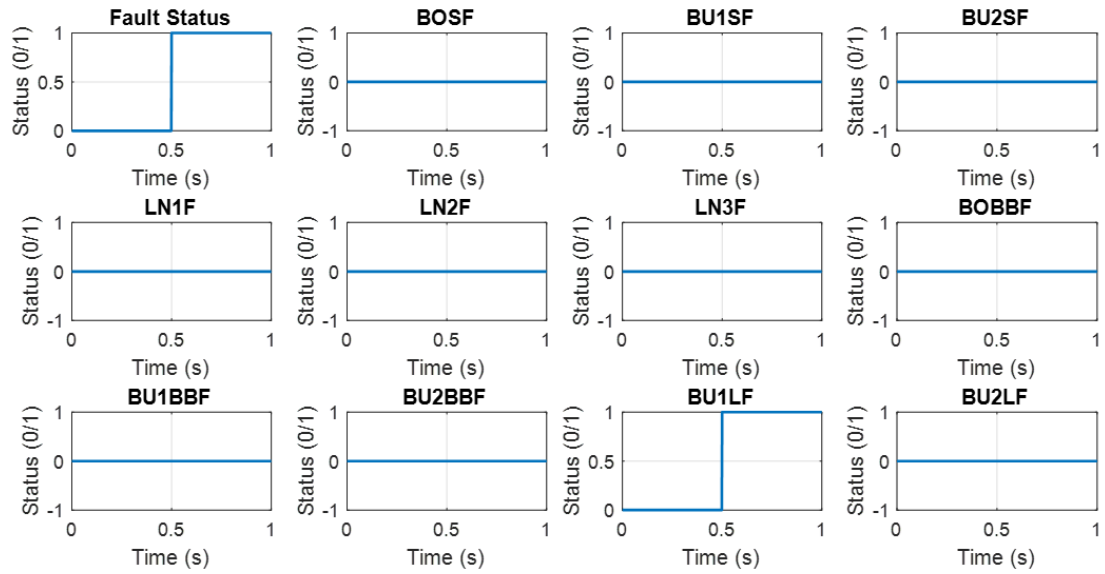
(a)



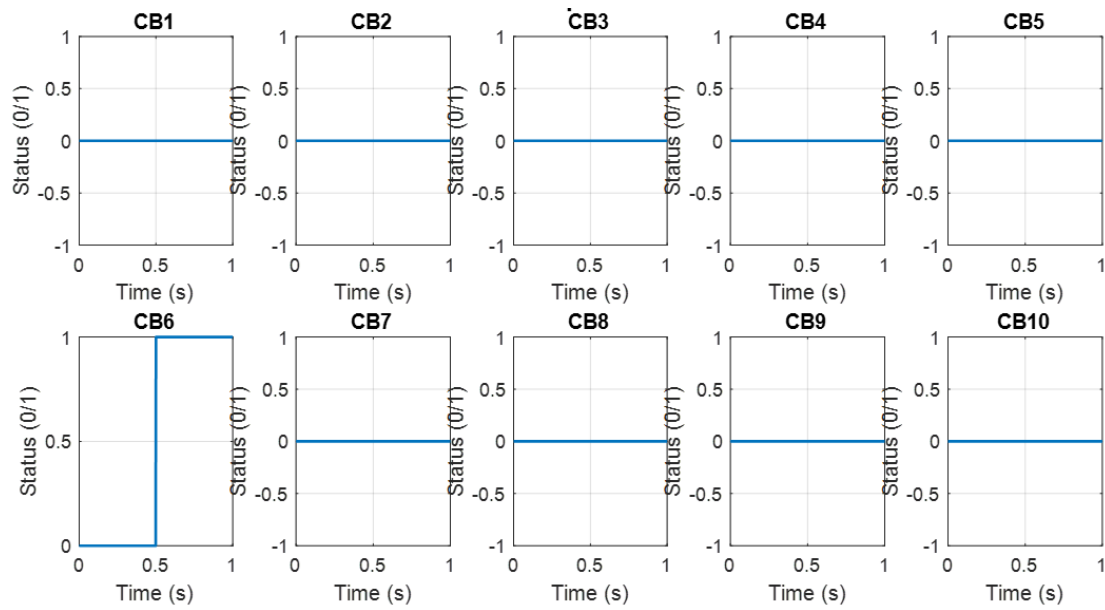
(b)

Figure 33: FDI Case-4 Load Component Fault Responses

(a) Converters Voltage & Current, (b) Transmission Cables Current.



(a)



(b)

Figure 34: FDI Case-4 Load Component Fault Detection & Isolation
 (a) Detection- Fault Status, (b) Isolation- Circuit Breakers Response.

Chapter 5

5.1 Summary and Future work

This project was undertaken to propose a solution to one of DCMG's major issues, fault detection and isolation. DC microgrids are emerging as a dependable and effective phenomenon for the power distribution system as technology advances. But their protection system still lacks the means to meet the desired needs. In this study, a machine learning-based fault detection and isolation algorithm is developed to protect DC microgrid systems from the influence of different faults. The suggested method begins with building a thorough DC microgrid model, which produces the necessary data for training the machine learning algorithm. To guarantee steady system operation, a hysteresis band controller is used as the feedback control technique. Once fault-related data has been carefully extracted, it is then fed into the ML algorithm, which is rigorously trained and optimized using the cross-entropy loss function and scaled conjugate backpropagation algorithm. The experimental results demonstrate the exceptional efficacy of the proposed methodology. Fault detection speeds reach an impressive 1 millisecond, accompanied by an astonishing 99.9% accuracy in fault classification. This rapid and precise diagnosis facilitates swift isolation of faults, minimizing both damage and system downtime. Consequently, the deployment of this intelligent defense mechanism paves the way for a future of DC microgrids operating with enhanced resilience and reliability, delivering power with increased confidence.

In terms of future work, there are a few areas that can be explored to make the fault detection and isolation algorithm for DC microgrids even better. One possibility is to make the algorithm capable of handling more complex fault situations by using techniques like ensemble learning or multi-label classification. Another idea is to incorporate advanced machine learning methods, such as deep learning, to improve the accuracy of fault detection and classification. To ensure that the algorithm is practical, it can be adapted for real-time implementation on specific hardware systems. It would also be valuable to test the algorithm in different operating conditions to see how well it performs in various situations. Lastly, integrating the algorithm with strategies to alleviate faults and conducting experiments on actual DC microgrid systems would be helpful in validating its effectiveness and real-world applicability.

Chapter 6

6.1 Conclusion & Recommendation

In this study, a machine learning-based fault detection and isolation algorithm is developed to protect DC microgrid systems from the influence of different faults. The goal was to design an effective approach that combines mathematical modeling, hysteresis band control, and supervised machine learning using neural networks. The workflow begins with the comprehensive modeling of the DC microgrid, encompassing both mathematical and physical aspects through the utilization of SIMULINK. A hysteresis band controller is employed as the feedback control strategy to ensure stable system operation. The algorithm extracts fault-related data from the DC microgrid, followed by the generation of a dataset for training the supervised machine learning algorithm. The neural network is trained using the cross-entropy loss function and optimized through the scaled conjugate backpropagation algorithm.

The suggested method excels in its experimental results, demonstrating outstanding fault detection capabilities. It pinpoints faults within just 1 millisecond and boasts an outstanding fault classification accuracy of 99.9%. This remarkable performance solidifies the technique's effectiveness in tackling fault detection challenges, offering a reliable and swift solution for safeguarding systems against malfunction. Our groundbreaking algorithm results aren't just numbers; they're a revolutionary leap for energy infrastructure. From safeguarding remote communities to unlocking renewable energy, this research extends beyond academia, paving the way for a future of robust, reliable, and sustainable energy for all. As we refine and implement this technology, we are prepared to transform how we generate, distribute, and utilize energy, leaving a legacy of innovation and a brighter future powered by clean, dependable electricity.

References

- [1] Ali, Zulfiqar, Yacine Terriche, Syed Zagam Abbas, Mustafa Alrayah Hassan, Muhammad Sadiq, Chun-Lien Su, and Josep M. Guerrero. "Fault Management in DC Microgrids: A Review of Challenges, Countermeasures, and Future Research Trends." *IEEE Access* (2021).
- [2] Konar, Srayashi, and Arindam Ghosh. "Interconnection of islanded DC microgrids." In *2015 IEEE PES Asia-Pacific Power and Energy Engineering Conference (APPEEC)*, pp. 1-5. IEEE, 2015.
- [3] Bhattacharya, Biswarup, and Abhishek Sinha. "Intelligent fault analysis in electrical power grids." In *2017 IEEE 29th International Conference on Tools with Artificial Intelligence (ICTAI)*, pp. 985-990. IEEE, 2017.
- [4] Skjong, Espen, Egil Rødskar, Maria Marta Molinas Cabrera, Tor Arne Johansen, and Joseph Cunningham. "The marine vessel's electrical power system: From its birth to present day." (2015).
- [5] Reilly, James T. "From microgrids to aggregators of distributed energy resources. The microgrid controller and distributed energy management systems." *The Electricity Journal* 32, no. 5 (2019): 30-34.
- [6] Lonkar, Manoj, and Srinivas Ponnaluri. "An overview of DC microgrid operation and control." In *IREC2015 The Sixth International Renewable Energy Congress*, pp. 1-6. IEEE, 2015.
- [7] Neves, Marcello da S., Maynara A. Aredes, Hamidreza Khezri, Elisa TH Ida, and Maurício Aredes. "Advantages of grid-tied DC microgrid." In *2017 Brazilian Power Electronics Conference (COBEP)*, pp. 1-6. IEEE, 2017.
- [8] Azer, Peter, and Ali Emadi. "Generalized state space average model for multi-phase interleaved buck, boost and buck-boost DC-DC converters: transient, steady-state and switching dynamics." *IEEE Access* 8 (2020): 77735-77745.
- [9] Pires, V. Fernão, Daniel Foito, Armando Cordeiro, and A. J. Pires. "A Bidirectional DC-DC Converter to Interlink Unipolar and Bipolar DC

- Microgrids." In 2021 9th International Conference on Smart Grid (icSmartGrid), pp. 37-42. IEEE, 2021.
- [10] Azeem, Omar, Mujtaba Ali, Ghulam Abbas, Muhammad Uzair, Ayman Qahmash, Abdulmohsen Algarni, and Mohammad Rashid Hussain. "A comprehensive review on integration challenges, optimization techniques and control strategies of hybrid AC/DC Microgrid." *Applied Sciences* 11, no. 14 (2021): 6242.
- [11] Hannan, M. A., MS Hossain Lipu, Pin Jern Ker, R. A. Begum, Vasilios G. Agelidis, and Frede Blaabjerg. "Power electronics contribution to renewable energy conversion addressing emission reduction: Applications, issues, and recommendations." *Applied energy* 251 (2019): 113404.
- [12] Chen, Bo, Jianhui Wang, Xiaonan Lu, Chen Chen, and Shijia Zhao. "Networked microgrids for grid resilience, robustness, and efficiency: A review." *IEEE Transactions on Smart Grid* 12, no. 1 (2020): 18-32.
- [13] Meghwani, Anju, Ramakrishna Gokaraju, Suresh Chandra Srivastava, and Saikat Chakrabarti. "Local measurements-based backup protection for DC microgrids using sequential analyzing technique." *IEEE Systems Journal* 14, no. 1 (2019): 1159-1170.
- [14] Srivastava, Chetan, and Manoj Tripathy. "DC microgrid protection issues and schemes: A critical review." *Renewable and Sustainable Energy Reviews* 151 (2021): 111546.
- [15] Thirumarimurugan, M., N. Bagyalakshmi, and P. Paarkavi. "Comparison of fault detection and isolation methods: A review." In 2016 10th International Conference on Intelligent Systems and Control (ISCO), pp. 1-6. IEEE, 2016.
- [16] Iqbal, Rahat, Tomasz Maniak, Faiyaz Doctor, and Charalampos Karyotis. "Fault detection and isolation in industrial processes using deep learning approaches." *IEEE Transactions on Industrial Informatics* 15, no. 5 (2019): 3077-3084.
- [17] Sah, Shagan. "Machine learning: a review of learning types." (2020).

- [18] Wang, Ting, Liliuyuan Liang, Sriram Karthik Gurumurthy, Ferdinanda Ponci, Antonello Monti, Zhiqing Yang, and Rik W. De Doncker. "Model-based fault detection and isolation in dc microgrids using optimal observers." *IEEE Journal of Emerging and Selected Topics in Power Electronics* 9, no. 5 (2020): 5613-5630.
- [19] Wang, Ting, Liliuyuan Liang, Zhiguo Hao, Antonello Monti, and Ferdinanda Ponci. "A Comprehensive Fault Detection and Isolation Method for DC Microgrids Using Reduced-Order Unknown Input Observers." *IEEE Transactions on Power Delivery* (2023).
- [20] Nalina, B. S., V. Kamaraj, and M. Ramesh Babu. "Fault Detection and Identification Strategy Based on Luenberger Observer for Bidirectional Interleaved Switched—Capacitor DC–DC Converter Interfaced Microgrids." *Journal of Electrical Engineering & Technology* 17, no. 4 (2022): 2329-2338.
- [21] Asadi, Samira, Navid Vafamand, Mehrdad Moallem, and Tomislav Dragičević. "Fault reconstruction of islanded nonlinear DC microgrids: An LPV-based sliding mode observer approach." *IEEE Journal of Emerging and Selected Topics in Power Electronics* 9, no. 4 (2020): 4606-4614.
- [22] Gajula, Kaushik, and Luis Herrera. "Detection and localization of series arc faults in DC microgrids using Kalman filter." *IEEE Journal of Emerging and Selected Topics in Power Electronics* 9, no. 3 (2020): 2589-2596.
- [23] Bayati, Navid, Hamid Reza Baghaee, Amin Hajizadeh, Mohsen Soltani, Zhengyu Lin, and Mehdi Savaghebi. "Local fault location in meshed DC microgrids based on parameter estimation technique." *IEEE Systems Journal* 16, no. 1 (2021): 1606-1615.
- [24] Augustine, Sijo, Matthew J. Reno, Sukumar M. Brahma, and Olga Lavrova. "Fault current control and protection in a standalone DC microgrid using adaptive droop and current derivative." *IEEE Journal of Emerging and Selected Topics in Power Electronics* 9, no. 3 (2020): 2529-2539.

- [25] Yang, Yachao, Chun Huang, Diehui Zhou, and Yong Li. "Fault detection and location in multi-terminal DC microgrid based on local measurement." *Electric Power Systems Research* 194 (2021): 107047.
- [26] Rao, G. Kesava, and Premalata Jena. "Fault detection in DC microgrid based on the resistance estimation." *IEEE Systems Journal* 16, no. 1 (2021): 1009-1020.
- [27] Saleh, Khaled, Ali Hooshyar, and Ehab F. El-Saadany. "Fault detection and location in medium-voltage DC microgrids using travelling-wave reflections." *IET Renewable Power Generation* 14, no. 4 (2020): 571-579.
- [28] Montoya, Rudy, Binod P. Poudel, Ali Bidram, and Matthew J. Reno. "DC microgrid fault detection using multiresolution analysis of traveling waves." *International Journal of Electrical Power & Energy Systems* 135 (2022): 107590.
- [29] Grcić, Ivan, Hrvoje Pandžić, and Damir Novosel. "Fault detection in dc microgrids using short-time fourier transform." *Energies* 14, no. 2 (2021): 277.
- [30] Jayamaha, D. K. J. S., N. W. A. Lidula, and Athula D. Rajapakse. "Wavelet-multi resolution analysis based ANN architecture for fault detection and localization in DC microgrids." *IEEE Access* 7 (2019): 145371-145384.
- [31] Bayati, Navid, Hamid Reza Baghaee, Mehdi Savaghebi, Amin Hajizadeh, Mohsen Soltani, and Zhengyu Lin. "EMD/HT-based local fault detection in DC microgrid clusters." *IET Smart Grid* 5, no. 3 (2022): 177-188.
- [32] Prince, Satyavarta Kumar, Shaik Affijulla, and Gayadhar Panda. "A fault detection technique based on line parameters in ring-configured DC microgrid." *International Journal of Emerging Electric Power Systems* 23, no. 4 (2021): 523-542.
- [33] Dhar, Snehamoy, Rajesh Kumar Patnaik, and P. K. Dash. "Fault detection and location of photovoltaic based DC microgrid using differential protection strategy." *IEEE Transactions on Smart Grid* 9, no. 5 (2017): 4303-4312.
- [34] Bayati, Navid, Ebrahim Balouji, Hamid Reza Baghaee, Amin Hajizadeh, Mohsen Soltani, Zhengyu Lin, and Mehdi Savaghebi. "Locating high-

impedance faults in DC microgrid clusters using support vector machines." *Applied Energy* 308 (2022): 118338.

- [35] Tan, Min Keng, Kar Leong Lee, Kit Guan Lim, Ahmad Razani Haron, Pungut Ibrahim, and Kenneth Tze Kin Teo. "Advanced Fault Detection in DC Microgrid System using Reinforcement Learning." In 2021 IEEE International Conference on Artificial Intelligence in Engineering and Technology (IICAET), pp. 1-6. IEEE, 2021.
- [36] Sharif, Amirhossein Akbari, Hossein Kazemi Karegar, and Saman Esmailbeigi. "Fault detection and location in dc microgrids by recurrent neural networks and decision tree classifier." In 2020 10th Smart Grid Conference (SGC), pp. 1-6. IEEE, 2020.
- [37] Abdali, Ali, Kazem Mazlumi, and Reza Noroozian. "Fast fault detection and isolation in low-voltage DC microgrids using fuzzy inference system." In 2017 5th Iranian Joint Congress on Fuzzy and Intelligent Systems (CFIS), pp. 172-177. IEEE, 2017.
- [38] Ramakrishna, A., & Vardhan, V. (2021). Machine learning techniques for fault detection and classification in power systems: A comprehensive review. *Electric Power Systems Research*, 193, 107236.
- [39] Al-Ghaili, A. M., & Abdel-Rahman, A. B. (2019). Fault detection and classification in power systems using machine learning techniques: A review. *Electric Power Systems Research*, 172, 52-64.
- [40] Gamage, R. T., & Saha, T. K. (2020). Machine learning techniques for fault detection and classification in power systems: A comprehensive review. *Electric Power Systems Research*, 180, 106010.
- [41] Shao, X., Jiang, J., Li, Y., & Chen, D. (2020). A comprehensive review of machine learning for fault detection and diagnosis in power systems. *IEEE Transactions on Smart Grid*, 11(2), 1657-1672.
- [42] Rana, M. M., Islam, S. M. R., & Ullah, M. M. (2020). Supervised machine learning techniques for fault detection and classification in power systems: A review. *Electric Power Systems Research*, 188, 106699.

- [43] Singh, S. N., & Singh, A. K. (2021). Supervised learning techniques for fault diagnosis in electrical power systems: A review. *International Journal of Electrical Power & Energy Systems*, 132, 106771.
- [44] Pandey, R. K., & Panigrahi, B. K. (2018). Fault detection and classification in power systems using machine learning techniques: A comprehensive review. *International Journal of Electrical Power & Energy Systems*, 98, 138-155.
- [45] Afshar, M. H., & Yavari, A. (2017). Fault detection and classification in power systems using supervised machine learning algorithms. *Electric Power Systems Research*, 142, 78-88.
- [46] Yao, Xujing, Xinyue Wang, Shui-Hua Wang, and Yu-Dong Zhang. "A comprehensive survey on convolutional neural network in medical image analysis." *Multimedia Tools and Applications* (2020): 1-45.
- [47] Kuang, L., & Wang, S. "A novel modified scaled conjugate gradient algorithm for deep learning neural networks." *Neural Computing and Applications* 32, no. 13 (2020): 10051-10064.
- [48] Yousefnezhad, M., & Hashemzadeh, A. "A novel scaled conjugate gradient method for training feedforward neural networks." *Soft Computing* 24, no. 16 (2020): 11997-12016.
- [49] Bengio, Yoshua, Ian Goodfellow, and Aaron Courville. *Deep Learning*. MIT Press, 2021.
- [50] Zhang, Jie, Yang Liu, Tianhong Wu, and Yun Qi. "Hyperparameters Optimization in Deep Learning: A Review." *Neurocomputing* 457 (2021): 622-634.
- [51] Wang, Q., & Gao, Y. (2022). Deep learning-based fault detection and classification in DC microgrids. *Electric Power Systems Research*, 207, 107276.
- [52] Khan, M. A., Ahmed, R., & Yilbas, B. S. (2022). Fault detection and classification in DC microgrids using convolutional neural networks. *Energies*, 15(1), 184.